Decimation Free Directional Filter Bank for Medical Image Enhancement

Developed by

Muhammad Khalid Khan Niazi
(Reg# 46-CS/MS/01)

Muhammad Aurangzeb Khan
(Reg# 51-CS/MS/01)

Supervised by

Dr. S. Tauseef-ur-Rehman

Department of Computer Science
Faculty of Applied Sciences
International Islamic University, Islamabad
(2004)

Acc. No. (FEC) T-1171

International Islamic University, Islamabad
Faculty of Applied Sciences
Department of Computer Science

Date: 11Th December, 2004

Final Approval

It is certified that we have read the project report submitted by Mr. Muhammad Khalid Khan Niazi (46-CS/MS/01) and Mr. Muhammad Aurangzeb Khan (51-CS/MS/01) and it is our judgment that this project is of sufficient standard to warrant its acceptance by the International Islamic University, Islamabad for the MS degree in Computer Science.

Committee

External Examiner

Dr. Syed Afaq Hussain
Head,
Department of Computer Science,
SZABIST, Islamabad.

Internal Examiner

Mr. Asim Munir
Assistant Professor,
Department of Computer Science,
Faculty of Applied Sciences,
International Islamic University, Islamabad.

Supervisor

Dr. S. Tauseef-ur-Rehman,
Head,
Department of Telecom & Computer Engineering,
Faculty of Applied Sciences,
International Islamic University, Islamabad.

A dissertation submitted to the
DEPARTMENT OF COMPUTER SCIENCE,
FACULTY OF APPLIED SCIENCES,
INTERNATIONAL ISLAMIC UNIVERSITY, ISLAMABAD as a partial fulfillment of the requirements for the award of the degree of MS in Computer Science.

Declaration

We hereby declare that this research, neither as a whole nor as a part has been copied out from any source. It is further declared that we have developed this technique entirely on the basis of our personal efforts under the sincere guidance of our supervisor.
No portion of this work presented in this report has been submitted in support of any application for any other degree or qualification of this or any other university or institute of learning.

Muhammad Khalid Khan Niazi
(46-CS/MS/01)

M. Khalid

Muhammad Aurangzeb Khan
(51-CS/MS/01)

Aurang Zeb

Dedication

Dedicated to our parents and family members who after Allah Almighty are most precious in our life and whose keen interest, encouragement and well wishing will bring inspired success to us in every field of life and hereafter. InshaAllah.

Also dedicated to Dr. Mohammad Asmat Ullah Khan whose encouragement and dedication to the cause made the dream a reality and living success.

Muhammad Khalid Khan Niazi
(46-CS/MS/01)

M. Khalid

Muhammad Aurangzeb Khan
(51-CS/MS/01)

Aurang Zeb

Acknowledgements

All praise to Allah Almighty, the most merciful, the most gracious. Without His help and blessing, we were unable to complete the project.

Thanks to our project supervisor Dr. S. Tauseef-ur-Rehman whose sincere efforts helped us to complete our project successfully. Without the great help, motivation and righteous guidance of Mr. Tauseef-ur-Rehaman it was impossible to complete this project.

Also thanks to Dr. Mohammad Asmat Ullah Khan, Who was ever ready for help, and whose frequent encouragement enables us to become familiar with research.

Thanks to our families who helped us during our most difficult of times and it is due to their unexplainable care and love that we are at this stage today. Without their unswerving love, encouragement, confidence, and support, we are sure that we would never have completed this project.

Muhammad Khalid Khan Niazi
(46-CS/MS/01)

M. Khalid

Muhammad Aurangzeb Khan
(51-CS/MS/01)

Aurang Zeb

Project in Brief

Project Title:	***Decimation Free Directional Filter Bank for Medical Image Enhancement.***
Objective:	**To keep the interest of the country foremost**
Undertaken by:	**Muhammad Khalid Khan Niazi** **Muhammad Aurangzeb Khan**
Supervised by:	**Dr. S. Tauseef-ur-Rehman** **Head Department of Telecommunication Engineering,** **International Islamic University, Islamabad.**
Starting Date:	**1st May 2003**
Ending Date:	11th Dec- 2004
Tools/languages:	**MATLAB 6.5**
Operating System	**Microsoft Windows XP**
System Used:	**Pentium-IV**

Abstract

Our proposed system is an orientation analysis tool. It differs from the past technique due to the fact that it is mainly concerned with the global direction rather than the local direction. So an image containing a certain feature in a specific direction will only be present in one of the directional images. In other words it can be stated that the output from decimation free directional filter bank is directionally orthogonal to the others. From the above discussion it can be deduced that our proposed system works better if the input image contains directional information. The proposed system takes a two dimensional gray scale image as an input. As the system is designed for Medical image processing, and we know that most of the Medical images are gray scale, that is the reason, the system takes gray scale images. It decomposes the input image into its global directional features. The final enhanced image is reconstructed by choosing pixels having large block energy.

Table of Contents

List of Figures

Chapter-1

INTRODUCTION

1. INTRODUCTION

Image processing systems which have directional sensitivity are popular in a variety of application areas. Systems which are composed of a bank of filters with wedge-shaped passbands are used in robotics, computer vision [1, 2], seismology [3-6], image enhancement [7], and image compression [8-16]. Image processing systems have also been designed which are based on two-dimensional Gabor filters. These filters also have directional sensitivity and are used in edge detection schemes, angularly adaptive filtering, texture analysis and classification, and orientation analysis [17]. Similarly, beamforming systems used in the processing of propagating waves in dispersive media are also used to separate signals into components with different directions of arrival and/or speeds of propagation. In addition to filter-based systems which have directional sensitivity, transforms with directional sensitivity, such as the Radon transform [18] and the Hough transform [19], are used in edge detection [20], linear feature detection and enhancement [21,22], reconstruction of data from projections, and the analysis and enhancement of multisensor array processing data. All of these various image processing systems fall into category of directional decomposition systems.

Directional analysis methods are applied in numerous 2-D and 3-D signal processing areas. Here some of the recently introduced methods are summarized briefly.

In the motion analysis and tracking area, recursive filters have been explore to extract directional motion parameters from long image sequences [23]. In [24], this directional temporal plane transform method is proposed so that the spatio-temporal image is transformed into a 2-D image on a directional temporal plane. Since object motion is represented by regions of this 2-D image, moving objects can be detected by simple 2-D image processing. Finally in [25], the 3-D continuous wavelet transform is proposed for target tracking.

In the fingerprint area, the majority of approaches are based on bitwise directional analysis. However, several approaches employ filter-based directional analysis. In [26], the directional properties of fingerprints are exploited as input features by computing one-dimensional Discrete Fourier transform (DFT) of the images over selected bands in four and eight directions. In [27], a method for enhancing fingerprint images is based on nonstationary directional Fourier domain filtering. Fingerprints are first smoothed using a directional filter whose orientation is matched everywhere to the local ridge orientation. In [28], the concept of the directional image is introduced and its application to segmentation is presented. The directional image can thought of as an image transform, where each pixel of the image represents a direction of the local gray level uniformity. The statistics derived from the directional image are used for the segmentation of the original image. The method is suited for simple images like fingerprints and other images that consist of only a background and a foreground. The directional image is partitioned into "homogeneous" connected regions according to the fingerprint topology, thus giving a synthetic representation which can be exploited as a basis for the classification in [29].

For shape analysis, two-dimensional edge detection can be performed by applying a suitably selected optimal edge filter in n directions [30]. To reconstruct the surface shape from shading images, it is shown that the local surface orientation is reconstructed from the directional derivatives of the image density in [31], For the second directional derivative edge detector, the smoothing operations are implemented by FIR digital filters [32]. A method based on the directional flow-change concept is proposed for recognizing planar

shapes [33]. In [34], the authors present a precise system for handwritten Chinese and Japanese character recognition, extracting directional element feature (DBF) from each character image. In [35], the authors propose directional erosions, which effectively implement a thinning algorithm and which they generalize to higher dimensions. To extract words from printed documents that have stray marks, the authors of [36] apply morphological operations based on multiple direction projection planes and skeleton images.

In medical image processing, the authors in [37] propose a directional filter for eliminating noise in MRI images. An image processing method for improving the quality of MRI images is proposed in [38]. The directions of various structural elements such as edges are extracted, and a directional adaptive filter is proposed as a one-dimensional smoothing process in the detected directions. In [39], the quantification of percent diameter stenosis in digital coronary arteriograms of low spatial resolution is considered by using the directional low-pass filter (DLF) developed to suppress quantum noise by averaging image intensity in a direction parallel to this vessel border. For chest X-ray images [40], a new filter is developed for enhancement of abnormal shadows, which is a combination of second-order difference filters wit) variable directions through minimum-value operation. It is shown that introducing oriented smoothness constraints results in a novel class of active contour models for segmentation. Its efficacy is further demonstrated on 2D MRI sequences [41].

One interesting area for directional analysis is color image processing. Several papers appear on this topic [41-44]. Processing of color image data using directional information has received increased attention lately due to the introduction of the vector directional filters. These rank-ordered type filters use the direction of color vectors to enhance, restore, and segment color images. This is very important in the case of color images, where the vector direction signifies the chromaticity of a given color. A. review of the theory of angular statistics along with some new theoretical results is presented in [45]. An approach for detecting edges in color images is discussed in [46].

There are many other interesting application areas for directional analysis. In [47], sonar images of the seafloor are classified by a sonar process on image texture directionality. The authors of [48] discuss automatically digitizing graphical topographic maps using directional analysis to extract important features. And it [49], a new indexing technique for image retrieval is introduced that calculates the histogram of the directional detail content in a given image. Finally, in image compression, directional information is used with other image compression scheme as in [50-52].

All of these examples illustrate the widespread use of directional filtering in signal processing applications, and serve as potential markets for the contribution, introduced in this thesis.

In general, filter based techniques result in decomposition where each band generated contains directional components which have a wide range of angular orientations. Such systems have a low-directional-resolution. The transform-based techniques result in a narrow range of angular orientations per component and are thus high-directional-resolution systems. In this thesis, a new framework for the directional decomposition of images is presented which is based on the theory of multidimensional multirate filter banks. In this chapter, some of the motivations and previous method for directional decompositions are discussed. The emphasis of the thesis is the application of multirate filter bank theory to the design of directional decomposition systems for Medical Image Enhancement. There are some limitations from which the existing directional decomposition systems suffer. Namely, the

existing directional decomposition systems do not, in general, allow for exact recovery of the input signal from the directional components. Furthermore, if the input signal is finite in extent, the representation of the signal in terms of its directional components can require an increased number of sample points than did the original input signal. Fortunately, these issues --exact reconstruction and information increase-- are ones which have been addressed in the multirate filter bank literature. Hence, the multirate filter bank framework allows for these limitations to be conveniently addressed. In addition, the union of these two techniques --directional decomposition and subband decomposition via multirate filter banks-- allows for many of the existing directional decomposition systems to be viewed using a single theoretical framework. Furthermore, the directional filter banks described in this thesis have applications in many areas. This greatly increases the scope of possible applications for multirate filter banks.

Subsection 1.1 briefly introduces various methods for directional analysis proposed in the past and at the end, Angiogram Images are briefly described in Subsection 1.2.

1.1 Previous Approaches

1.1.1 Bitwise Directional Analysis

This concerns only local directionality generated by local pixel computation. Therefore, cost of the processing is performed with a windowing function. It can be implemented easily and customized for given problems to provide local directional information despite noise sensitivity. This category of directional analysis is used primarily on binary imagery.

1.1.2 Filter-Based Decompositions

For filter-based methods, a set of filters is applied to a given image to extract directional information. This method is more robust against noise than bitwise operators, but most of them use non-separable 2-D filter prototypes. Two dimensional Gabor filtering is a typical example [53]. Other examples that appear in the literature are the two-dimensional continuous wavelet transforms [54], and the steerable filters [55].

1.1.3 Transform-Based Analysis

Transform-based methods can have more directional resolution than filter-based analysis approaches, often with higher complexity than a filter-based method. The Radon and Hough transforms are typical example [56].

1.2 Angiogram Images

Angiography is a major application in an area called contrast enhancement radiography. Historically, angiographic imaging (called Angiograms) has been the standard for the cardiovascular imaging. In angiography, a catheter is inserted into the body and positioned within the anatomical region understudy. A contrast agent is injected through the catheter, and X-Ray projection imaging is used to track the flow of contrast through the anatomy. Typical examples of angiogram images are shown in Figure 1.1.

Figure 1.1 Angiogram Image of Heart

Chapter-2

NOTATIONS & BACKGROUND MATERIAL

2.1 Image

A monochrome image is a 2-dimensional light intensity function f(x,y), where x and y are spatial coordinates and the value of f at (x,y) is positional to the brightness of the image at that point. If we have a multicolor image, f is a vector, each component of which indicates the brightness of the image at point (x,y) at the corresponding color band.

A digital image is an image f(x,y) that has been discretized both in spatial coordinates and in brightness. It is a represented by a 2-dimensional integer array, or a series of 2-dimensional arrays, one for each color band. The digitized brightness value is called the gray level value.

Each element of the array is called a pixel or a pel derived from the term "picture element". Usually, the size of such an array is a few hundred pixels by a few hundred pixels and there are several dozens of possible different gray levels. Thus, a digital image looks like this:

$$\mathbf{f(x,y)} = \begin{pmatrix} f(0,0) & f(0,1) & \cdots & f(0,N-1) \\ f(1,0) & f(1,1) & \cdots & f(1,N-1) \\ \vdots & \vdots & & \vdots \\ f(M-1,0) & f(M-1,1) & \cdots & f(M-1,N-1) \end{pmatrix}$$

2.2 Image Types

Following are the four major categories of images:

- Intensity Images
- Binary Images
- Indexed Images
- RGB Images

2.2.1 Intensity Images

An intensity image is a data matrix whose values have been scaled to represent intensities. Intensity image looks like as shown in Figure 2.1. When the elements of an intensity image are of class uint8, or class unit16, they have integer values in the range [0,255] and [0, 65535], respectively. If the image is of class double, the values are floating-point numbers. Values of scaled, class double intensity images are in the range [0, 1] by convention.

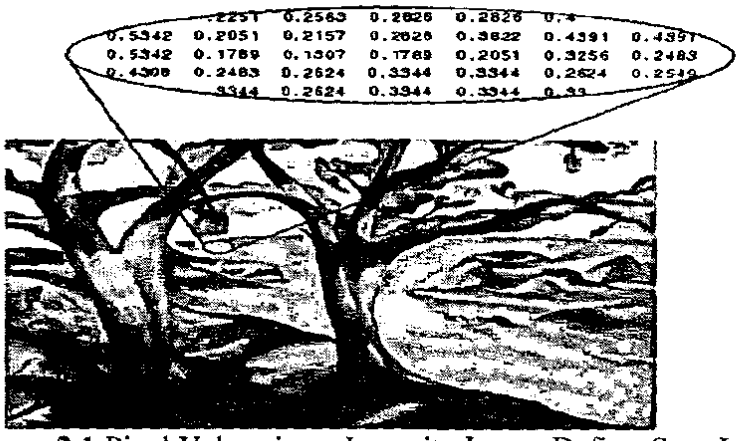

Figure 2.1 Pixel Values in an Intensity Image Define Gray Levels

2.2.2 Binary Image

Binary image is a logical array of 0s and 1s. In binary images usually object is represented in white and background in black color. Binary image looks like as shown in Figure 2.2.

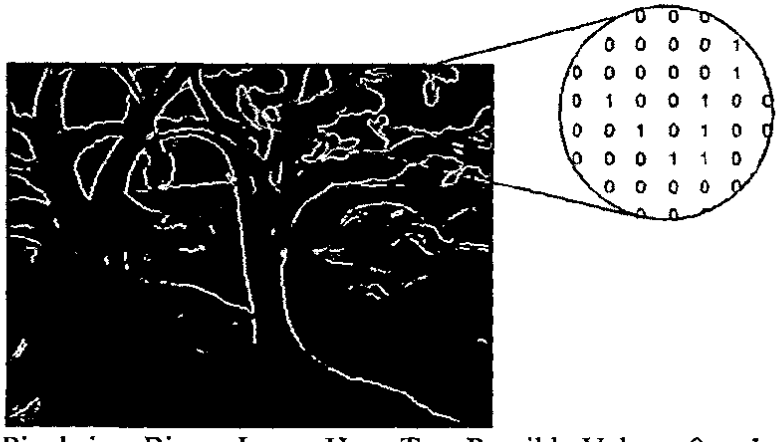

Figure 2.2 Pixels in a Binary Image Have Two Possible Values: 0 or 1

2.2.3 Indexed image

An indexed image has two components: a data matrix of integers, X, and a colormap matrix, map. Matrix map is an m X 3 array of class double containing floating-point values in range [0, 1]. The length, m, of the map is equal to the number of colors it identifies. Each row of map specifies the red, green, and blue components of a single color. An index image uses "direct mapping" of pixel intensity values to color map values. The color of each pixel is determined by using the corresponding value of integer matrix X as a pointer into map. If X is of class double, then all of its components with values less than or equal to 1 point to the first row in map, all components with value 2 point to second row, and so on. If X is of class uint8 or uint16, then all components with value 0 point to the first row in map, all components with value 1 point to the second row, and so on. Index image is shown in Figure 2.3.

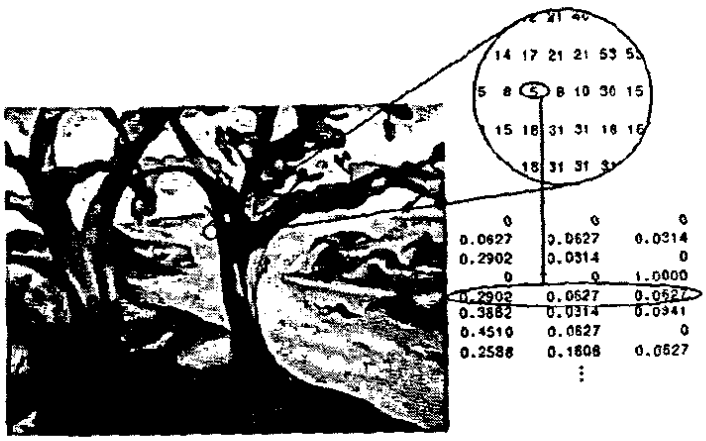

Figure 2.3 Pixel Values Are Indices to a Colormap in Indexed Images

2.2.4 RGB Image

An RGB color image is an M x N x 3 array of color pixels. Where each color pixel is a triplet corresponding to the red, green, and blue components of an RGB image at a specific spatial location. An RGB image may be viewed as a "stack" of three gray-scale images that, when fed into the red, green, and blue inputs of color monitor, produce a color image on the screen. By convention, the three images forming an RGB color image are referred to as the red, green, and blue component images. The data class of the component images determines their range of values. If an RGB image is of class double, the range of values is [0, 1]. Similarly, the range of values is [0, 255] or [0, 65535] for RGB images of class uint8 or uint16, respectively. The number of bits used to represent the pixel values of the component images determines the bit depth of an RGB image. Figure 2.4 shows RGB image.

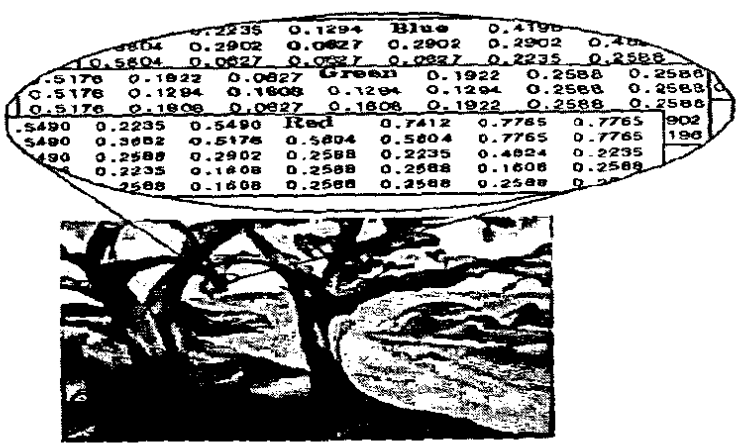

Figure 2.4 The Color Planes of an RGB Image

2.3 Image Processing

Image processing has been developed in response to the three major problems concerned with images:

- Image digitization and coding to facilitate transmission, printing and storing of images.
- Image enhancement and restoration in order, for example, to interpret more easily images of the surface of other planets taken by various probes.
- Image segmentation and description and an early stage in Machine Vision.

2.3.1 Image Enhancement

Enhancement is to process an image so that the result is more suitable than the original image for a specific application. This process includes adjustment of brightness or contrast, edge detection an edge sharpening, removal of small irrelevant features (termed noise), and adjustment for background intensity variation.

Image enhancement can only improve and clarify information that is already present in an image: it cannot recover what was never there in the first place! Therefore, at the stage of image capture it is essential to seek the best image quality by suitable sample preparation, adjustment of instrumentation, choice of lighting, etc. We state this as a principle:

"It is better, and often easier, to improve quality at the stage of image capture rather than by subsequent processing."

But in real life problem it's not the case, for example, in angiographic image it is not possible to have ideal light conditions. So in these cases we need a post processing (image enhancement) on the images to improve their quality. Image enhancement transforms a given image to a new image, where pixel intensities in the new image are function of the pixel intensities in the original image.

Image enhancement approaches fall into two broad categories:

- Spatial Domain Enhancement
- Frequency Domain Enhancement

2.3.1.1 Spatial Domain Enhancement

The term spatial domain refers to the image plane itself, and approaches in this category are based on direct manipulation of pixels in an image. The term spatial domain refers to the aggregate of pixels composing an image. In Figure 2.5, one of spatial domain images is shown.

Figure2.5 Spatial-domain image.

Spatial enhancement relies on changing the gray scale representation of pixels to give an image with more contrast for interpretation. It applies the same transformation function to all pixels with a given gray scale in an image. However, it does not take full advantage of human recognition capabilities even though it may allow better interpretation of an image by a user. Interpretation of an image includes the use of brightness information, and the identification of features in the image. Spatial enhancement is also the mathematical processing of image pixel data to emphasize spatial relationships. This process defines homogeneous regions based on linear edges.

Spatial enhancement techniques use the concept of spatial frequency within an image. Spatial frequency is the manner in which gray-scale values change relative to their neighbors within an image. If there is a slowly varying change in gray scale in an image from one side of the image to the other, the image is said to have a low spatial frequency. If pixel values vary radically for adjacent pixels in an image, the image is said to have a high spatial frequency.

Spatial enhancement involves the enhancement of either low or high frequency information within an image. Algorithms that enhance low frequency image information employ a "blurring" filter (commonly called a low pass mask) that emphasizes low frequency parts of an image while de-emphasizing the high frequency components. The enhancement of high frequency information within an image is often called edge enhancement. It emphasizes edges in the image while retaining overall image quality. Some of the spatial domain enhancement methods are given below:

- Gray Scale Manipulation
- Histogram Equalization
- Image Smoothing
- Image Sharpening
- High Boost Filtering

2.3.1.2 Frequency Domain Enhancement

The second broad category of image enhancement is the frequency domain enhancement. Filtering in the frequency domain is particularly effective. Selected frequencies can be filtered in or out. High-pass, low-pass and band-reject filters can easily be implemented. The resulting filtered images do not lose as much information as some of the simpler filtering methods. A particularly good example of such selective filtering is if the power spectrum of the noise in an image is known then it can be removed very effectively with minimal impact on the remainder of the image information content. Frequency domain enhancement involves frequency domain transforms. These transforms change an image from its spatial domain form of brightness to a frequency domain of fundamental frequency components. Because the Fourier transforms maps from the spatial domain to the frequency domain, it is natural to use it for detecting **texture** within an image. Textures are areas of an image which have similar elements which repeat in space, although not necessarily with strict regularity. One of the most commonly used is the Fast Fourier Transform (FFT).

The two-dimensional FFT is a mapping of image pixel values into the image *spatial* frequency space. By performing a two-dimensional FFT on an image, we are creating a two-dimensional map of all spatial frequencies within an image. Every output image pixel, as a result of the FFT, has a real and an imaginary number associated with it. The real pixels form an image that may be thought of as the magnitude of the spatial frequencies present in an

image, and the imaginary pixels form and image representing the phase of the spatial frequencies. The highest spatial frequency that can be present in an image is equivalent to every other pixel having black-and-white values. Therefore, if an x and y axis are used to represent spatial frequencies on a plot, the width of the plot will, at most, be the total width of the image divided by 2.

A useful way to display the spatial frequencies within an image is by using a *star diagram* representation of the magnitude of the complex two-dimensional FFT. In such a diagram, the lowest frequency component within an image (the average value of the image) is shown at the center of the diagram, and spatial frequencies increase pixel by pixel away from the center of the diagram. The brightness of the pixels at each x and y position relate to the relative occurrence of that spatial frequency in the original image. Spatial frequencies only exist up to the Nyquist frequency in the x and y directions, so the display is reflected about the center of the diagram. Furthermore, information in the +x and +y direction from the diagram center duplicates information in the -x and -y direction of the diagram. An example of frequency domain image is shown in Figure 2.6.

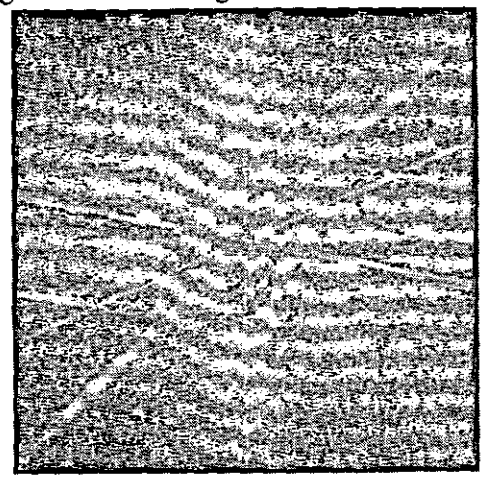

Figure 2.6 Frequency Response of the Cameraman

A two-dimensional FFT image may be useful in itself in developing an understanding of individual images, but Fourier Transform theory lends itself to image enhancement techniques as well. The ability to produce a two-dimensional FFT star diagram is known as the running of a *forward FFT*. This process can also be thought of as transforming an image from the normal *time domain* to the *frequency domain*. The resulting frequency domain image may be transformed back to the time domain by performing an *inverse two-dimensional FFT*. If no changes are made to the spatial frequency complex image, the inverse two-dimensional FFT will provide the exact same image that we began with. Fourier theory, however, tells us that we may perform certain operations, called *convolutions*, in the frequency domain that may enhance the image after the inverse two-dimensional FFT. These frequency convolutions are not to be confused with the kernel convolutions of spatial domain.

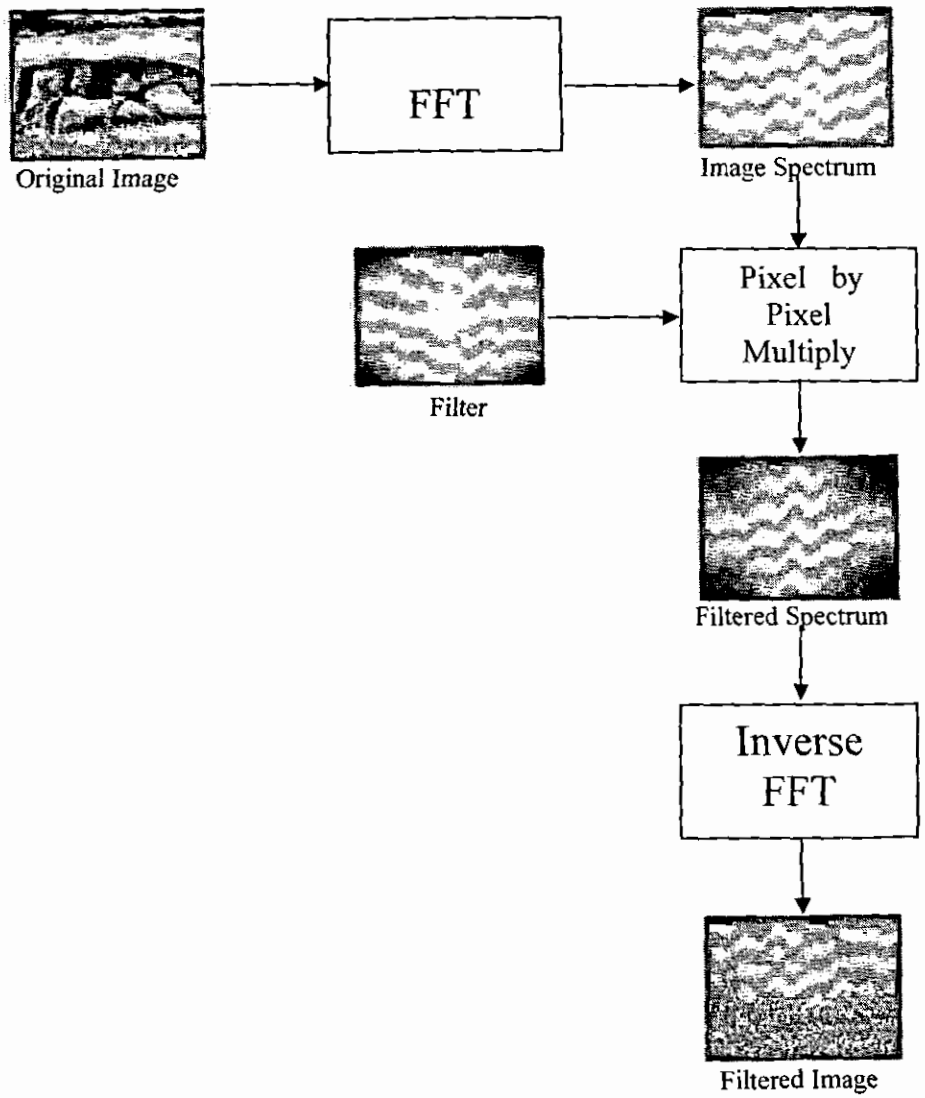

Figure 2.7 Block diagram of frequency domain filtering

A convolution in the frequency domain is a simple multiplication of an image with mask that may be arbitrarily designed by a user, multiplied by the complex frequency domain image. The resultant frequency domain image is then run through the inverse two-dimensional FFT process to yield a transformed image. This process of convolution in the frequency domain is extremely valuable in the spatial enhancement of image data. Block diagram of frequency domain filtering is shown in Figure 2.7.

We may perform the operations of spatial domain convolution in a more complete and flexible manner. In addition, there are some functions that may be done by frequency convolution that as yet have not been achieved by spatial domain convolution, such as *noise removal* from an image, and *image restoration*. Some of the frequency domain enhancement methods are given below:

- Low Pass Filtering

- High Pass Filtering
- Band Pass Filtering
- Homomorphic Filtering

2.4 Filters

Filters are used to stop or pass selected frequencies of an image. There are many types of filters but most are a derivation or combination of four basic types:

- Lowpass Filters
- Highpass Filters
- Bandpass Filters
- Bandstop or Notch Filter

The Bandpass and Bandstop filters can be created by proper subtraction and addition of the frequency responses of the Lowpass and Highpass filter. Figure 2.8 shows the frequency response of these filters.

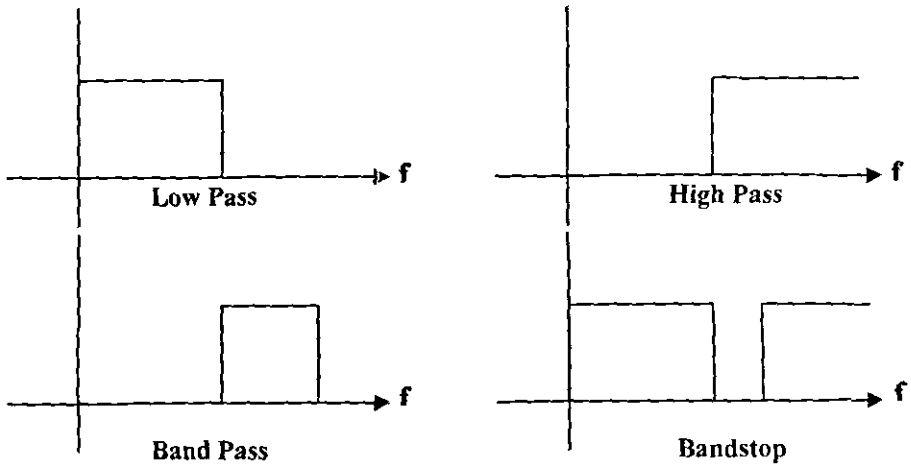

Figure 2.8 Frequency response of 1-dimensional low pass, band pass and band stop filters.

The low pass filter passes low frequencies while attenuating the higher frequencies. High pass filters attenuate the low frequencies and pass higher frequencies. Bandpass filters allow a specific band of frequencies to pass unaltered. Bandstop filters attenuate only a specific band of frequencies. To better understand the effects of these filters, imagine multiplying the function's spectral response by the filter's spectral response. There is one problem with the filters shown in Figure 2.8. They are ideal filters. The vertical edges and sharp corners are non-realizable in the physical world. Although we can emulate these filter masks with a computer, side effects such as blurring and ringing become apparent.

2.5 Filter Bank

An analysis-synthesis filter bank is an array of selective filters designed to allow specific information to be extracted in the analysis section and reconstructed in the synthesis section. Figure 2.9 shows a filter bank structure. Each of the subbands the analysis section extracts frequency components based on the associated frequency partition map as in Figure 2.10.

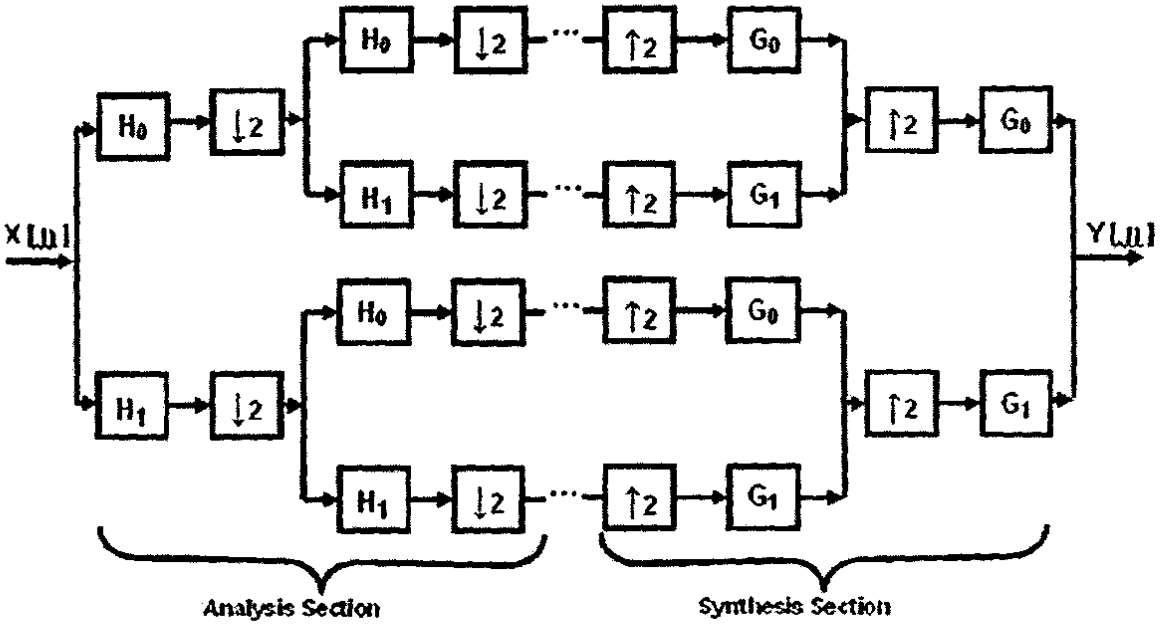

Figure 2.9 A typical implementation of a tree-structured filter bank.

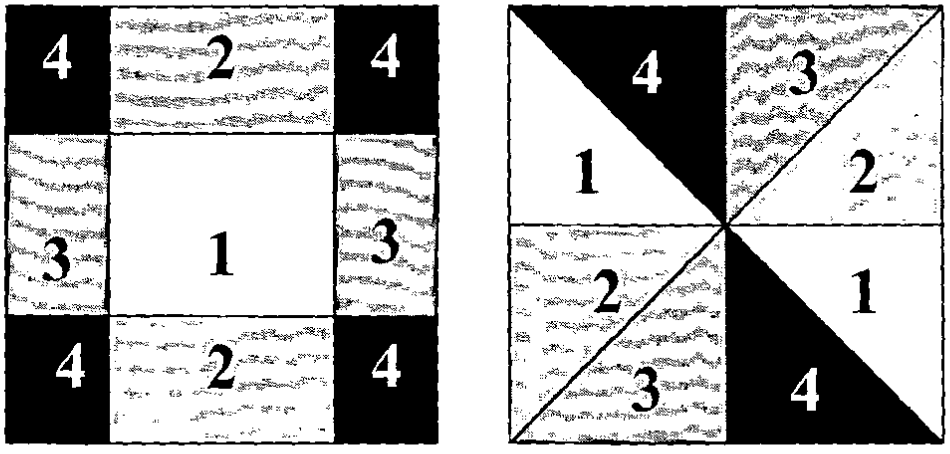

(a) (b)

Figure 2.10 Example of frequency partition maps for filter banks. Each of the subbands extracts the assigned, frequency component, (a) Typical filter bank case. (b) Directional filter bank case.

The subbands in the synthesis section perform the duel operations enabling perfect reconstruction. In image compression, which is typical application area of filter banks, using both analysis and synthesis system are essential. In other applications, it is often only necessary to use the analysis or synthesis bank. As shown in Figure 2.9, the component of the analysis section are the downsampler ↓2 and the analysis filters H_0 and H_1 the synthesis section, the upsampler ↑2 and the synthesis filters G_0 and G_1 are used. A typical choice for the downsampler and the upsampler is a row-wise or column wise down/up sampler. For the filter prototypes used in filter banks, FIR filters a commonly chosen [57, 58].

There are many kinds of filter banks based on the various possible configurations, e.g., the components used, the way they are connected, and so on. Most filter banks are designed to be maximally decimated, perfectly reconstructing, and separable. A maximally decimated filter bank has to have the minimum number of pixel in each subband in the analysis section and should allow for perfect reconstruction (or near-perfect reconstruction) in the synthesis section. In other words, the total number of pixels in an input image should equal the total number of pixels over all the subband images at any stage of the analysis or synthesis system. Given a 1-D filter whose length is M, and M × M 2-D filter, for N × N image, separable filtering can yield M/2 times fewer multiplications per pixels than non-separable 2-D filtering.

2.6 Quincunx Resampling

"A resampling matrix is a square matrix whose entries are all integers and whose determinant is non-zero. The dimension of the matrix is equal to the dimension of the signal on which it is operating."

"A Diagonal sampling is sampling that is done by a diagonal resampling matrix whose elements are 2" for a positive integer n. Note that the name diagonal results from the fact that the matrix is diagonal, not from the sampling direction."

"A generalized quincunx resampling matrix is a resampling matrix whose entries are ±1, and determinant is 2".

There are eight quincunx resampling matrices, depending on their sampling lattice vectors [59], as provided in equation (2.13). Since Q_1 is the most commonly used quincunx resampling matrix, we will use it by default unless specifically mentioned otherwise.

$$Q_1 = \begin{pmatrix} 1 & 1 \\ -1 & 1 \end{pmatrix} \qquad Q_2 = \begin{pmatrix} 1 & -1 \\ 1 & 1 \end{pmatrix}$$

$$Q_3 = \begin{pmatrix} -1 & 1 \\ 1 & 1 \end{pmatrix} \qquad Q_4 = \begin{pmatrix} 1 & 1 \\ 1 & -1 \end{pmatrix}$$

$$Q_5 = \begin{pmatrix} -1 & -1 \\ 1 & -1 \end{pmatrix} \qquad Q_6 = \begin{pmatrix} -1 & 1 \\ -1 & -1 \end{pmatrix}$$

$$Q_7 = \begin{pmatrix} 1 & -1 \\ -1 & -1 \end{pmatrix} \qquad Q_8 = \begin{pmatrix} -1 & -1 \\ -1 & 1 \end{pmatrix} \qquad (2.6.1)$$

2.6.1 Quincunx Downsampling

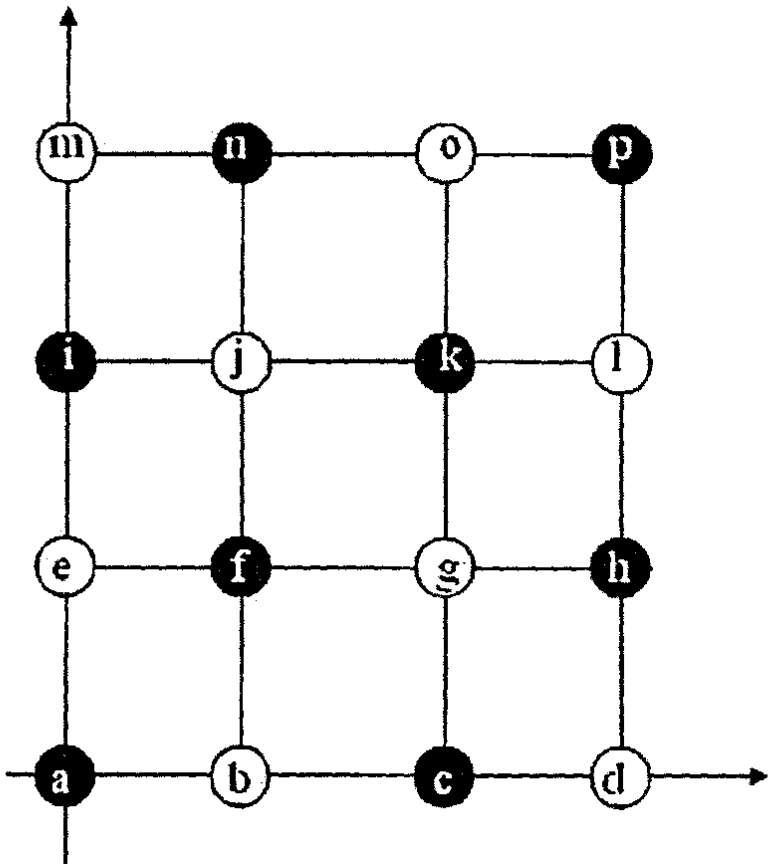

(a)

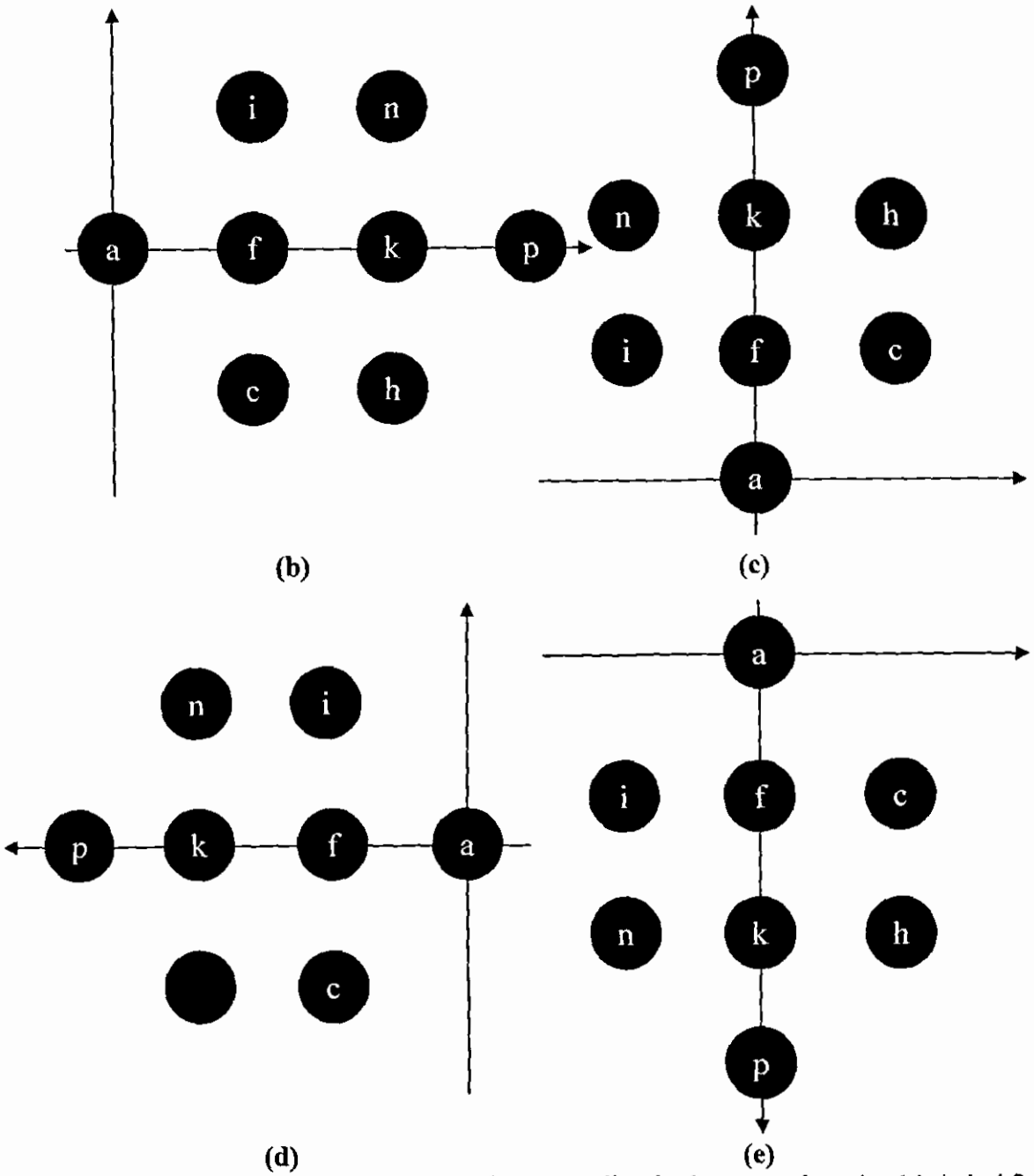

Figure 2.11 Illustration of Qunicunx downsampling in the space domain; (a) A 4×4 2-D input. Quincunx downsampled output by (b) Q_1 (c) Q_2 (d) Q_3 and (e) Q_4.

2.6.2 Quincunx Upsampling

Like other typical filter banks, the synthesis system of the directional filter bank the duel of the analysis system. Therefore, the role that quincunx upsampling plays for the DFB can be understood in a similar way.

2.7 Diamond-conversion Resampling

"A unimodular matrix is a resampling matrix whose determinant is ±1. Note that the inverse matrix of a unimodular matrix is also unimodular."

One of attractive advantages of the directional filter bank is the fact that it can be implemented by only one filter prototype, which is a strong motivation to use unimodular matrices in a DFB. Because of the structure of a directional filter bank, as we will see in Section 2.8, five different filter prototypes need to be designed, shown in Figure 2.12. By using carefully designed unimodular matrices, the filter design process can be reduced to require only one filter prototype $H_0(\omega)$. This results from the fact that a unimodular matrix can transform a given frequency component arrangement. Therefore, if the unimodular matrices that change frequency components from $R_0^i(\omega)$ to $H_0^i(\omega)$, for i = 1, 2, 3, and 4, respectively, are found, then the systems in Figure 2.13 (a) and (b) are identical and only one filter prototype $H_0(\omega)$ is needed. Therefore, $H_0(\omega)$ can replace the four remaining filters $R_0^i(\omega)$ by using unimodular matrices.

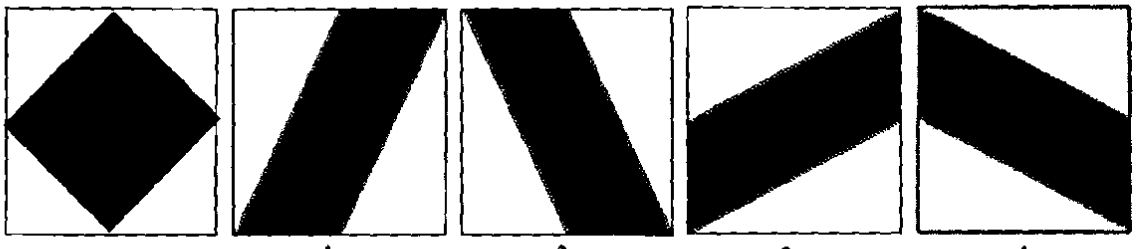

Figure 2.12 Five passbands for directional filter banks.

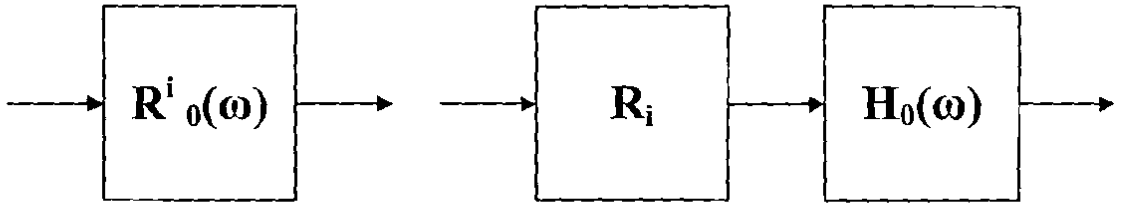

Figure 2.13 Two identical structures in a directional filter bank (DFB). (a) Using $R_0^i(\omega)$ alone and (b) a unimodular matrix with $H_0(\omega)$.

"A *diamond-conversion* matrix is a unimodular matrix that can change the frequency components from the four parallelograms $R_0^i(\omega)$, for i =1, 2, 3, and 4, to the diamond shape $H_0(\omega)$", as shown in Figure 2.12.

Therefore, the $H_0(\omega)$ with R_i, i = 1, 2, 3, 4, replaces $R_0^i(\omega)$, i = 1, 2, 3, 4 which simplifies the system implemented by only one filter prototype.

2.8 Overview of 2^n-band DFB

In the remaining text, we concentrate primarily on the analysis section of the DFB's since the synthesis section can be understood as the duel system of the analysis section.

2.8.1 The Two-band DFB

As shown in Figure 2.14, A two-band DFB has a modulator, a pair of diamond filters $H_0(\omega)$ and $H_1(\omega)$, and quincunx sampling matrix. The directional frequency components labeled as in Figure 2.14 can be successfully extracted by the two-band DFB structure.

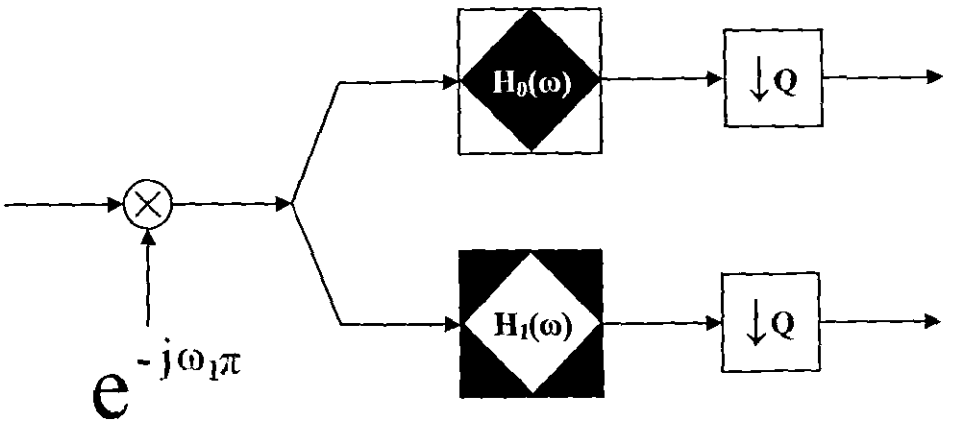

Figure 2.14 A two-band DFB structure with frequency partition maps.

2.8.2 The Four-band DFB

A four-band DFB is composed of two-band DFB's arranged in a tree structure, as shown in Figure 2.15. After the modulator, the constituent frequency components are shifted, resulting in a diamond-like shape. Then, via the diamond filters, $H_0(\omega)$ and $H_1(\omega)$, each of the four frequency regions is filtered and followed by a quincunx downsampler. By cascading another set of two-band DFB's at the ends of the first two-band DFB, a four-band directional decomposition is achieved as shown in Figure 2.15.

2.8.3 The 2^n-band DFB

The two-band and four-band DFB's lead to 2^n-band extensions that can be useful in practical applications. To expand to eight bands, we apply a third stage in cascade. With an input whose directional frequencies ate labeled as in Figure 2.16 (a), an eight-band DFB generates the eight subband outputs shown in Figure 2.16 (b). Note that each of the subband images is smaller than the original input, which is obvious for the maximally decimated DFB. Figure 2.17 contains more details for the eight-band DFB. First, note that the shape of each of the four input frequency components is now a parallelogram, which is the reason we need four additional filter passbands, as in Figure 2.12. Inserting four diamond-conversion matrices allows us to use the diamond filters, $H_0(w)$ and $H_1(w)$, again. Also note that there is no longer a modulator at this stage.

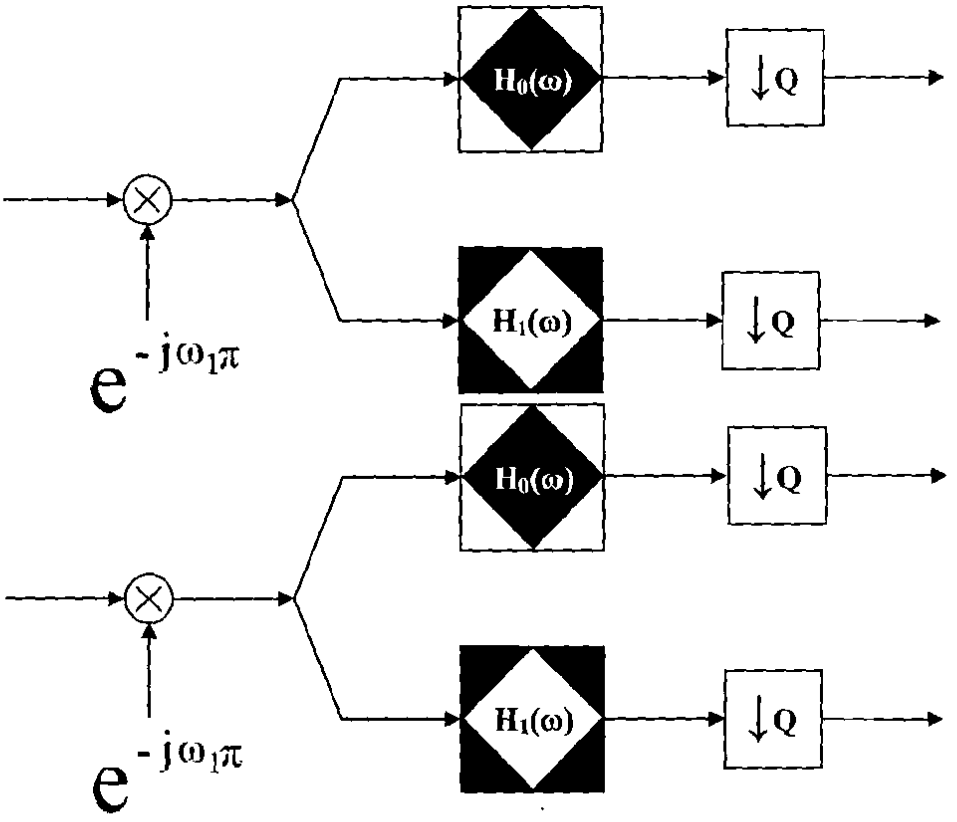

Figure 2.15 A four-band DFB structure with frequency partition maps.

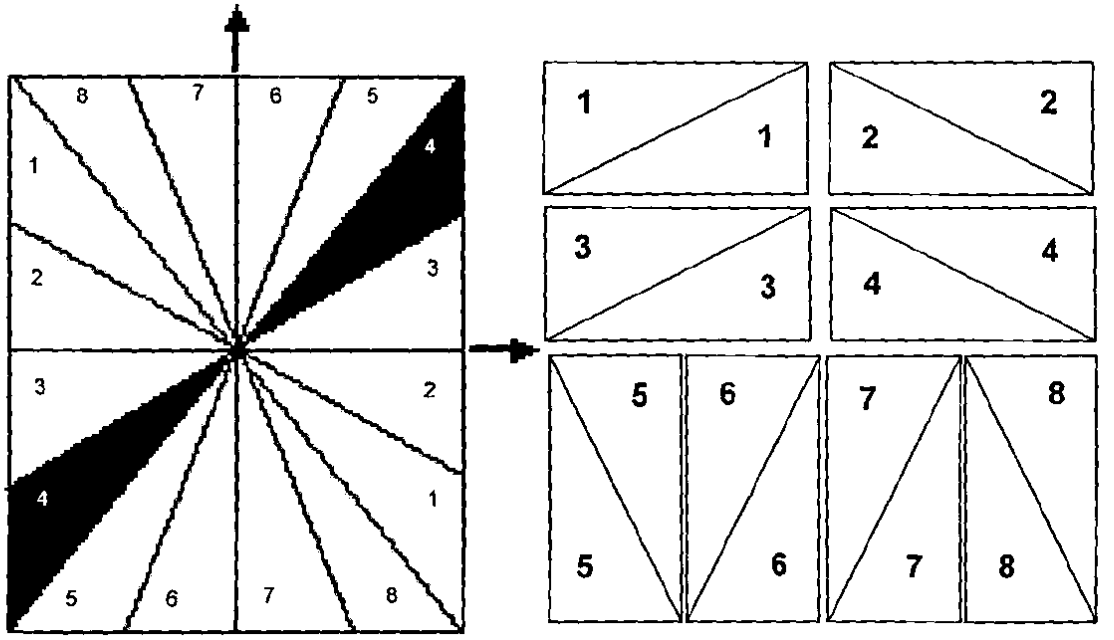

(a) (b)

Figure 2.16 The frequency partition map for an eight-band DFB.(a) Input, (b) Eight subband outputs.

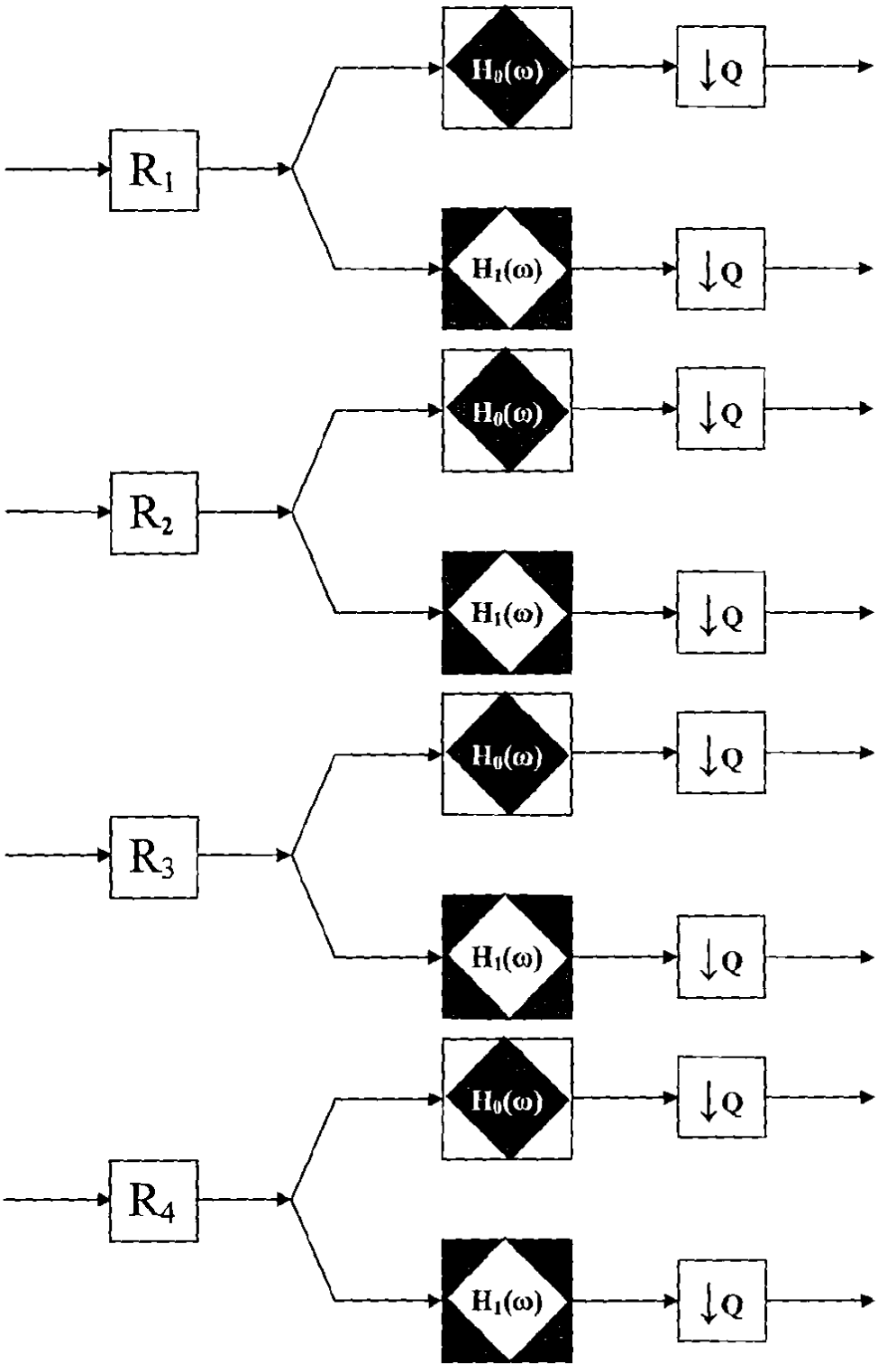

Figure 2.17 An eight-band DFB structure with frequency partition maps.

Chapter-3

PREVIOUS WORK

Among the various approaches for extracting directional information, the DFB has some attractive features that others do not have. Most of the DFB work was pioneered by Bamberger, Smith and Sang [60-62] and most of the background provided in this section was quoted from their work. In [63], they showed that the output of the Radon transform was conceptually identical to the DFB when a large number of bands are used. A non-2^n band DFB for image compression was considered in [60]. Also, the parallel-structured DFB was proposed in [64] to get rid of redundant computation and improve visual information in subbands, in [sang], author proposed a decimated filter bank in which he proposed a technique to remove the frequency scrambling from the output subbands. In this work, a way is proposed to remove the two modulators in the first two stages along with the downsampling matrices from the over all parallel-structured DFB.

As one of the applications for DFB's, a fingerprint image was successfully enhanced based on the perfect reconstruction property of the DFB [60]. Also, DFB's were analyzed from a different and useful viewpoint in [65]. They provided an overall viewpoint to analyze directional filter banks.

3.1 Frequency Scrambling

Despite the successful directional frequency decomposition using the efficient structure of the DFB, the main drawback of directional filter banks is that the decomposed subband outputs are distorted visually from the original input image as illustrated in Figure 3.1 (b). Sang developed [62] a system in which he proposed the idea of removing the frequency scrambling. In this section we will discuss the idea of elimination of frequency scrambling proposed by Sang.

Even if each of the sub-bands contains its corresponding directional frequency content in the frequency domain, the subbands are visually distorted in the space domain. Therefore, spatial processing of the subbands for signal processing applications is virtually impossible, although one can still perform pixel-based and energy-based post-processing as described by Bamberger [60]. This spatial subband distortion property has restricted the use of the DFB to a very limited number of image processing applications.

The reason for this drawback is seen in the frequency mappings in Figure 3.2. Comparing the differently shaded regions in Figure 3.2 (a) and (b), we see that the low frequency area is severely misplaced in its subband as shown in Figure 3.2 (b). We refer to this distortion as *frequency* scrambling [62]. The severely misplaced low frequency components generate visually distorted subband images. In [64], another structure for implementing a DFB was proposed so that the resulting subband images would have more intuitive visual information, but it replaced the initial tree-structured DFB's with parallel-structured ones, where each of the subbands filters needs to be designed separately. Thus, it sacrifices computational efficient achieve visualizable subbands.

In the following sections, Section 3.2 to Section 3.4, the previous drawbacks will be removed while all of the structural advantages of DFB's are retained, so is each of the subbands can provide more accurate visual information within a computationally efficient structure. By virtue of the new structure of the DFB, spatial processing of subbands is straightforward and hence the DFB's can have more widespread use.

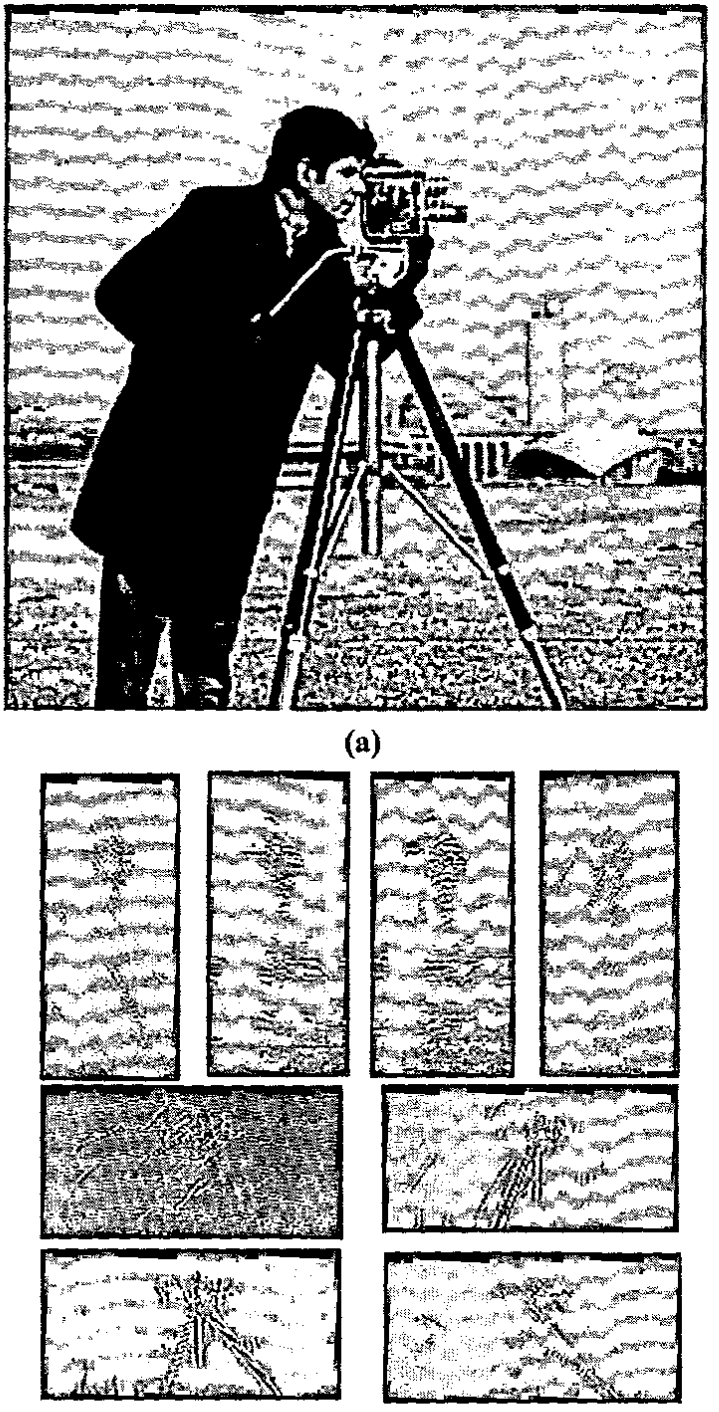

Figure 3.1 Decomposition by the previously proposed directional filter. The original cameraman image, (b) Its decomposed directional subband based on [61].

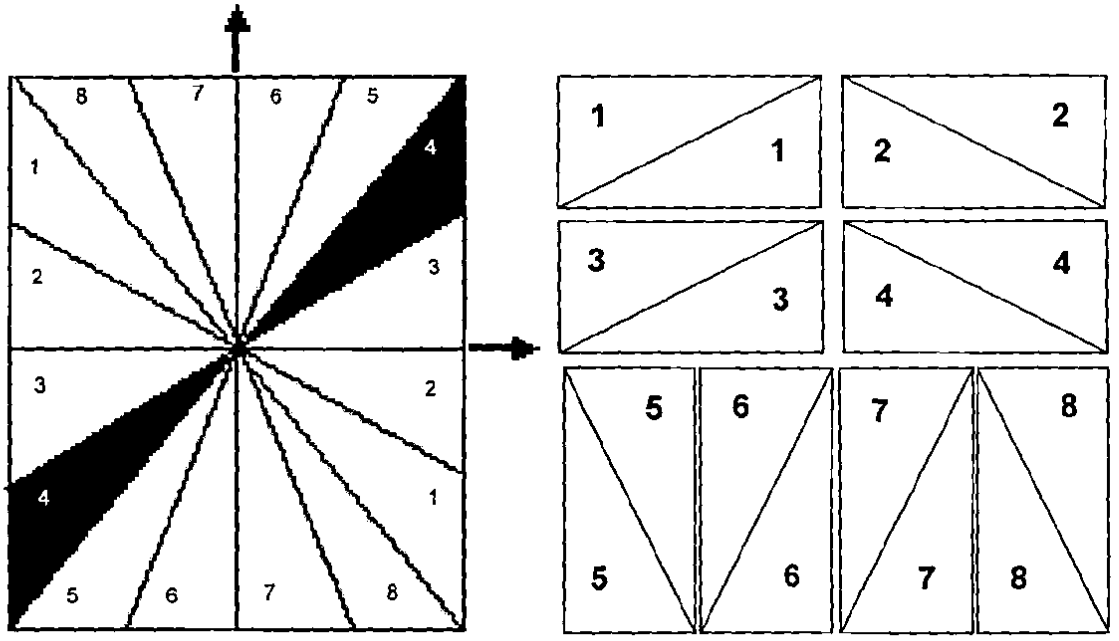

(a) (b)

Figure 3.2 frequency partition map for the eight-band directional filter bank, (a) Directional frequencies of input to be decomposed, (b) Decomposed frequency maps of the eight subbands.

3.2 Visualized Directional Subbands

Frequency scrambling occurred for two reasons. One was because the modulators in first two stages result in significant frequency shifting. However, they were removed easily or *pushed* to the end of the analysis section by using the modulated filter Figure 3.3 (b) as proposed in [64]. The other reason for frequency scrambling was that the overall downsampling matrix was not diagonal, which resulted from the quincunx and the diamond-conversion matrices. Unlike typical diagonal downsampling, quincunx downsampling induces frequency expansion that contains *rotation*. The diamond-conversion matrices after the second stage also skew the frequency components, as shown in Figure 2.17.

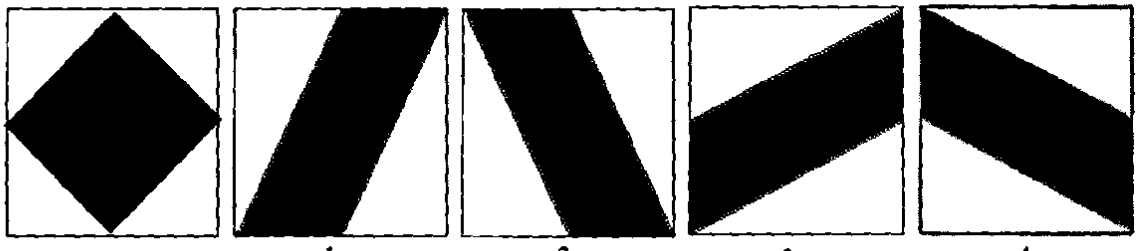

$H_0(\omega)$ $R^1{}_0(\omega)$ $R^2{}_0(\omega)$ $R^3{}_0(\omega)$ $R^4{}_0(\omega)$

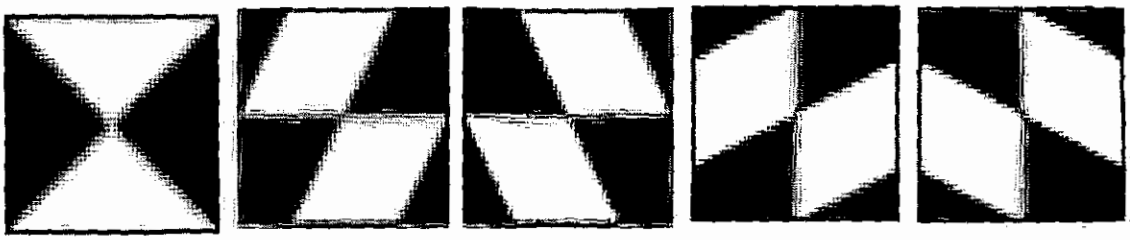

Figure 3.3 Five passbands for directional filter banks, (a) With the modulator; the first two stages, (b) Without the modulators the overall downsampling matrix is not diagonal, which results from the quincunx and the diamond-conversion matrices.

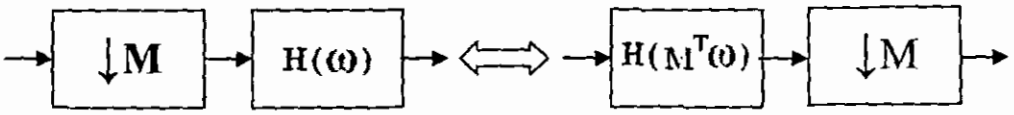

Figure 3.4 The multirate system identity.

For better understanding, note that the tree-structured DFB can be simplified using the multirate system identity in Figure 3.4. By using this identity, all of the sampling matrices can be gathered at the end of the analysis section so that the corresponding overall sampling can be determined easily, and all of the filters at each of the stages can be combined at the beginning of the analysis section.

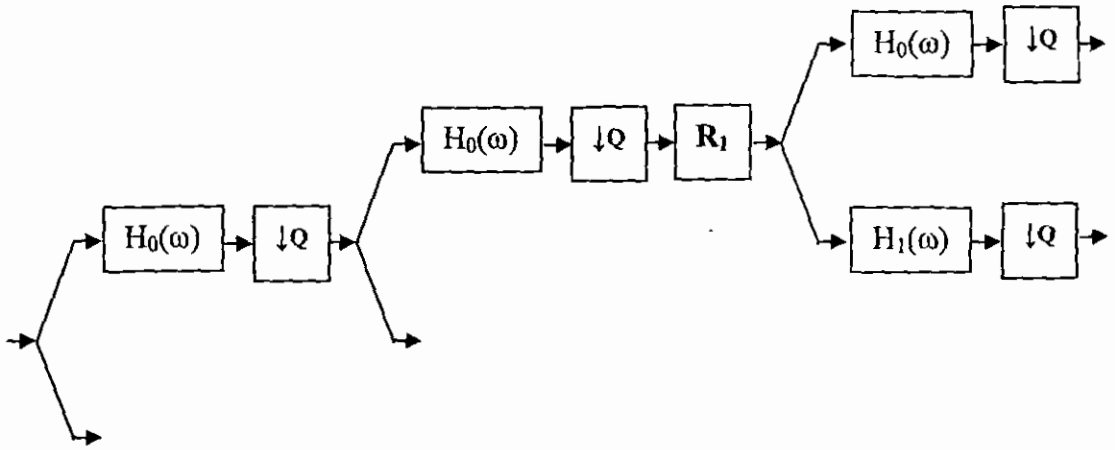

(a)

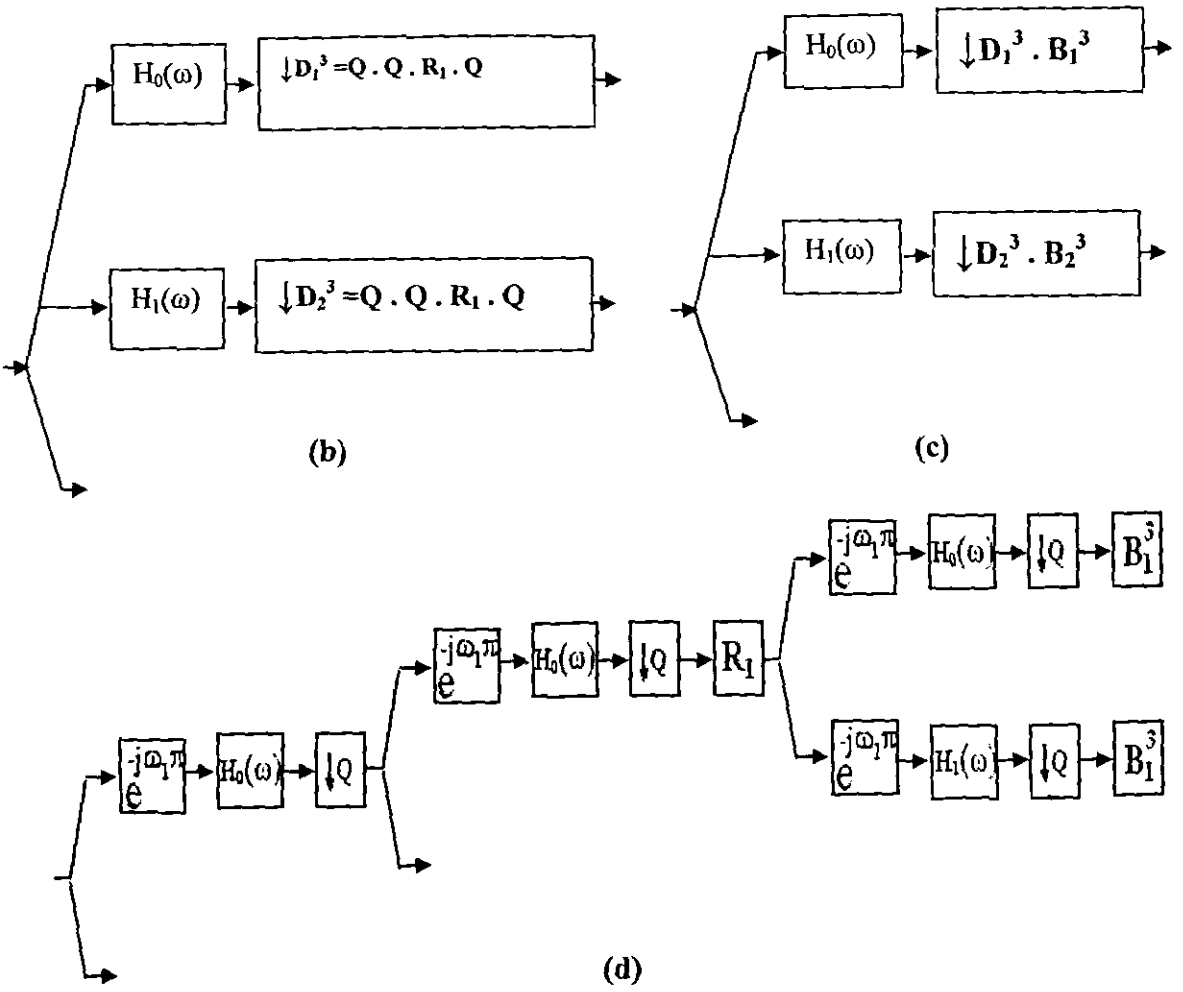

Figure 3.5 Introducing backsampling; (a) Two paths in an eight band DFB. (b) Simplified identical structure. (c) Adding backsampling matrices. (d) Two paths if an eight band DFB with the backsampling matrices.

An example of the eight-band DFB is given in Figure 3.5. Let the overall filter and sampling matrix be $H_i^n(\omega)$ and D_i^n, for i = 1,2,... , 2^n, for the analysis section of the 2^n-band DFB, respectively. As shown in Figure 3.5, all of the filters and resampling matrices in each of the subband paths can be combined into the overall filters H_i^3 (ω) and the overall downsampling D_i^3 matrices, for i = 1,2,... ,8, respectively, as shown in Figure 3.5 (a) and (b). Bamberger [64] used this to implement the visually enhanced parallel-structured DFB. Lin and Vaidyanathan [65] showed that other directional-like separable filter banks can be constructed based on this viewpoint. Sang [62] introduced another unimodular matrix, which is called a backsampling matrix, features in the previously proposed DFB.

Let B_i^n be the backsampling matrix for the i^{th} subband of a 2^n-band DFB. Note that the overall downsampling matrix D_i^3 is non-diagonal. It not only downsamples row-wise or column-wise but also introduce geometrical changes such as rotations and/or skewing. By adding the backsampling matrices B_i^3 as shown in Figure 3.5 (c), the new overall downsampling matrix $D_i^3 \bullet B_i^3$ can return the overall sampling *back* to the typical diagonal

downsampling matrix under which all of the subband images can retain their unscrambled visual information in the space domain. In order to preserve the computational efficiency in the original tree-structured DFB while achieving visualizable subbands simultaneously, we append the backsampling matrices at the end of the analysis section in the tree-structured DFB as shown in Figure 3.5 (d). This is identical to Figure 3.5 (c). Note that the first two stages of the DFB do not use any resampling matrix, only the quincunx matrix which is used twice. The overall sampling for the two quincunx matrices can be viewed as a diagonal resampling matrix followed by a rotation. For example,

$$Q_1 * Q_1 = \begin{bmatrix} 0 & 2 \\ -2 & 0 \end{bmatrix} = \begin{bmatrix} 2 & 0 \\ 0 & 2 \end{bmatrix} \begin{bmatrix} 0 & 1 \\ -1 & 0 \end{bmatrix}.$$

Without the modulators, the first two stages do not generate any frequency scrambling. Therefore, as long as the overall resampling matrix in the third stage is a diagonal downsampling, then an eight-band DFB can be simplified conceptually to just *filtering* by $H_i^3(\omega)$ the *diagonal* downsampling by $D_i^3(\omega) \cdot B_i^3(\omega)$ .Then each subband output can save the visual appearance as the input images as is the case with traditional typical filter.

This idea can be generalized for a 2^n-band analysis section as in Section 3.3. By using the multirate system identity, all of the filters and resampling matrices are combined into $H_i^n(\omega)$ and D_i^n, respectively. A backsampling matrix B_i^n makes the overall downsampling matrix diagonal for the visualizable subband images. This consideration results in appending only one backsampling matrix B_i^n at the end of the 2^n-band analysis section so that the DFB can achieve visualizable subbands with a minimum amount of additional computation. In other words, the sampling over a: of the bands after the second stage should correspond to diagonal downsampling. Therefore, in terms of computational expense, the directional filter banks proposed by Sang [62] here have the exactly the same amount of computation as the initial structure [61] plus the backsampling by the matrix B_i^n.

3.3 Resampling Matrices for the DFB

In this section, all three of the resampling matrices-diamond-conversion, quincunx: and backsampling-used in the DFB are summarized and specified. Since the DFB is a tree-structured filter bank, each of the three resampling matrices can be used repeatedly in the following tree structure.

- **Expanding Tree Structure**

Up to the second stage, the tree can be expanded easily by cascading the blocks as in Figure 2.12. After the second stage, different rules should be applied as follows.

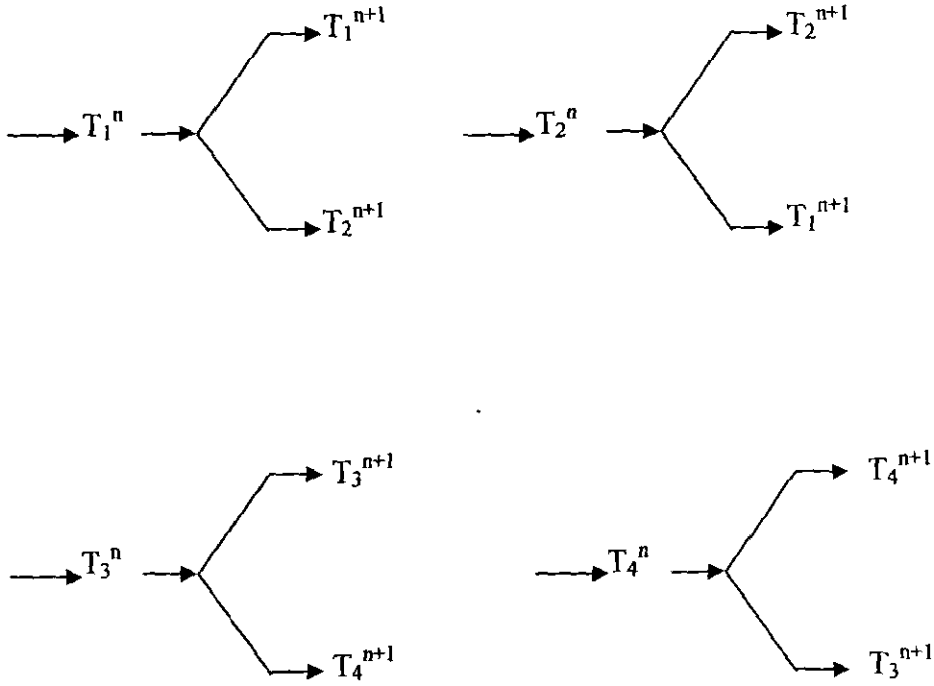

Figure 3.6 Expanding tree for the new DFB.

1. Define a *path type* as T_i^n at the n^{th} stage ($n > 2$), where *i* is called the path type index, that is $i = 1, 2, 3$, and 4. The path type T_i^n determines all of the resampling matrices that are needed at the i^{th} path in the n^{th} stage ($n > 2$).
2. At the second stage, i.e., $n = 2$, T_i^2 is initially assigned to the four subbands in consecutive order.
3. Then at the n^{th} stage, where $n > 2$, the path types for the succeeding stages are determined as shown in Figure 3.6.
4. For any T_i^n, all three resampling matrices, quincunx Q_i^n, diamond-conversion R_i^n, and backsampling B_i^n matrices, can be determined as follows.

- **Quincunx Matrix**

Among the eight quincunx matrices given in Equation (2.13), two of them can be used. For the first two stages, either Q_1 or Q_2 can be used. Note that the overall sampling in the first two stages is $Q_1 \cdot Q_1$ or $Q_2 \cdot Q_2$, which is a clockwise rotation of the image diagonally downsampled, so that a counterclockwise rotation man need to be added after the first two stages. For the remaining stages, in order to keep the simple rule for the expanding tree as in Figure 3.6, for any T_i^n path where n is a positive integer and $i = 1, 2, 3$, and 4, Q_i^n is defined as follows:

$$Q_i^n = \begin{cases} Q_2 & \text{if i is 1 or 4, for all n} \\ Q_1 & \text{if i is 2 or 3, for all n} \end{cases}$$

- **Diamond-conversion Matrix**

Finding the expected diamond-conversion matrices is accomplished by using an appropriate choice of a change of variables matrix ([66], [60]). Based on this method the four diamond-conversion matrices that will be used in this thesis are

$$R_1 = \begin{pmatrix} 1 & 1 \\ 0 & 1 \end{pmatrix} \qquad R_2 = \begin{pmatrix} 1 & -1 \\ 0 & 1 \end{pmatrix}$$

$$R_3 = \begin{pmatrix} 1 & 0 \\ 1 & 1 \end{pmatrix} \qquad R_4 = \begin{pmatrix} 1 & 0 \\ -1 & 1 \end{pmatrix}$$

For any T_i^n, $R_i^n = Ri$ for i = 1, 2, 3, and 4, respectively.

- **Backsampling Matrix**

As mentioned in Section 3.2, for any 2^n-band (n > 2) DFB, B_i^n makes the overall downsampling in the analysis section *diagonal*. The recursive equation for B^n is given below.

$$B_i^n = \left([B^{(n-1)}]^{-1} R_i^n * Q_i^n \right)^{-1} * T_i, \text{ Where}$$

$$T_i = \begin{cases} \begin{pmatrix} 1 & 0 \\ 0 & 2 \end{pmatrix} & \text{If i = 1 or 2} \\ \begin{pmatrix} 2 & 0 \\ 0 & 1 \end{pmatrix} & \text{If i = 3 or 4} \end{cases}$$

$$B_i^3 = R_{5-i}^3, \quad \text{where i = 1 , 2, 3, 4}$$

3.4 New Tree-structured Directional Filter Banks

By using the three newly-defined, resampling matrices, $\mathbf{R}_i^n$, $\mathbf{Q}_i^n$, and $\mathbf{B}_i^n$, the new directional filter bank can separate not only directional frequency components but also directional spatial information in subbands. For instance, the subband outputs for the cameraman image obtained by using the new DFB are given in Figure 3.7. As expected, each of the subbands preserves the spatial information within the subband, in contrast to the earlier work shown in Figure 3.1. Note that each of maximally decimated subbands has the assigned directional spatial information. For instance, in the second subband, one of the tripod's legs is directionally visualized as well as the cameraman's body contour that has a similar direction as the tripod's leg. But, in the fourth subband, most of the directional information that is captured in the second subband is missing, while another tripod's leg is captured. Also notice that the subbands are able to capture more delicate directional differences. For instance, note that the orientation of the portion of the profile from the elbow to shoulder of the cameraman is slightly different from that of the tripod's left leg in the input picture. Comparing the second subband with the eighth subband, the arm contour captured in the latter subband, while the left tripod leg is in the second subband expected.

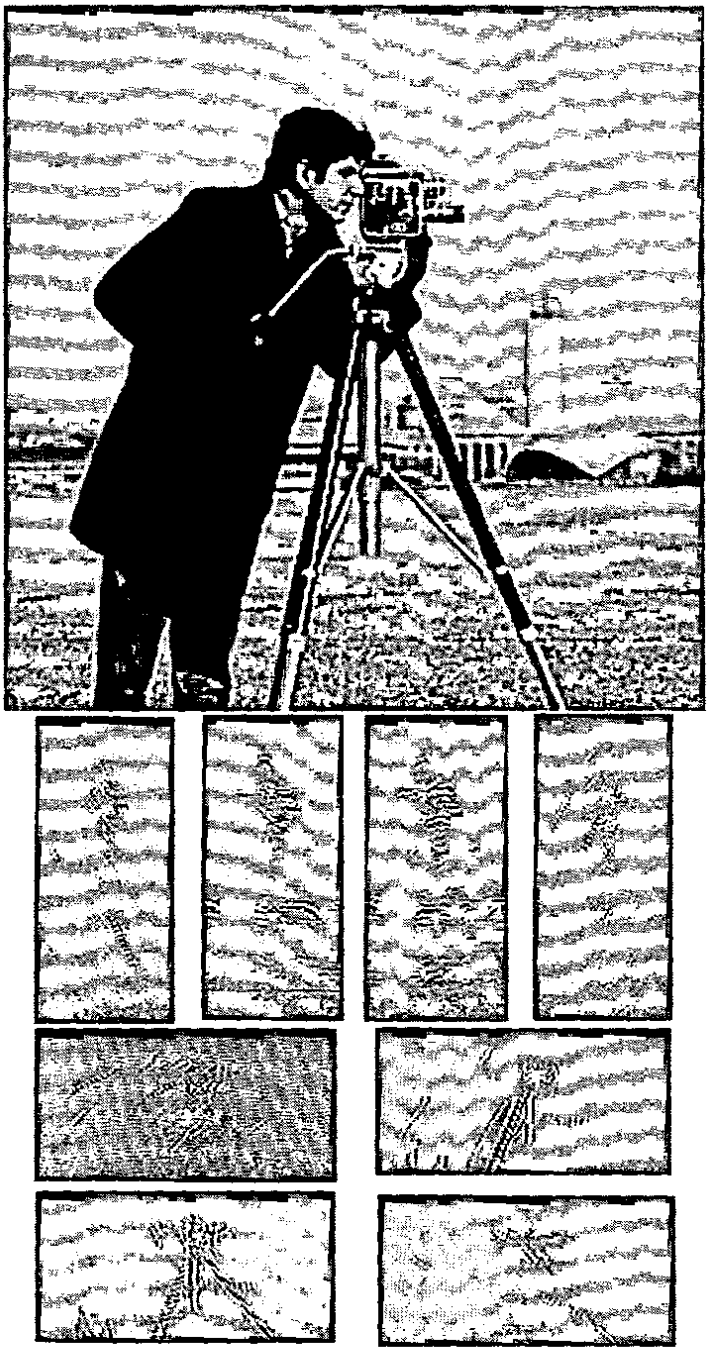

Figure 3.7 Subband images generated by eight-band DFB proposed by Sang [62].

Chapter-4

DESIGN AND STRUCTURE OF PROPOSED SYSTEM (DECIMATION FREE DIRECTIONAL FILTER BANK)

There are several different areas of image processing where directional decompositions have been applied. These applications include robotics, computer vision, seismology, image compression, image analysis, and image enhancement. At the heart of these directional decomposition-based systems is an *orientation analysis* stage. The orientation analysis attempts to provide a measure of how strongly oriented an image is in a particular range of directions. The orientation of an image is very much a perceptual and application dependent quantity. The degree of an orientation of an image (or subimage) in a particular direction can be defined in a variety of ways. Our proposed system is an orientation analysis tool. Figure 4.1 shows the block diagram of the proposed system. It differs from past techniques discussed in sections 1.1 due to the fact that it is mainly concerned with the global direction rather than local direction. So an image containing a certain feature in a specific direction will only be present in one of the directional image. To be very precise, it can be stated that each output from Decimation Free Directional Filter bank is directionally orthogonal to the other output of the system. From the above discussion it can be deduced that our proposed system works better if the input image contain directional information. The proposed system takes a two dimensional gray scale image as an input. As the system is designed for medical image processing, and we know that most of the medical images are gray scale, that is the reason, the system takes gray scale images. It decomposes the input image into its global directional features. All the output images from the system have the same size and dimension. The final enhanced image is reconstructed by choosing pixels having large block energy. Our Proposed system can be decomposed into two stages. The sections that follow address the issues regarding these stages.

4.1 Decimation Free Directional Filter Bank

Decimation free directional filter bank is a set of directionally orthogonal filters which extracts directional information from the image. Decimation free directional filter bank can be implemented in parallel form as well as in a tree structure. The parallel implementation is more efficient than tree structure. Tree structure is easy to understand as compare to parallel structure. Later on, the chapter contains a detailed discussion on both forms of implementation. Figure 4.2 shows the schematic diagram of Decimation free directional filter bank. The figure reveals that the implementation scheme followed is a tree structure one. Here tree structure is used only for the sake of comparison with the previous system, understanding and simplicity. A Decimation free directional filter bank takes an image as an input in a spatial domain, and outputs eight directionally orthogonal directional images. Size of each directional image is same as input image. Decimation free directional filter bank can be further subdivided into three subsections on the basis of tree structure implementation.

4.1.1 First Stage of Decimation Free Directional Filter Bank

First stage of decimation free directional filter bank comprise of two filters with hourglass shape like passband. Due to their shape, they are referred as hourglass filters. Block diagram of first stage is shown in Figure4.3. First stage of Decimation free directional filter bank decomposes the spectrum of the input image into two hourglass shape passbands. These two output directional images have same size as input image but the directional information present in each of these two directional images is orthogonal to each other.

All the filters used in decimation free directional filter bank are non-ideal. Ideal filters are avoided to avoid ringing artifacts. So, design of all filters of decimation free directional

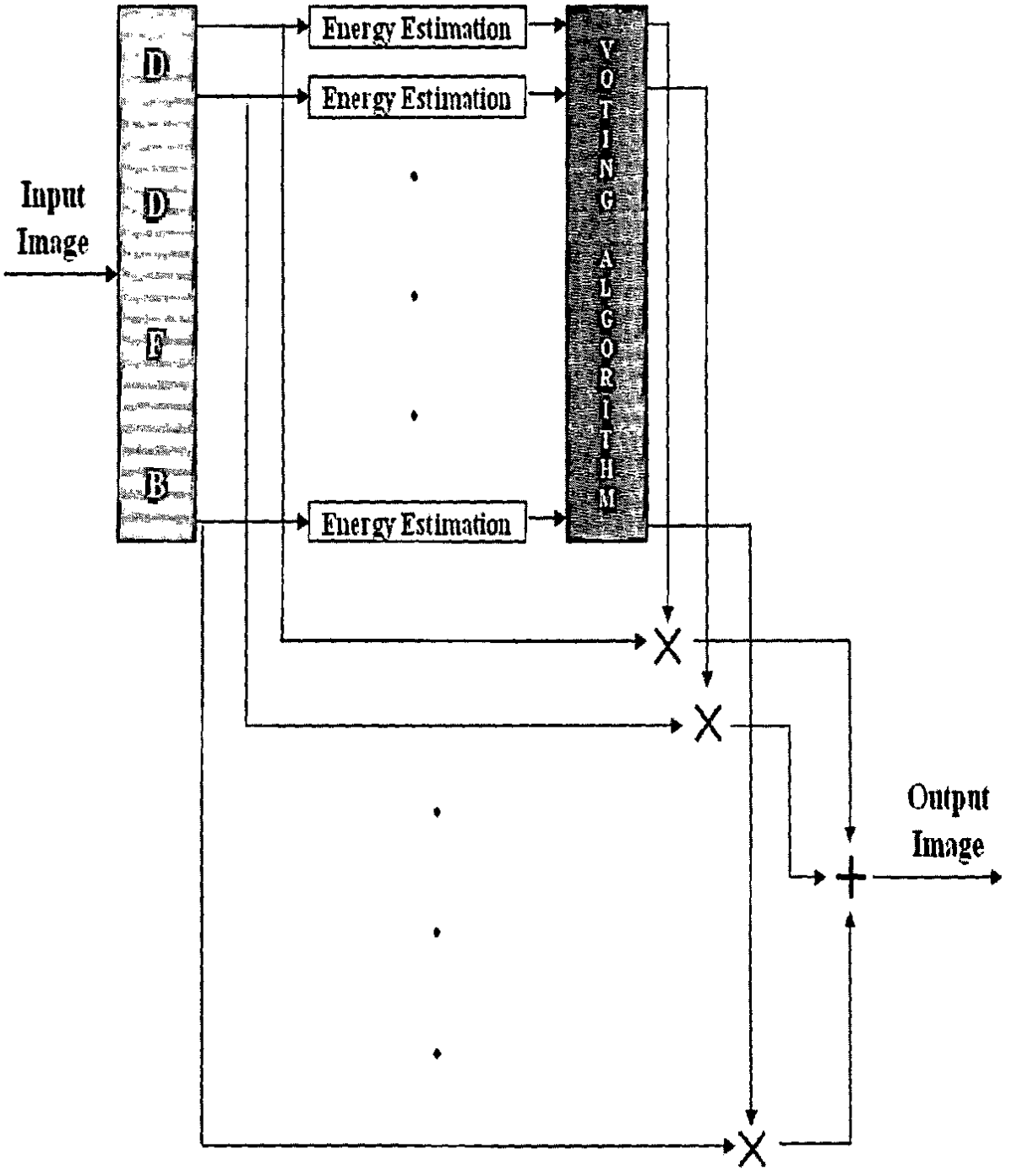

Figure 4.1 Block Diagram of the proposed system.

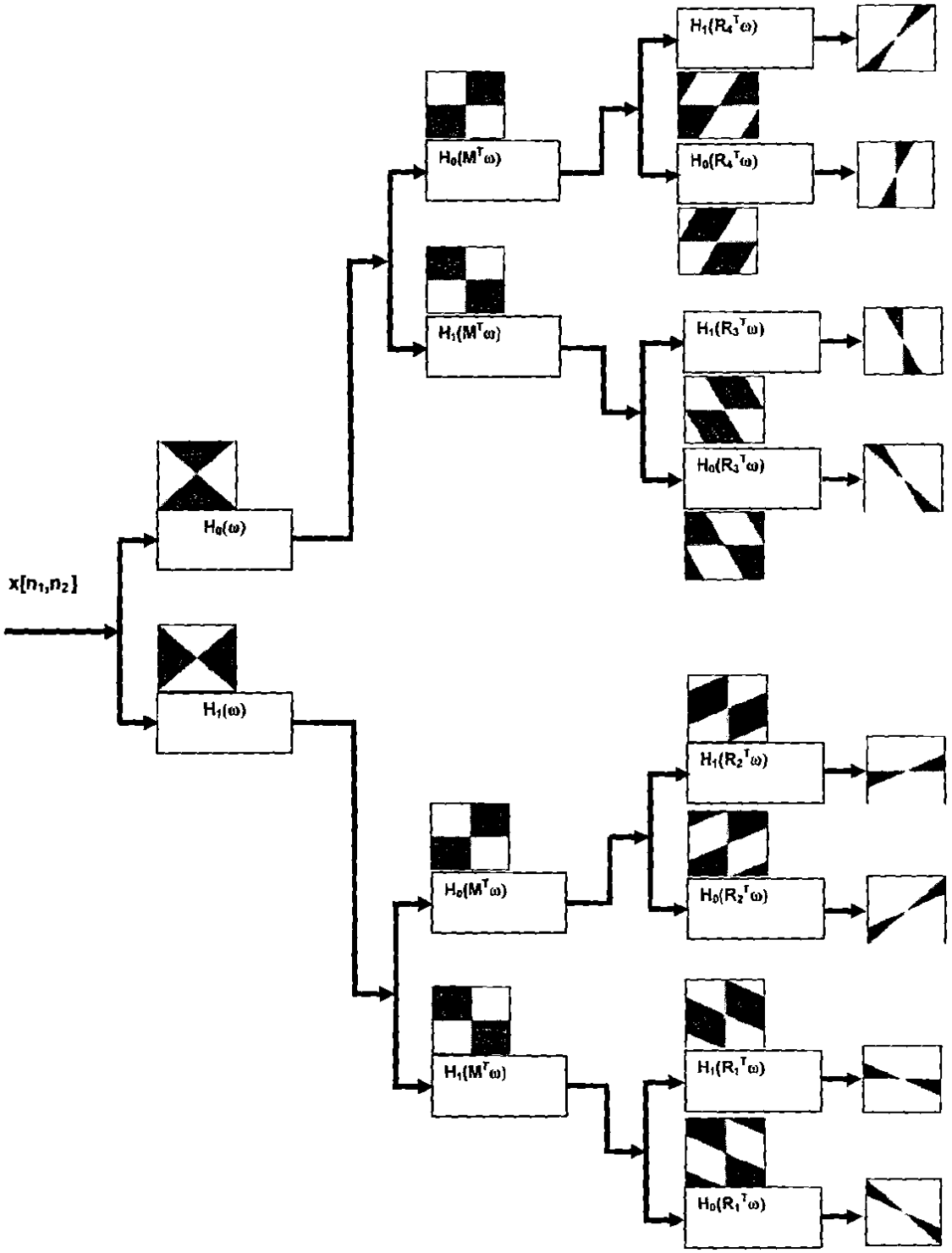

Figure4.2 Schematic diagram of Decimation Free Directional Filter Bank

filter bank requires great care. The following subsection describes the issues regarding the design of first stage filters of decimation free directional filter bank.

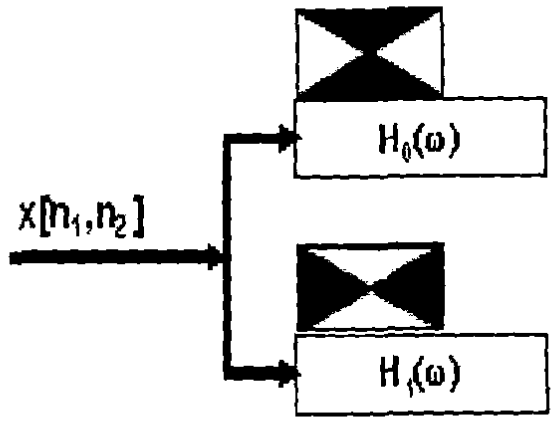

Figure 4.3 Block Diagram of First Stage.

4.1.1.1 Design of Hourglass Shaped Filters

First stage filters of decimation free directional filter bank have hourglass like passband. Both first stage filters are constructed from one-dimensional Lowpass filter. One-dimensional Low pass filter is a non-ideal finite impulse response (FIR) filter with fifty one (51) tapes. We have designed an odd length filter to have full sample delay instead of fractional delay. Following are the steps to design a non-ideal hourglass filter $\mathbf{H_0(\omega)}$.

- The very first step in the design is to take a one-dimensional low pass filter. For a one-dimensional filter, two parameters must be selected: the cutoff frequency, fc, and the length of the kernel, K. We desire to have cutoff frequency $\pi/2$ to avoid aliasing and folding while downsampling by a factor of two. We choose K as fifty one (51), to have full sample delay. The cutoff frequency (normalized frequency) is expressed as a fraction of the sampling rate, and therefore must be between 0 and 0.5. Following are the coefficients of the filter.

n	coefficients
-25	0.0011340930
-24	0
-23	-0.0020874578
-22	0
-21	0.0034173449
-20	0
-19	-0.0052135012
-18	0
-17	0.0075914137
-16	0
-15	-0.0107118931
-14	0
-13	0.0148202587
-12	0
-11	-0.0203297421
-10	0
-9	0.0280173467
-8	0
-7	-0.0395562122
-6	0
-5	0.0593253958
-4	0
-3	-0.1034561628
-2	0
-1	0.3174198746
0	0.5
1	0.3174198746
2	0
3	-0.1034561628
4	0
5	0.0593253958
6	0
7	-0.0395562122
8	0
9	0.0280173467
10	0
11	-0.0203297421
12	0
13	0.0148202587
14	0
15	-0.0107118931
16	0
17	0.0075914137
18	0
19	-0.0052135012
20	0
21	0.0034173449
22	0
23	-0.0020874578
24	0
25	0.0011340930

All these coefficients are present in a column vector. To make a two dimensional filter $h[n_1,n_2]$, from this one-dimensional vector we have to multiply this column vector with its transpose. Figure 4.4 shows the frequency domain picture of the resulting filter.

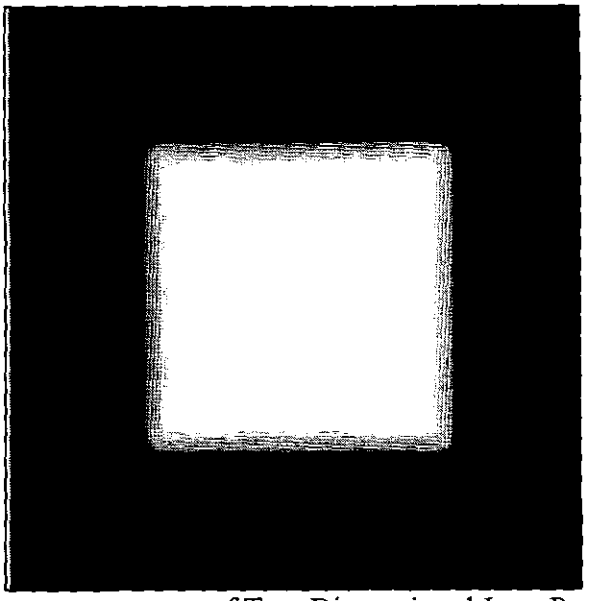

Figure 4.4 Frequency response of Two Dimensional Low Pass Filter with cutoff frequency $\pi/2$.

- Now perform downsampling on $h[n_1,n_2]$. The downsampling performed on $h[n_1,n_2]$ is a directional one. Directional downsampling which is used in this particular step is known as Quincunx downsampling as discussed in chapter 2. We have to downsample the filter by two with Quincunx method. Mathematically the whole operation can be written as:

$$h_d[\mathbf{n}] = x[M\mathbf{n}].$$

Here $\mathbf{n}$ is a row vector containing n_1 and n_2, and M is a two by two matrix of integers. Here M is chosen such that the determinant of M remains two. The result from the determinant decides, by how much the image is to be downsampled. In words, the whole above process can be stated as, to fill a point in an resulting image we multiply the co-ordinates of the resulting image with M. The resulting vector is the co-ordinates of the image from where we have to pick the value and put it in the resulting image. In frequency domain the same relation can be written as

$$X_d(\omega) = \frac{1}{|\det M|} \sum_{k \in N(M^T)} x\left(M^{-T}(\omega - 2\pi k)\right)$$

Where $N(M^T)$ is the set of the form $M^T x$, with $x \in [0,1)^D$. The frequency domain picture of the resulting filter is shown in Figure 4.5.

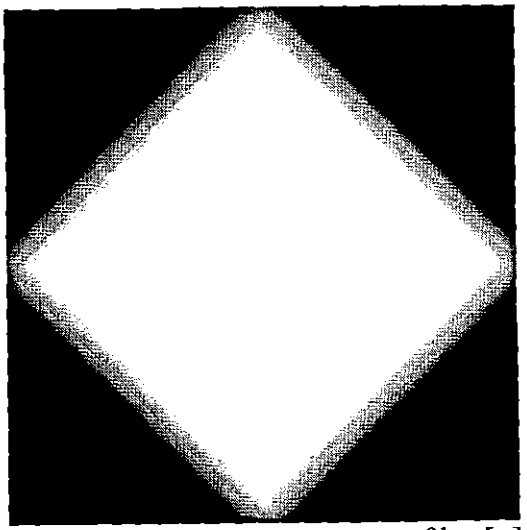

Figure 4.5 Frequency response of $h_d[n]$.

- Delaying a signal in the frequency domain is known as modulation. The third and final step in the design of hourglass filter is to modulate the downsampled filter in ω_1 direction by π. Mathematically it can be stated as:

$$H_0(\omega_1, \omega_2) = H_d(\omega_1 - \pi, \omega_2).$$

Figure 4.6 shows the Frequency domain picture of the above operation. The resulting filter from the above operation is known as Hourglass filter.

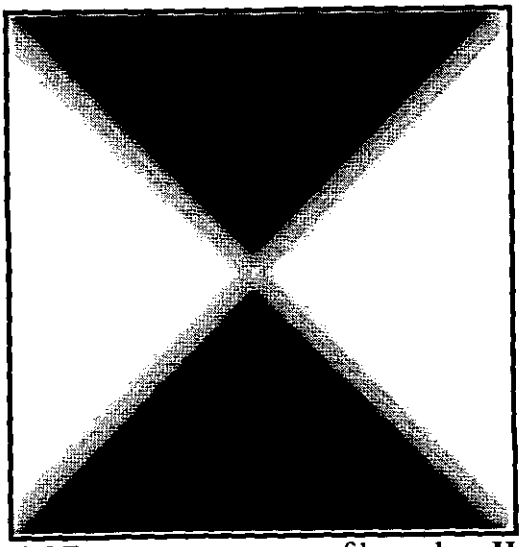

Figure 4.6 Frequency response of hourglass $H_0(\omega_1, \omega_2)$.

- Second hourglass filter, $H_1(\omega_1, \omega_2)$, can be obtained by modulating the $H_0(\omega_1, \omega_2)$ in both ω_2, and ω_1 direction by π. Mathematically, it can be stated as:

$$H_1(\omega_1, \omega_2) = H_0(\omega_1 - \pi, \omega_2 - \pi).$$

Figure 4.7 shows the frequency domain picture of the above transformation.

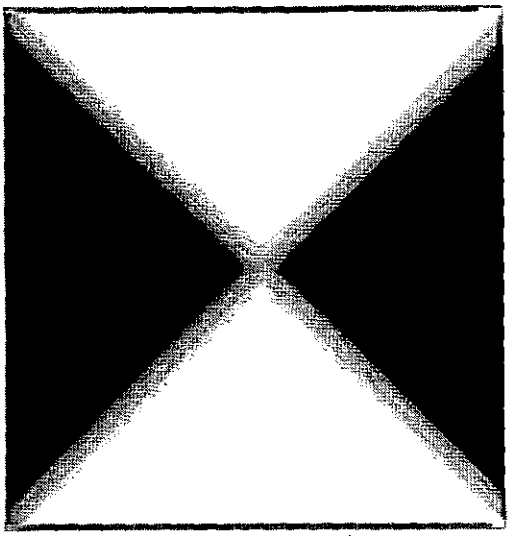

Figure 4.7 Frequency response of hourglass $H_1(\omega_1, \omega_2)$.

The input image after passing through the first stage have hourglass shaped like pass band. These images are now used as an input as shown in Figure 4.2 to the second stage. In the next section, we will discuss issues regarding second stage of decimation free directional filter bank.

4.1.2 Second Stage of Decimation Free Directional Filter Bank

Output from the first stage is used as an input to the second stage. Second stage requires two filters each to be operated on each of the output from first stage. The output from the second stage increases the angular resolution by two. So, the output from the second stage contains four directional images having orientation $0\text{-}45^0$, $45^0\text{-}90^0$, $90^0\text{-}135^0$ and $135\text{-}180^0$. In the section to follow, we will discuss issues regarding the design of second stage filters.

4.1.2.1 Design of Second Stage Filters

Second stage filters have checkerboard like pass band, as shown in the Figure 4.2. Due to this very reason they are normally referred as checkerboard filters. As like the first stage they are also non-ideal filters to avoid ringing. To design checkerboard filters, following two steps are necessary.

- Take both the filters, which are created in section 4.1.1.1.
- Now perform upsampling discussed in chapter 2, on each of the filter. The upsampling performed in this section is also directional in nature. Mathematically, the operation can be written as:

$$x_u = \begin{cases} x_0[M^{-1}n] & , \text{if } \mathbf{n} \in \mathbf{L(M)} \\ 0 & , \text{otherwise.} \end{cases}$$

In frequency domain, the same operation can be written mathematically as;

$$X_u(\omega) = \sum_{n \in I(M)} x[M^{-1}n] e^{-j\omega^T n} = \sum_{m \in N} x[m] e^{-j\omega^T Mm}$$

$$= X(M^T \omega)$$

Figure 4.8 and Figure 4.9 shows the result of transformation on H_1, and H_0 of the above equation.

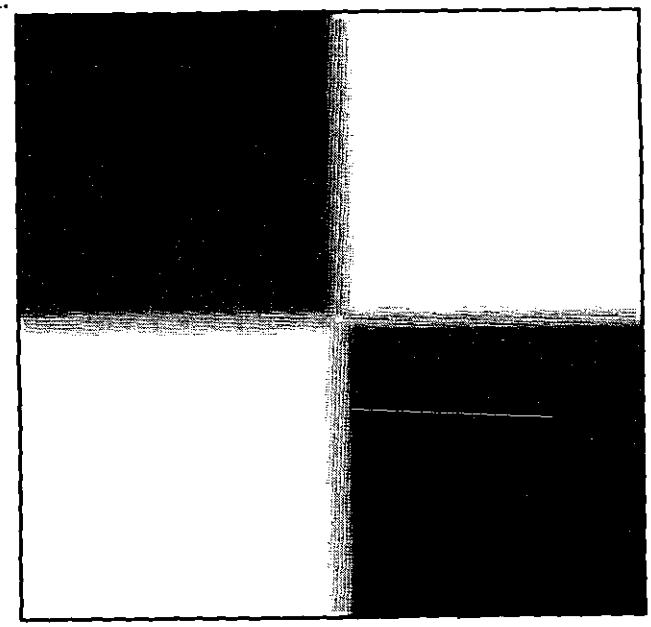

Figure 4.8 Frequency of checkerboard filter $\mathbf{H_1}$ $(M^T\omega)$.

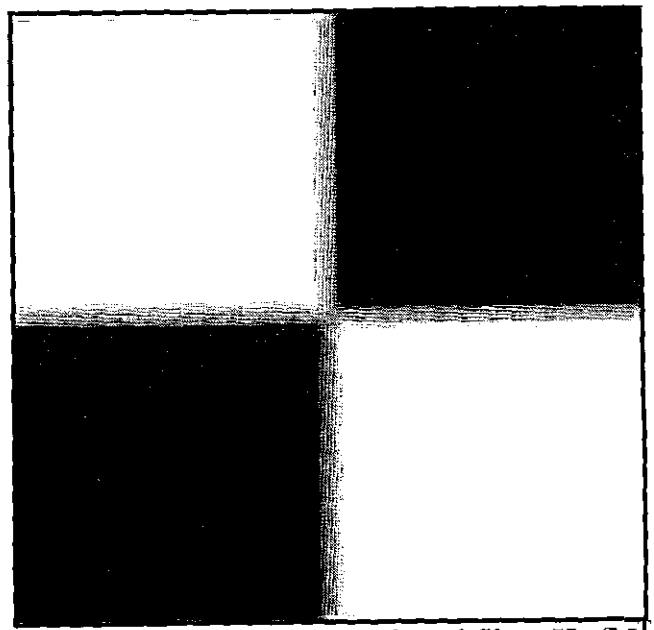

Figure 4.9 Frequency of checkerboard filter $\mathbf{H_0}$ $(M^T\omega)$.

The output from the decimation free directional filter bank up till second stage when unit impulse is given as input is shown in Figure 4.10.

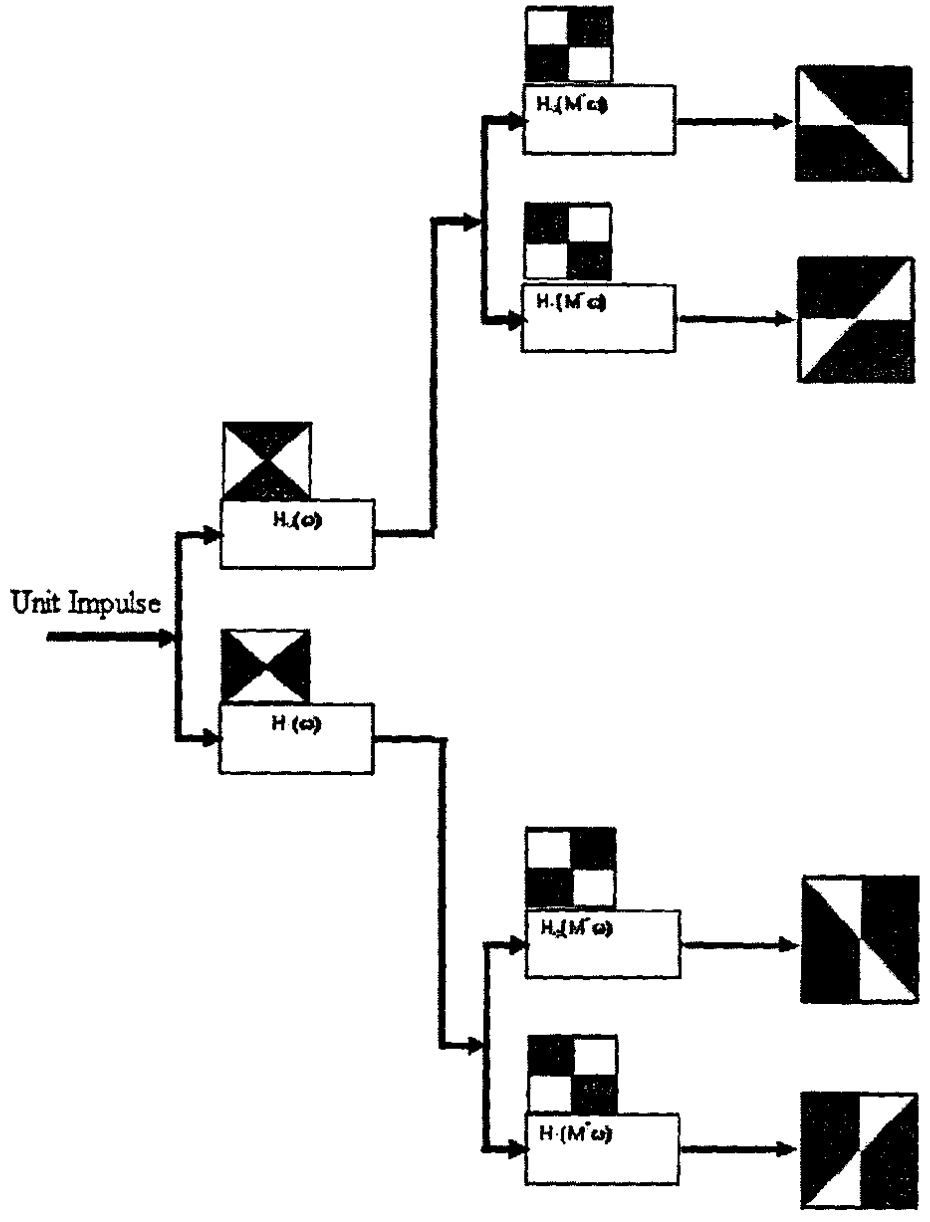

Figure 4.10 Output Frequency responses from second stage.

4.1.3 Third Stage of Decimation Free Directional Filter Bank

The output from the second stage are fed as input to the third stage. The output from the third stage are wedge shaped like frequency responses. Third stage requires eight different filters. Due to the very reason, third stage filters design requires more complex procedure. In the section below, we will discuss all the issues regarding design of third stage filters.

4.1.3.1 Design of Third Stage Filters

Design of third stage filters requires resampling to be done in four different ways to both of the filters designed during the first stage. The resampling matrices are same as discussed in section 3.3. Mathematically, resampling in the frequency domain is given by:

$$X(\omega) = \sum_{n \in L(R)} x[R_i^{-1}n] e^{-j\omega^T n} = \sum_{m \in N} x[m] e^{-j\omega^T R_i m}$$

$$= X(R_i^T \omega)$$

where R_i, is a resampling matrix. Its equivalent mathematical form in the spatial domain is given by the equation:

$$x_u = \begin{cases} x_0[R_i^{-1}n] & , \text{if } n \in L(M) \\ 0 & , \text{otherwise.} \end{cases}$$

Where R_i, is same as discussed above. Figure 4.2 shows the wedge shaped frequency domain responses of decimation free directional filter bank.

We are referring the outputs from third stage as directional images rather than directional subbands due to the only reason that each output from decimation free directional filter bank has the same size as the input image.

4.1.4 Parallel Implementation of Decimation Free Directional Filter Bank

Decimation free directional filter bank can be implemented in parallel structure by just using the outputs of the third stage of decimation free directional filter bank tree structure when a unit impulse is given as input. Figure 4.11 shows the parallel structure of decimation free directional filter bank. The implementation requires less computation and hence more efficient than tree structure. The simplicity in decimation free directional filter bank has it much convenient to implement the whole structure in the parallel form.

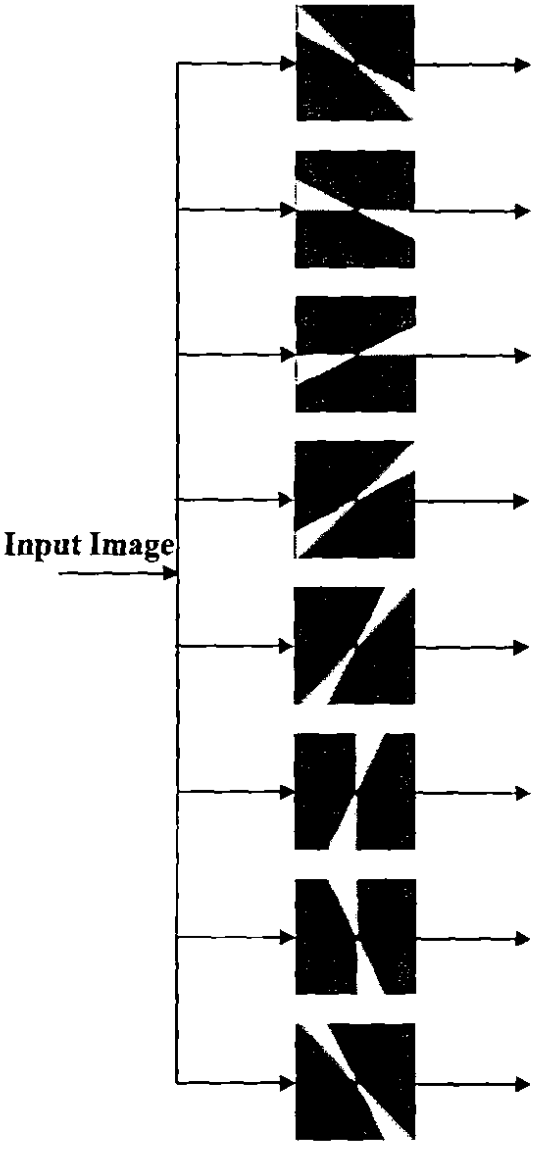

Figure 4.11 Parallel Structure of decimation free directional filter bank.

Chapter-5

APPLICATION OF DECIMATION FREE DIRECTIONAL FILTER BANK TO MEDICAL IMAGE ENHANCEMENT

The detection and enhancement of Coronary arterial trees (CAT's) in an angiogram image is an important pre-processing task that will greatly reduce the stress on further processing such as 3-D reconstruction of CAT model. Conventional techniques make use of gradient operators to detect CAT structure. However, the gradients are local operators that do not provide continuous map of arterial trees especially in noisy environment. We propose a decimation-free directional filter bank (DFB) structure. It provides output in the form of directional images as opposed to directional sub-bands provided in previous DFBs. The presence of directional images facilitates any further spatial processing if needed. However, we have to prepare an angiogram image before it can be given as input to the proposed DFB structure due to the fact that angiograms acquired are low in contrast. The preparation steps involve removing non-uniform illumination from the image. Then proposed DFB structure outputs directional images. The final enhanced result is constructed on a block-by-block basis by comparing energy of all the directional images and picking one that provides maximum energy. The enhancement that results in the final image is due to the fact that we can separate omni-directional background noise from CAT structure which is pre-dominantly a directional feature.

5.1 Introduction

Angiograms are images of blood vessel structures (vasculature) that are acquired using either magnetic resonance imaging or X-Ray methods. Angiograms are required not only for diagnosis but also for treatment planning, where accurate delineation of any lesion and information concerning its blood supply is important. Typical features that clinicians look for in angiograms include the number and position of feeding vessels (arteries) as well as the way in which blood is drained from the lesion. Very often the presence of abnormal or unusual vessels structure, position or geometry may be the only clue to existence of an abnormality. Some types of lesion are associated with a specific vascular structure. The analysis of angiogram which are high resolution X-Ray two dimensional (2-D) images containing projections of coronary arterial trees (CAT's) is done through several techniques. One such technique is biplane angiography where a sequence of usually orthogonal projection pairs is constructed. Although biplane angiogram provide information for resolving many types of ambiguity, such as artery crossing and overlapping due to projection of three dimensional (3-D) objects on the plane, the related high overhead costs have limited its use by the majority of medical labs. The other methods include single-view cine-angiograms [67], and motion estimation [68]. All the above methods are concerned with visualization of CAT's in an X-Ray angiogram. The X-Ray angiograms acquired are generally, low in contrast with spatially varying average brightness, and noisy background. The example of one such image is shown in Figure 1.1.

Primarily, we are concerned here with enhancing angiogram image to make it suitable for further processing that include 3-D construction of CAT's structure [67]. The enhancement problem may be considered as an image segmentation problem in the sense that angiogram should be partitioned into two classes, each one belonging either to the vascular structure or the background.

Figure 5.1 Angiogram Image of Heart

From signal processing point of view, the CAT's segmentation problem can be dealt with either in spatial domain or Fourier domain. The spatial domain techniques employed for CAT extraction mainly make use of gradient edge detection algorithms. Morphological edge detectors have been used for automatic recognition of arterio-venous intersection in [69]. A line finding algorithm along with a probabilistic relaxation scheme has been used for the extraction and subsequent description of blood vessel patterns in retinal images [70]. Gradient based feature extraction techniques are helpful in reliably locating blood vessels and got their motivation from enhancement of fingerprint images. However, these algorithms do not result in a continuous map of the artery trees. An individual blood vessel may be broken into several segments due to the presence of non-uniform background and the local character of gradient operator [71]. On the other hand, Fourier domain CAT's extraction techniques employ sector Filters to enhance directed line segment in an image but fail to produce good results in the presence of blob type objects [72]. Bamberger et.al. proposed directional filter banks (DFB) in [60] to extract directional features present in an image. Recently there has been extensive activity in the area of feature detection and image enhancement using DFB. Few examples include wavelet image Denoising [73], fingerprint image enhancement [74], fingerprint image enhancement in a binary domain [75]. Since angiogram background noise is omni-directional and CAT's structure is highly directional in nature, it is conjectured that, in general, a DFB will help us in substantially reducing the noise while preserving the directional features.

In this chapter, we proposed a directional Filter bank (DFB) based enhancement technique for X-Ray angiograms that helps in better visualization of coronary arterial trees. Furthermore, the proposed method can also be utilized as a pre-processing step in accurate reconstruction of 3-D CAT's. Our proposed DFB structure differ with the previous DFB in the sense that our proposed algorithm provides output in the form of directional images for further spatial domain processing, whereas, the previous techniques provide directional sub-bands that need interpolation to get approximated directional images [60]. The creation of

directional images has been made possible in the proposed structure due to absence of decimators.

In the sections that follow we will describe first the make-up steps for an angiogram image, then develop the theory of decimation free directional Filter bank structure, discuss the creation of directional images, and finally reconstruct the enhanced image.

5.2 Angiogram Image Enhancement

An angiogram image enhancement algorithm receives an input angiogram image, applies a set of intermediate steps on the input image and finally outputs the enhanced image. We begin with a test image shown in Figure 5.1 and apply various processing steps sequentially.

The details of these steps come next.

5.2.1 Non-uniform Illumination Correction

An input angiogram image has a varying illumination pattern that needs to be removed. Although, there are many spatial domain techniques available to get rid of non-uniform illumination structure, we opted for Homomorphic filtering to extract non-uniform illumination of the test image. An image **f(x ,y)** can be expressed as a product of illumination and reflectance components i.e.

$$f(x,y) = i(x,y) * r(x,y).$$

By taking the natural logarithm of input image **f(x , y)** in the spatial domain we have transformed the image into sum of its illumination and reflectance parts. This is shown in equation form as below:

$$f(x,y) = ln\{i(x,y)\} + ln\{r(x,y)\}.$$

This is followed by taking discrete Fourier transform (DFT) of the logarithmic image. Now based on the fact that illumination is a slowly-varying pattern that will appear as low frequency content in the Fourier domain. Therefore, we applied a non-ideal Butterworth Lowpass Filter to extract the Lowpass region of the image. The transfer function of a Butterworth Lowpass Filter of order **n**, and with cutoff frequency at a distance D_0 from the origin is defined as

$$H(u,v) = 1/(1+[D(u,v)/D_0]^{2n}),$$

where **D (u, v)** is a radial distance from the origin. After filtering the image, inverse DFT has been applied to transform the filtered image from Fourier domain back to spatial domain. Finally illumination pattern present in an image can be obtained by taking exponential of the resulting output in the spatial domain. The extracted illumination pattern can be subtracted from the test image to obtain a uniformly illuminated image as shown in Figure5.2. In our test image case, we employed D_0 as **12**, and order **n** of the Butterworth Filter was **2**.

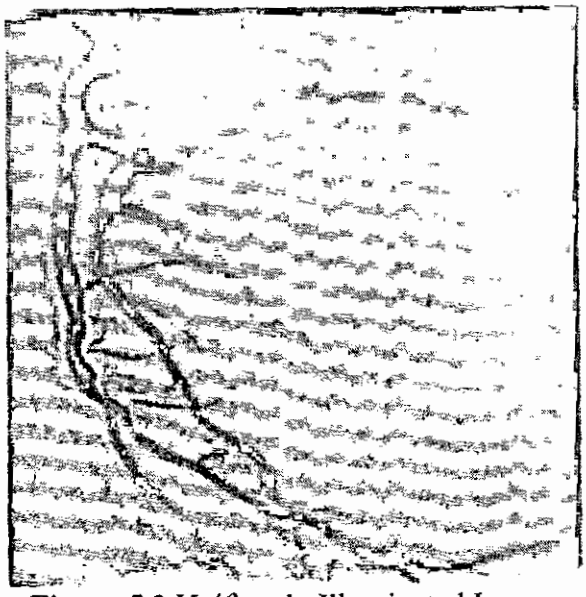

Figure 5.2 Uniformly Illuminated Image.

5.2.2 Normalization

Normalization is a pixel-wise operation. The main purpose of normalization is to get an output image with desirable mean and variance, which facilitates the subsequent processing. The uniformly illuminated image is normalized by the following formula.

$$N(i,j) = \begin{cases} M_0 + \sqrt{\frac{VAR_0(img-M)^2}{VAR}} & \text{if } img(i,j) > M \\ M_0 - \sqrt{\frac{VAR_0(img-M)^2}{VAR}} & \text{otherwise} \end{cases}$$

Where M and VAR denote the estimated mean and variance of input image and VAR_0, M_0 are desired variance and mean values respectively. After normalization the output image is ready for next processing step.

The result of the above mentioned process is shown in Figure 5.3. We note that Figure 5.3 image has got its contrast back but with uniform illumination pattern.

5.3 Creation of Directional Images

This section has been divided into two sections. The first section deals with the structure for designing fan filters, while the second describes the creation of directional images employing structure of first section.

5.3.1 Design of Directional Filters

The directional analysis employed in this section decomposes the spectral region of a given image into wedge-shaped passband regions. It is easily shown that these wedge-shaped regions correspond to directional components of an image. The filters related to wedge-shaped regions are commonly referred to as fan filters. The schematic diagram of our

proposed structure is shown in Figure 4.2. The structure is in the form of a tree with two band splits at the end of each stage, where each split increases the angular resolution by the factor of two.

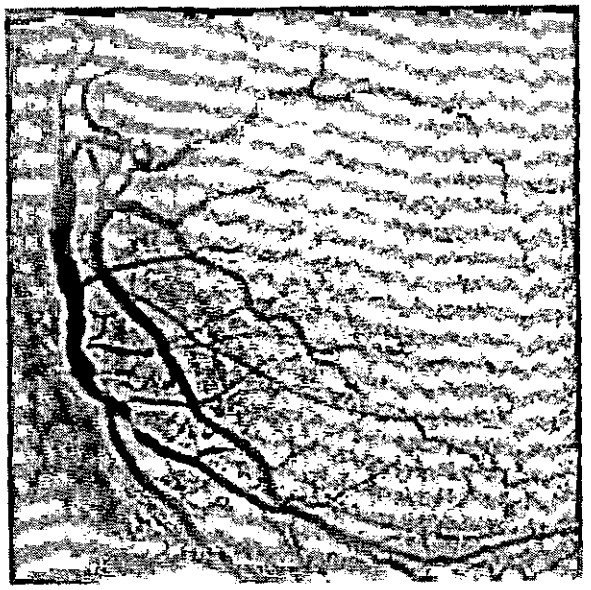

Figure 5.3 Normalized Image with VAR_0 =1200 and M =.120.

The first stage employs the complementary hour-glass filters. The filters for next two stages are obtained by linear transformation of the first stage hour-glass filters. For implementing linear transformation, the uni-modular matrices $\mathbf{M}_i$ and $\mathbf{R}_i$ are utilized. The rules for the selection of these matrices are presented in [76]. Once the filters for each stage are implemented, we can combine them on branch by branch basis to get the required fan filters as shown at the end of third stage in Figure 4.2.

One important difference between our proposed structure and DFB structure presented in [76] is the absence of decimator. It was pointed out in [60] that if sub-bands need to be processed for directional energy estimates, the decimation present in the conventional filter bank structure poses problem. This means that two samples located at the same spatial index $(\mathbf{n}_1, \mathbf{n}_2)$ in two different sub-bands i and j, will not necessarily correspond to same spatial region in the original image. This problem was circumvented in [60] by employing nearest-neighborhood or bilinear interpolation to make all sub-bands of the same size. However, in our structure, decimators at each stage are taken out and filters are designed by linear transformation in the frequency domain to get fan filters. Furthermore, to avoid ringing artifact in the output, ideal fan filters are avoided by employing non-ideal hour-glass filters using an FIR Lowpass filter.

5.3.2 Directional Images

The first step employed in directional images creation is to remove the spatial varying mean term by filtering with a Highpass filter. In this chapter, rectangularly separable

Highpass filter was used. The one-dimensional filter had a nominal cutoff frequency of $\pi/16$ and 40dB stop band attenuation.
The result of Highpass filtering the image in Figure 5.3 is shown in Figure 5.4. Comparing Figure5.4 with Figure 5.3, we note that arterial tree has uniform gray level throughout the image, however, in Figure 5.3; arterial tree has varying gray level from black to highest gray levels.

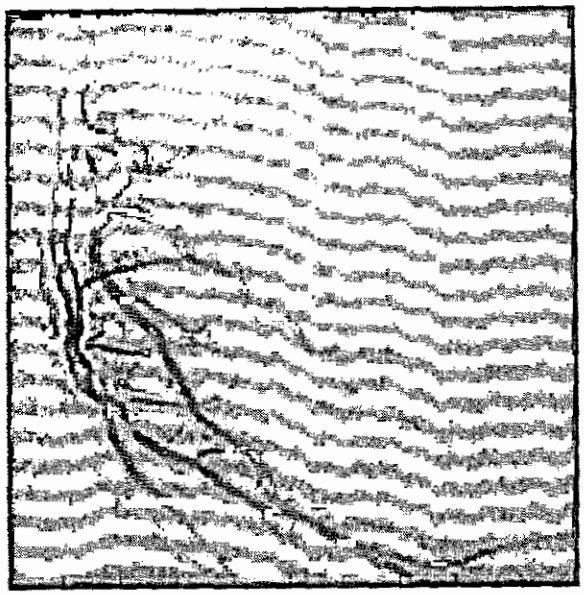

Figure 5.4 Highpass Image with cutoff frequency $\pi/16$.

Directional images are obtained by applying all directional Filters constructed in previous section. These directional images can be regarded as decomposition of the original image in eight pieces based on direction. Directional images contain features associated with global directions rather than local directions. By creating directional images we have divided noise of the original image into eight different directions, thus reducing noise energy eight times.

Filters constructed during directional filter bank are eight in numbers. Each of the third stage filters contains transition on both sides of their pass band. So, in total there are sixteen transition regions. As earlier mentioned, these directional filters are directional orthogonal to each other. So, the part of the image which just lies in the transition region would be missed.

The solution to the above mentioned problem is to use overlapping filters. Overlapping filters are filters which have directional sensitivity, but they are not directionally orthogonal. Figure 5.5 contains frequency response of these overlapping filters. The white region in Figure 5.5 is assumed to be stop band. The overlapping effect has made these filters to pick the parts of the images lying in the transition regions but on the cost of directional orthogonality. Filter (a), (b), (c), and (d) can be constructed on the same lines as discussed in previous chapter. Filter (e) of Figure 5.5 is constructed by simply adding the responses of second, third, fourth, and fifth branch of third stage of Figure 4.2. Filter (f) of Figure 5.5 can be constructed by just adding the remaining filters of third stage of Figure 4.2. Directional images obtained by the overlapping filters are shown in Figure 5.6.

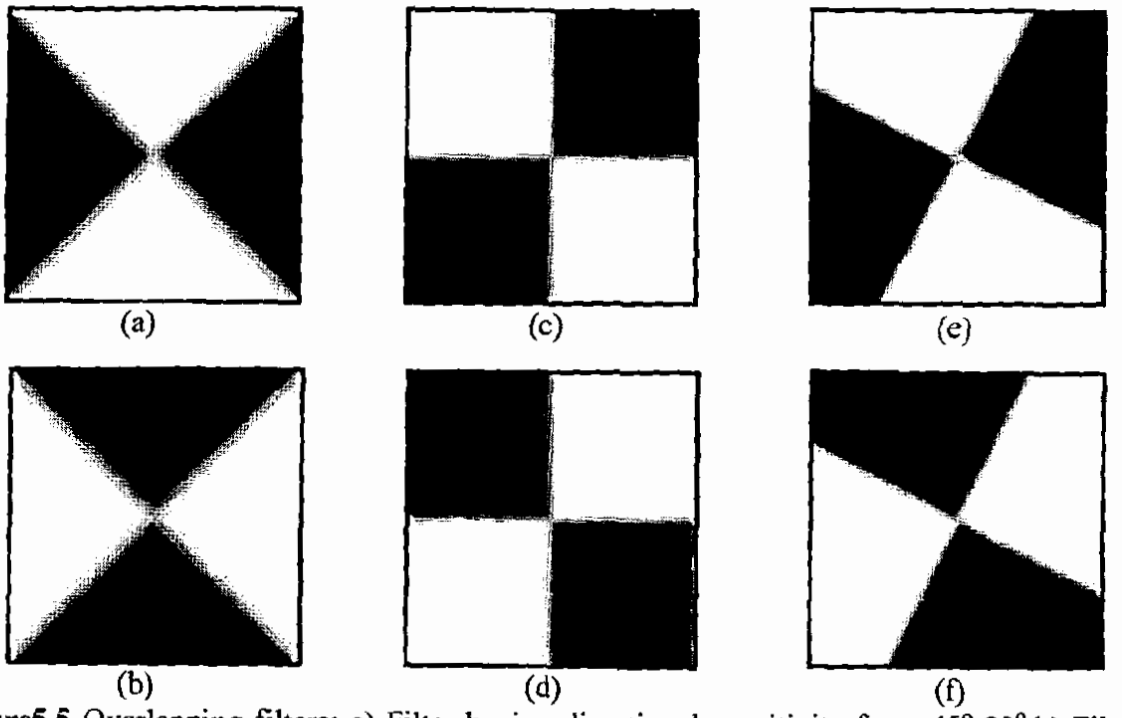

Figure5.5 Overlapping filters; a) Filter having directional sensitivity from 45°-90° b) Filter having directional sensitivity from -45°-45° c) Filter having directional sensitivity from 90°-180° d) Filter having directional sensitivity from 0°-90° e) Filter having directional sensitivity from 67.5°-157.5° f) Filter having directional sensitivity from -22.5°-67.5°.

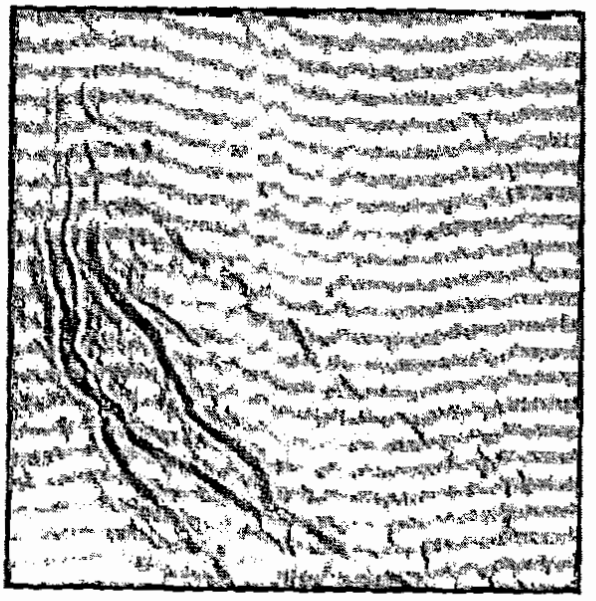

(a)

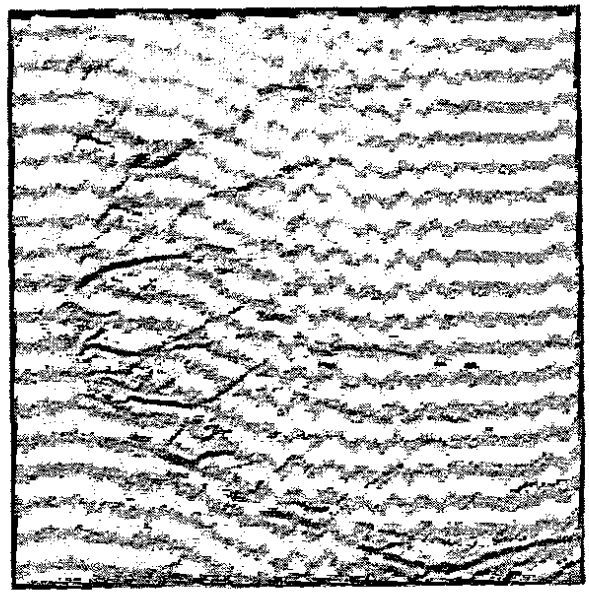

(b)

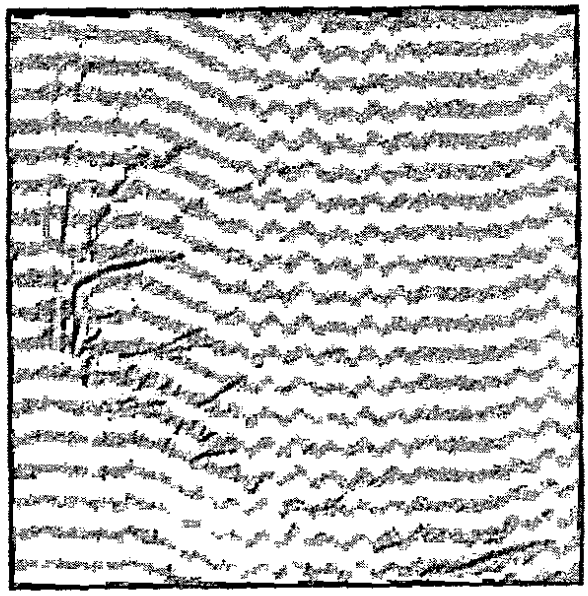

(c)

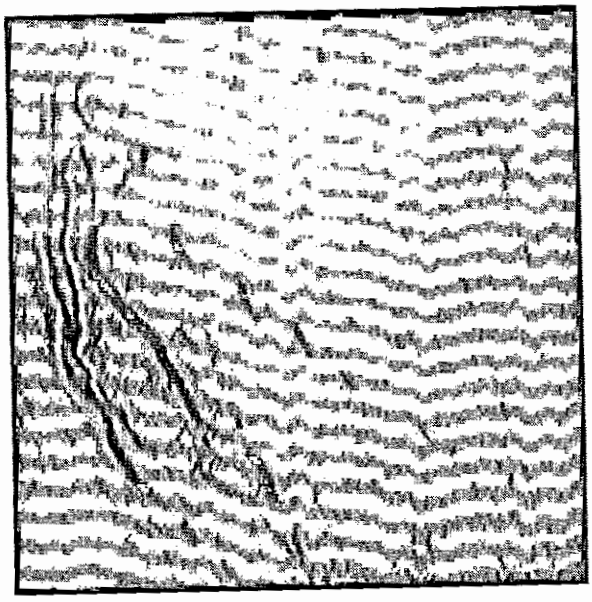

(d)

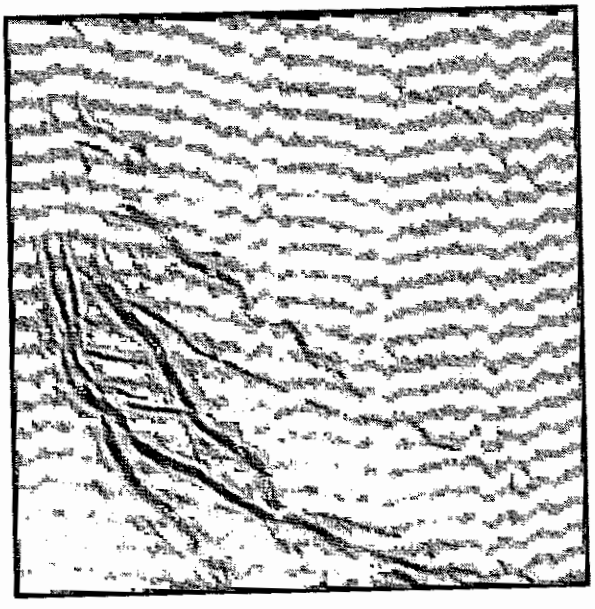

(e)

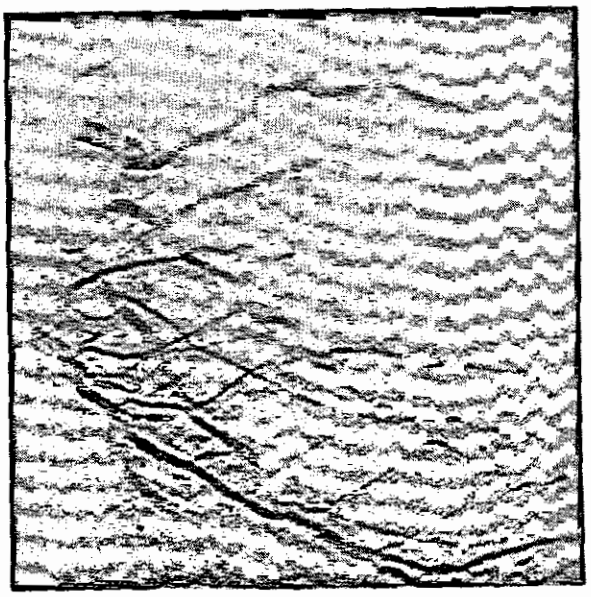

(f)

Figure 5.6 Directional Images of Figure 5.1; a) Direction 67.5°-157.5° b) Direction 157.5°-67.5° c) Direction 0°-90° d) 90°-180° e) 45°-135° f) 135°-45°.

5.4 Noise Removal

Noise removal is accomplished by first calculating the block based directional energy of each directional image. The directional energy of a block (X, Y) including the pixel (x , y) from the kth directional image is calculated as

$$E_k(X,Y) = \sum_{x=0}^{m_k} \sum_{y=0}^{n_k} \left| f_k(X,Y;x,y) \right|$$

where, f k is the directional image. The noise free directional images represented by Ak are obtained by the equation.

$$A_k = \begin{cases} f_k(X,Y;x,y) & \text{if } E_k(X,Y) > T \\ f_k(X,Y;x,y) & \text{if otherwise} \end{cases}$$

Here, T represents the threshold.

5.5 Reconstruction of Enhanced Image

Enhanced image is constructed from the directional images according to the following equation,

$$E_k = MAX\,[\,Y_{(1\le k\le 6)}\,(i,j)\,]$$

where f_{hf} is high-frequency output image from directional filter bank and f_i represents *ith* directional image. For every block (X,Y) of the original image we select a replacement from the six directional images based on maximum directional energy. Now it is advantageous to accentuate the contribution to enhancement made by the high-frequency components of an angiogram image. In order to do so we adopted the well-known enhancement process referred to as ***high-frequency emphasis***, where we added our enhanced high-frequency angiogram image with that of original angiogram image. The resultant image will be similar in contents to the original image but with emphasis to the high frequency features of the image. The final enhanced angiogram image thus obtained is shown in Figure 5.7. We note the clarity of the CAT's structure and other detail that simply are not visible in the original image. Comparing the result with the original image shown in Figure 5.1 reveals that the whole coronary tree-structure is intact while the spatial noise has been cleaned substantially.

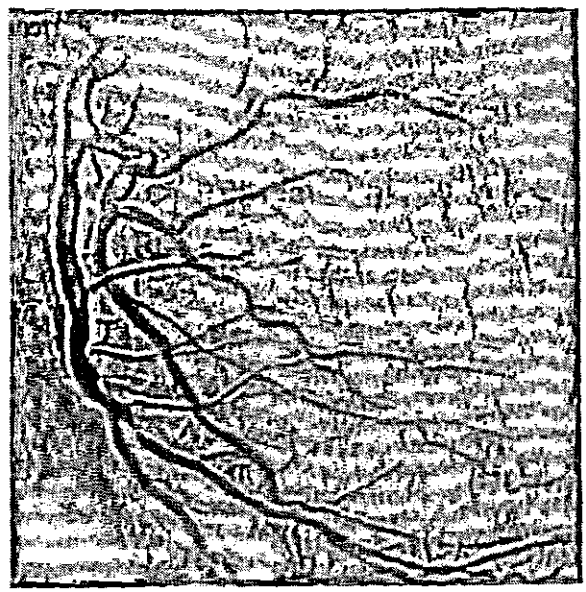

Figure 5.7 Final result high frequency emphases

Chapter-6

APPLICATION OF DECIMATION FREE DIRECTIONAL FILTER BANK TO FACE RECOGNITION

This study addresses new face recognition method based on Principal Component Analysis (PCA) and Decimation Free Directional Filter Bank (DFB) responses. Our method consists of two parts. One is the creation of directional images using DFB from the original face image. The other is transforming the directional images into eigenspace by PCA, which is able to optimally classify individual facial representations. PCA analysis is primarily used as a dimensionality reduction technique with least consideration to the recognition aspect. The basic idea of combining PCA and DFB is to provide PCA with some recognition ability. In our system recognition ability of the PCA is enhanced by providing directional images as inputs. The experiment results showed the remarkable improvement of recognition rate of 21-25% in Olivetti data set.

6.1 Introduction

Face recognition is largely motivated by the need for surveillance and security, telecommunication and digital library, human-computer intelligent interaction, and smart environments [77-80]. The face recognition primarily based on the understanding how people process and recognize each others face, and the development of corresponding computational modal for automated face recognition.

Developing a computational modal for the recognition of natural objects such as human faces is quite difficult, because they are complex and multidimensional. The general approach is to start with a given set of features and then attempts to derive an optimal subset (under some criteria) of features leading to high recognition performance. Principal component analysis (PCA) is a popular technique used to derive a starting set of features for face recognition. Turk and Pentland [81] develop a well-known PCA-based face recognition method, referred to as Eigenfaces method. More recently, a principal component analysis of imagery has also been applied for robust target detection [82,83], nonlinear image interpolation [84], visual learning for object recognition [85,86], and visual servoing for robotics [87].

However, these authors have used PCA analysis primarily as a dimensionality reduction technique and did not the recognition aspect. This is due to the fact that PCA is based on the optimal representation of the data in the sense of mean-square error. One way to improve the PCA stand-alone recognition performance, one needs to combine further this optimal representation criterion with some discrimination criterion.

One widely used discrimination criterion in the face recognition community is the Fisher linear discriminant (FLD, a.k.a. linear discriminant analysis, or LDA) [88], which defines a projection that makes the within-class scatter small and the between-class scatter large. As a result, FLD derives compact and well-separated clusters. FLD is behind several face recognition methods [89,90]. As the original image space is high dimensional, most of these methods apply PCA first for dimensionality reduction, as it is the case with the Fisher faces method due to Belhumeur et al.[90]. Subsequent FLD transformation is used then to build the most discriminating features (MDF) space for classification [89]. The drawback of FLD is that it requires large training sample size for good generalization.

In contrast, one can provide a preprocessing step that outputs discriminating feature classes. Then PCA can be used with each class to reduce the dimensionality. This view is described [91], where the Gabor filter responses are used as input vectors to the PCA. It is mentioned that Gabor filter responses works well with PCA and results in a system that is less sensitive to the rotation and illumination with improved classification. However, as

described [92], Gabor filter bank has overlapping and missing subband regions. the DFB, on the other hand, is a contiguous subband representation as shown in Fig. 1 Accordingly, a DFB can represent linear patterns, as found around eyes, nose and mouth area, more effectively, than a Gabor filter bank. The positive effect, in case of Gabor filter bank, of extracting special frequency and directional feature and suppressing noise component is much offset by the negligence of useful information existing outside the specified frequency range. This study represents Decimation Free Directional Filter Bank (DFB) as a preprocessing step to provide directional discriminating feature spaces. DFB based directional analysis has played a major role in wavelet image Denoising [62], fingerprint image enhancement [60], fingerprint image enhancement in a binary domain [75]. In our work, DFB effectively decomposes the face image into eight directional images and each directional image contains directional features associated with a particular direction. This preprocessing can be regarded as a discrimination process. Then PCA is used with each directional image in isolation. Finally, the PCA outputs based on each directional image is analyzed for recognition purpose.

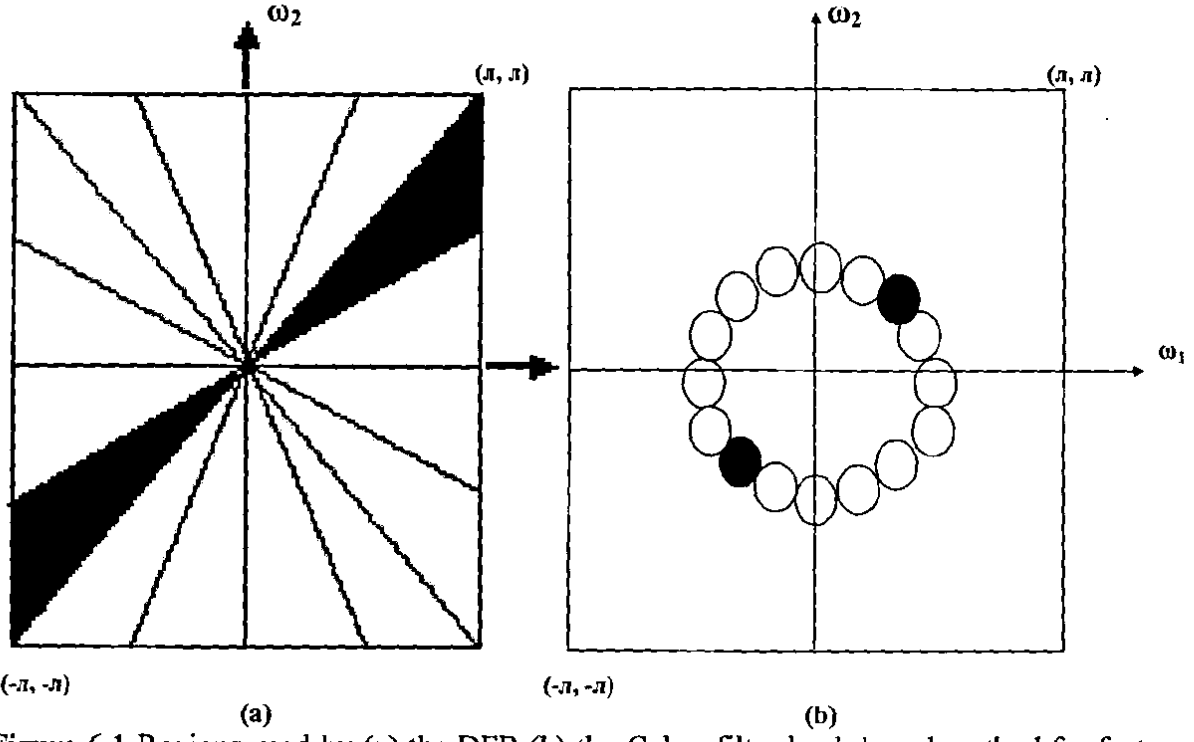

Figure 6.1 Regions used by (a) the DFB (b) the Gabor filter bank-based method for feature extraction.

6.2 Creation of Directional Images

This section has been divided into two subsections.

6.2.1 Directional Filter Design

The directional analysis employed in this section decomposes the spectral region of a given image into wedge-shaped passband regions. It is easily shown that these wedge-shaped

regions correspond to directional components of an image. The filters related to wedge-shaped regions are commonly referred to as fan filters.

The schematic diagram of DFB structure is in the form of a tree with two-band splits at the end of each stage Figure 4.2, where each split increases the angular resolution by the factor of two. The first stage employs the complementary hour-glass filters. The filters for next two stages are obtained by linear transformation of the first stage hour-glass filters. For implementing linear transformation, the uni-modular matrices **M** and $\mathbf{R}_i$ are utilized. The rules for the selection of these matrices are presented by Park et. al. [73]. Once the filters for each stage are implemented, they can be combined on branch by branch basis to get the required fan filters as shown at the end of third stage in Figure 4.2.

$$R_1 = \begin{pmatrix} 1 & 1 \\ 0 & 1 \end{pmatrix} \quad R_2 = \begin{pmatrix} 1 & -1 \\ 0 & 1 \end{pmatrix}$$

$$M = \begin{pmatrix} 1 & 1 \\ -1 & 1 \end{pmatrix}$$

$$R_3 = \begin{pmatrix} 1 & 0 \\ 1 & 1 \end{pmatrix} \quad R_4 = \begin{pmatrix} 1 & 0 \\ -1 & 1 \end{pmatrix}$$

One important difference between present proposed structure and DFB structure presented [73], is the absence of decimator. It was pointed out [74] that if sub-bands need to be processed for directional energy estimates, the decimation present in the conventional filter bank structure poses problem. This means that two samples located at the same spatial index (n_1, n_2) in two different sub-bands i and j will not necessarily correspond to same spatial region in the original image. This problem was circumvented [21] by employing nearest neighborhood or bilinear interpolation to make all sub-bands of the same size. However, in the present structure, decimators at each stage are taken out and filters are designed by linear transformation in the frequency domain to get fan filters. Furthermore, to avoid ringing artifact in the output, ideal fan filters are avoided by employing non-ideal hour-glass filters using an FIR Lowpass filter.

6.2.2 Directional Images

Directional images are obtained by applying all directional filters constructed as above. Figure 6.2 shows a facial image whose eight directional images are shown in Figure6.3. These directional images can be regarded as decomposition of the original image in eight pieces based on direction. Directional images contain features associated with global directions rather than local directions. By creating directional images, noise of the original image was divided into eight different directions, thus reducing noise energy eight times.

Figure 6.2 Test Facial Image.

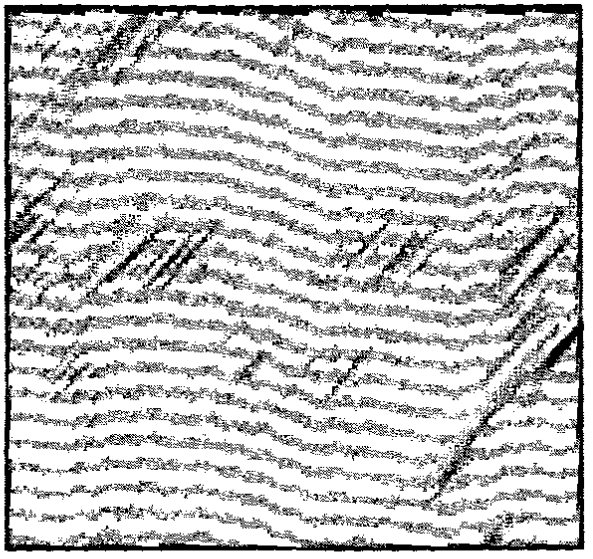

(a)

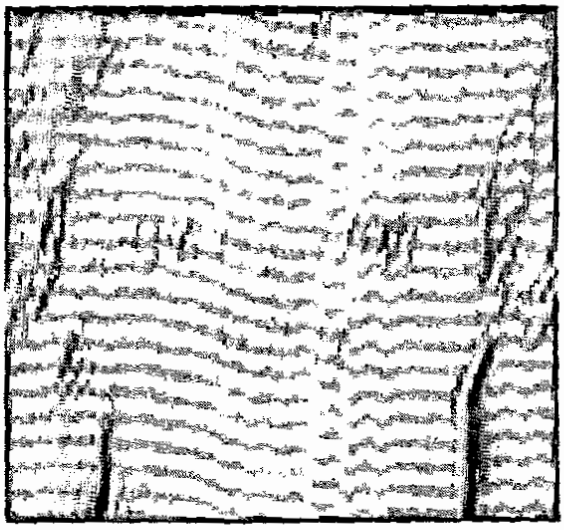

(b)

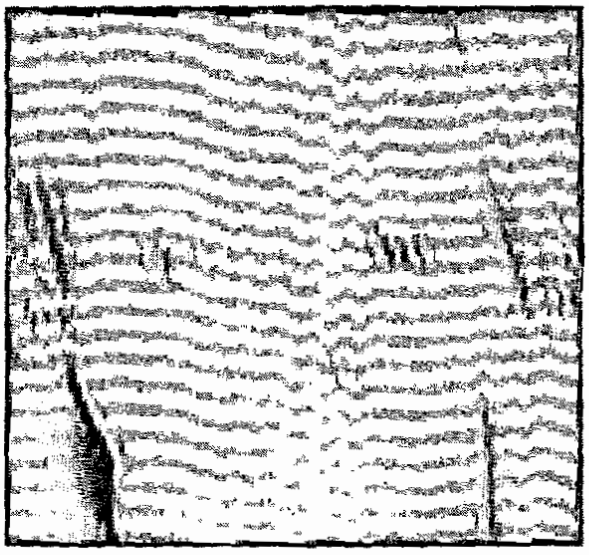

(c)

(d)

(e)

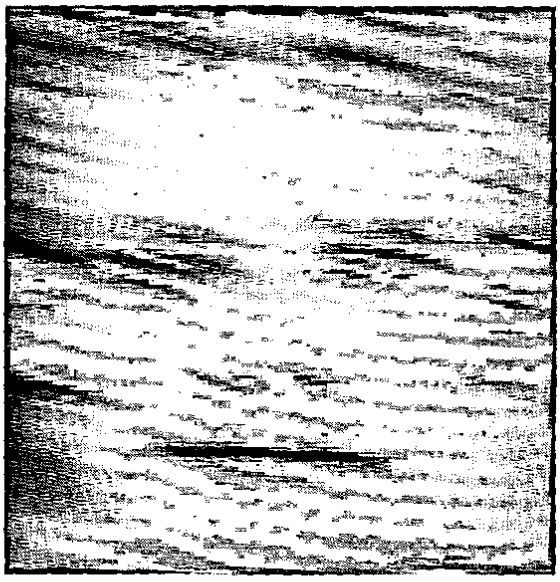

(f)

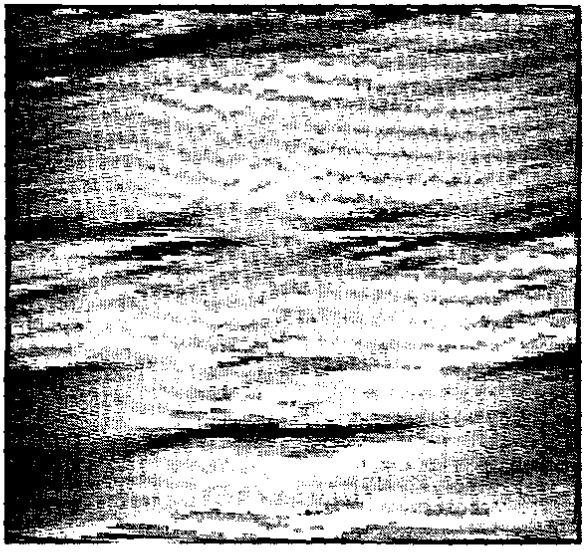

(g)

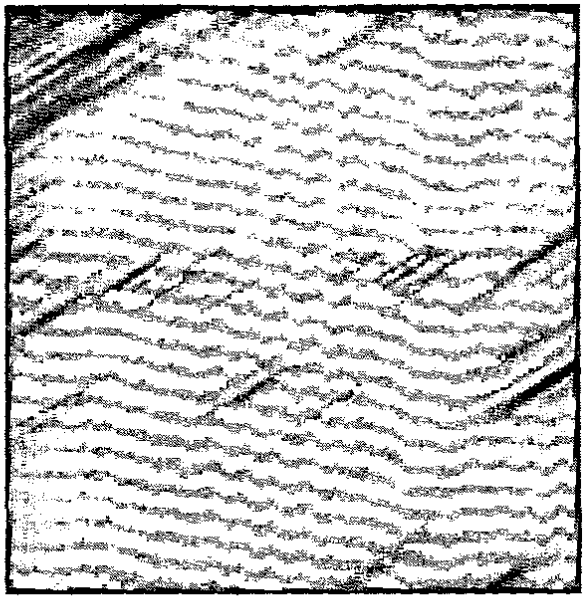

(h)

Figure 6.3 Creation of directional image: a) Directional image 1. b) Directional image 2. c) Directional image 3. d) Directional image 4. e) Directional image5. f) Directional image 6. g) Directional image 7. h) Directional image 8.

6.3 Principal Component Analysis (PCA)

PCA generates a set of orthonormal basis vectors, known as principal components (PCs) that maximize the scatter of all projected samples. Let $X = [X_1, X_2, \ldots, X_n]$ be the sample set of the original images. After normalizing the images to unity norm and subtracting grand mean a new image set $Y = [Y_1, Y_2 \ldots Y_n]$ is derived. Where each

$$Y_i = (y_{i_1}, y_{i_2}, \ldots, y_{i_N})^t, i = (1, 2, \ldots, n).$$

The covariance matrix of normalized image is defined as

$$\sum Y = \frac{1}{n} \sum_{i=1}^{n} Y_i Y_i^t = \frac{1}{n} Y Y^t \qquad (1)$$

And the eigenvector and eigenvalues matrices Φ, Λ are computed as

$$\sum Y\Phi = \Phi\Lambda . \qquad (2)$$

Note that YY^t is an N×N matrix while Y^tY is an n×n matrix. If the sample size n is much smaller than the dimensionality N, then the following method saves some computation [83]

$$(Y^tY)\Psi = \Psi\Lambda_1 \qquad (3)$$

$$\delta = Y\Psi \qquad (4)$$

Where: $\Lambda_1 = \text{diag}(\lambda_1, \lambda_2, \ldots, \lambda_n)$, and $6 = [\Phi_1, \Phi_2, \ldots, \Phi_n]$. If one assumes that eigenvalues are sorted in decreasing order, $\lambda_1 \geq \lambda_2 \geq \ldots \geq \lambda_n$, then the first m leading eigenvectors define matrix P

$$P = [\Phi_1, \Phi_2, \ldots, \Phi_m]. \quad (5)$$

The new feature set Z with lower dimensionality m (m << N) is then computed as

$$Z = P^t Y \quad (6)$$

6.4 Proposed System

In proposed system the directional features will be used as the training set images of PCA and recognition process is performed on these images. Block diagram of proposed system is shown in Figure 6.4.

The steps involved in the proposed system are as follows:

1) Obtain face images $I_1, I_2, \ldots, I_M$ of Olivetti face dataset shown in Figure 6.5. This data set is composed of 400 images from 40 galleries which is constructed under various depth and plane rotations. Dataset is composed of 10 face images per a person so we have defined one as a training set and the other nine sets as testing sets in turn. We have passed whole dataset through DFB and got eight directional images for each dataset image. Then we created eight new datasets by combining same directions of all the images. After that PCA is performed on each directional dataset.
2) Constructed 10304×40 matrix where the column vector V_i was the data of training image.
3) Compute the average face vector AVG,

$$AVG = \frac{1}{M}\sum_{i=1}^{M} V_i$$

4) Subtract the mean face,

$$d_i = V_i - AVG$$

5) Compute the covariance matrix:

$$C = \frac{1}{M}\sum_{n=1}^{M} d_n d_n^t = A A^t$$

where: A = [d1, $d_2, \ldots, d_M$]. AA^t is a very large matrix so Turk and Pentland suggested [83] a way to reduce it. They proposed that instead of AA^t, A^tA can be used.

6) Compute the M eigenvectors u_i of A^tA.
7) Keep only K eigenvectors (corresponding to the K largest eigenvalues).
8) Calculate weights of the training images by projecting mean subtracted images on the eigenvectors.
9) For recognition of any image first calculate weights for this image and then compare it with the weights of the training image.

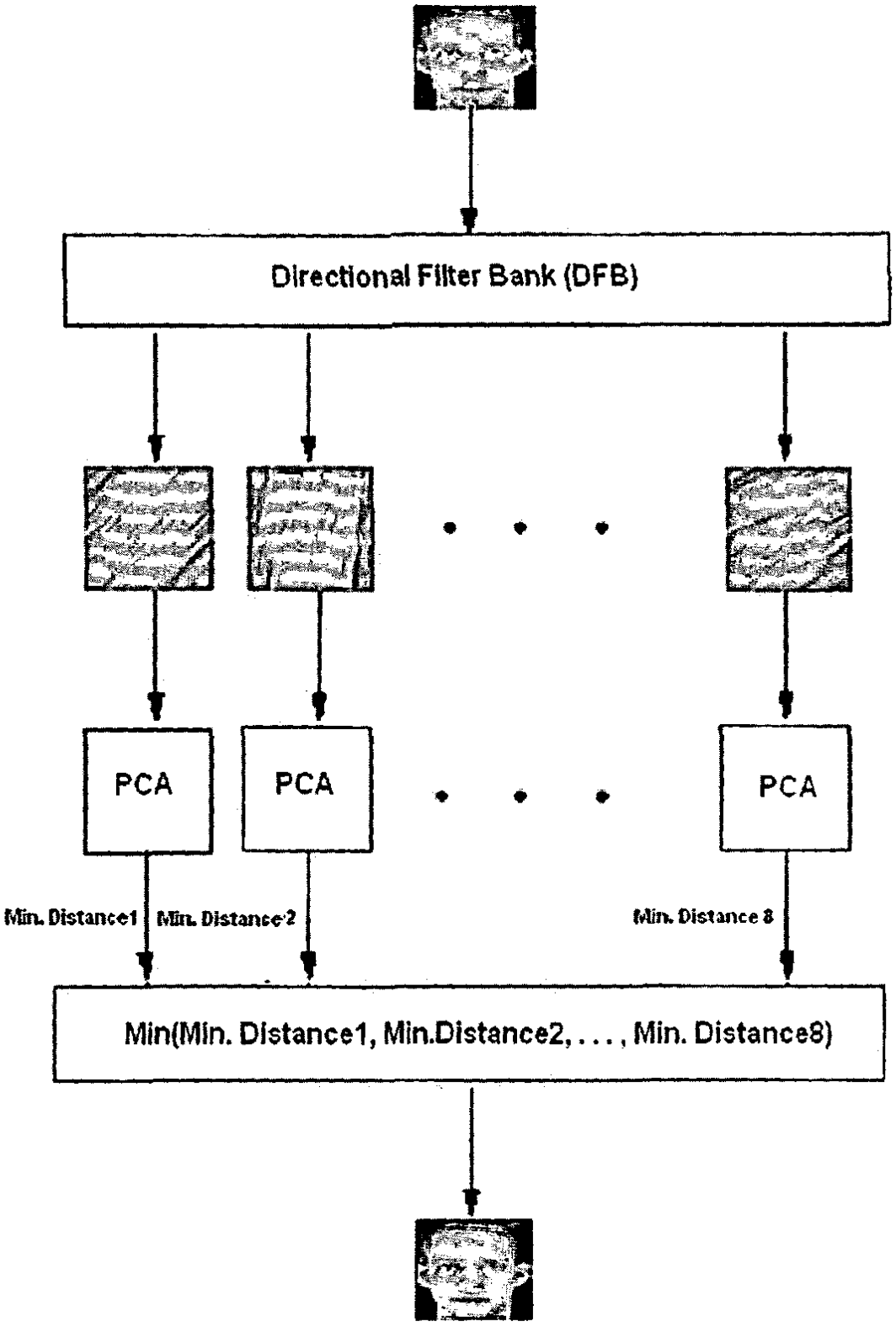

Figure 6.4 Block diagram of proposed system.

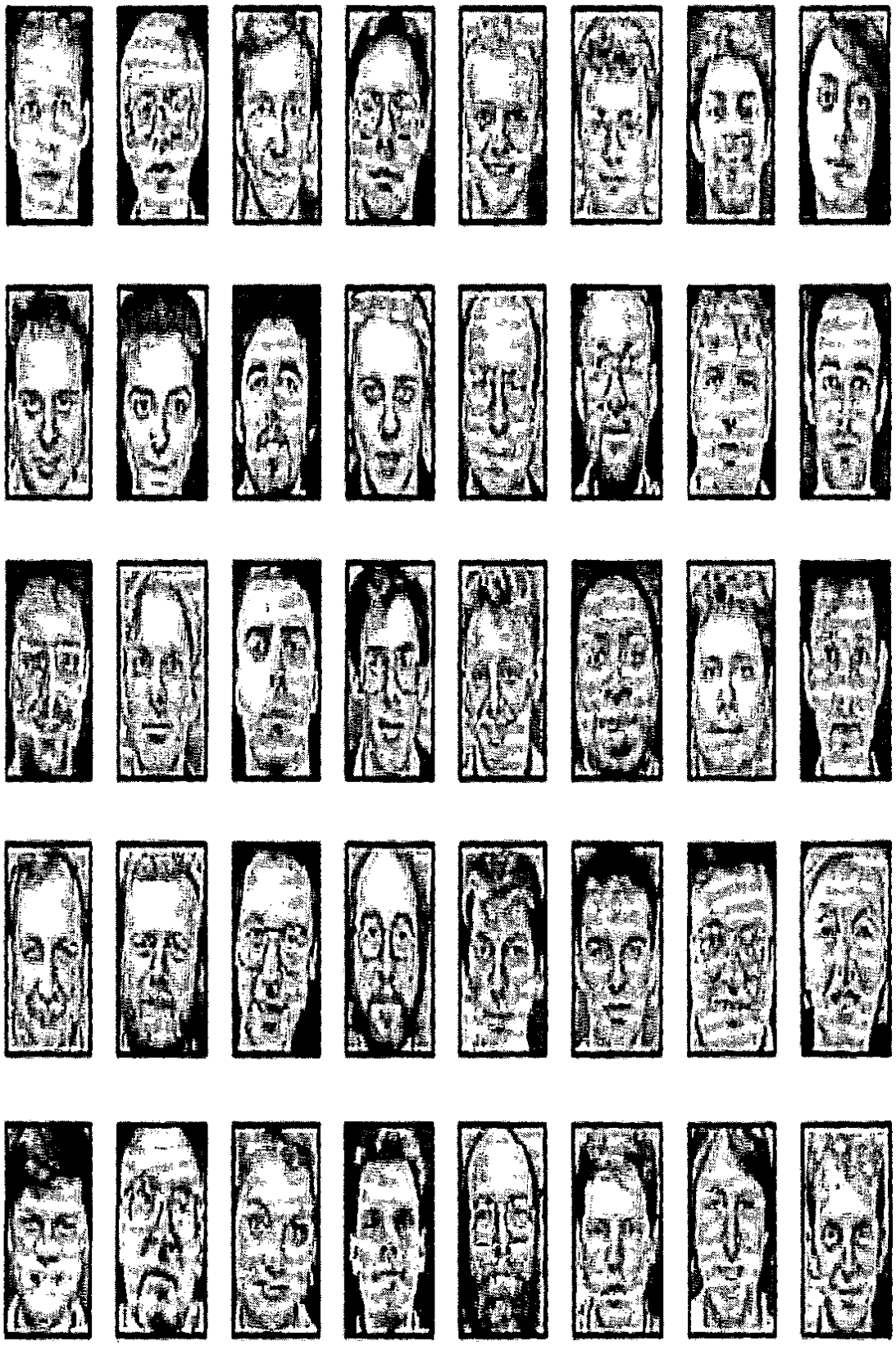

Figure 6.5 Face images of Olivetti dataset.

6.5 Simulation Results

Figure 6.6 shows three curves comparing PCA, DFB-PCA, Gabor filter bank-PCA (GFB-PCA). We see that Gabor filter bank-PCA performs well when the number of Eigenfaces were less than and equal to five but it is overshadowed by DFB-PCA as the number of Eigenfaces are increased. We can confirm the remarkable improvement of recognition rate of __21.25% whereas Gabor filter Bank-PCA gives 11% recognition rate against PCA when tested on Olivetti dataset. Further, when the number of Eigenfaces were less than and equal to five but it is overshadowed by DFB-PCA as the number of Eigenfaces are increased. We can confirm the remarkable improvement of recognition rate of 21.25% whereas Gabor filter bank-PCA gives 11% recognition rate against PCA when tested on Olivetti dataset. Further, this study investigated the question of which directional image is most effective input for PCA. The Figure 6.7 shows a bar diagram of various directional images. It can be seen that direction 8 is providing 66% recognition rate. This confirms the observation that directional image 8 is providing the optimal discriminating features.

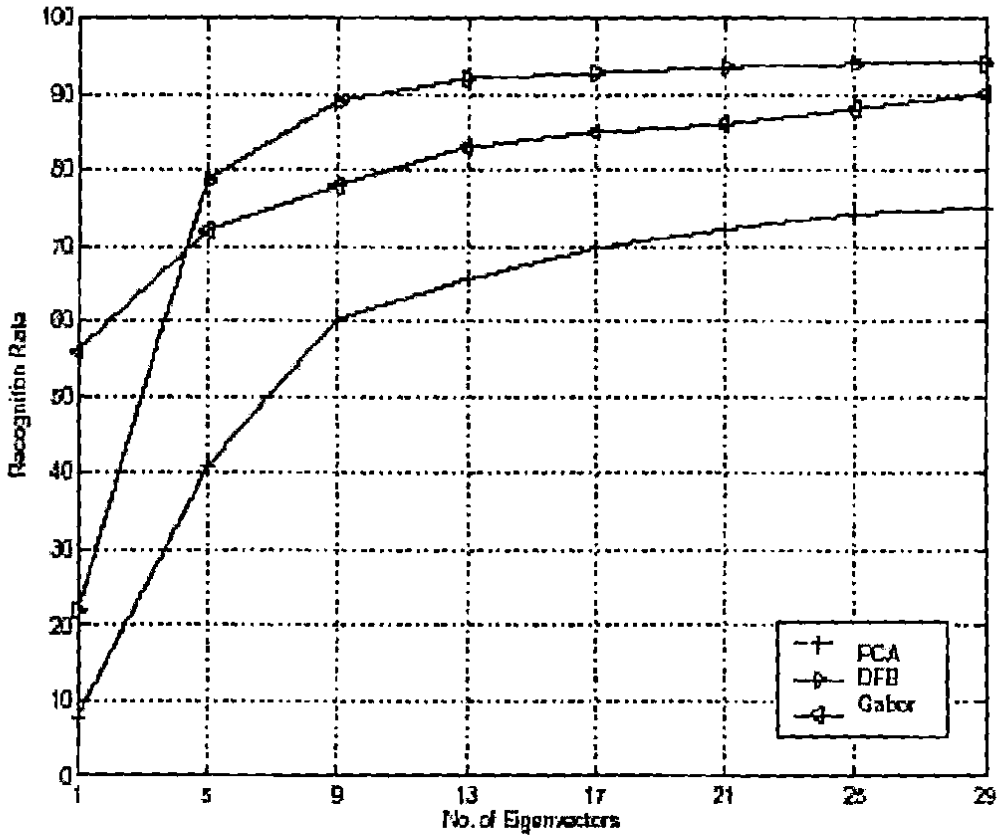

Figure 6.6 Comparison of PCA, DFB-PCA and Gabor filter bank-PCA.

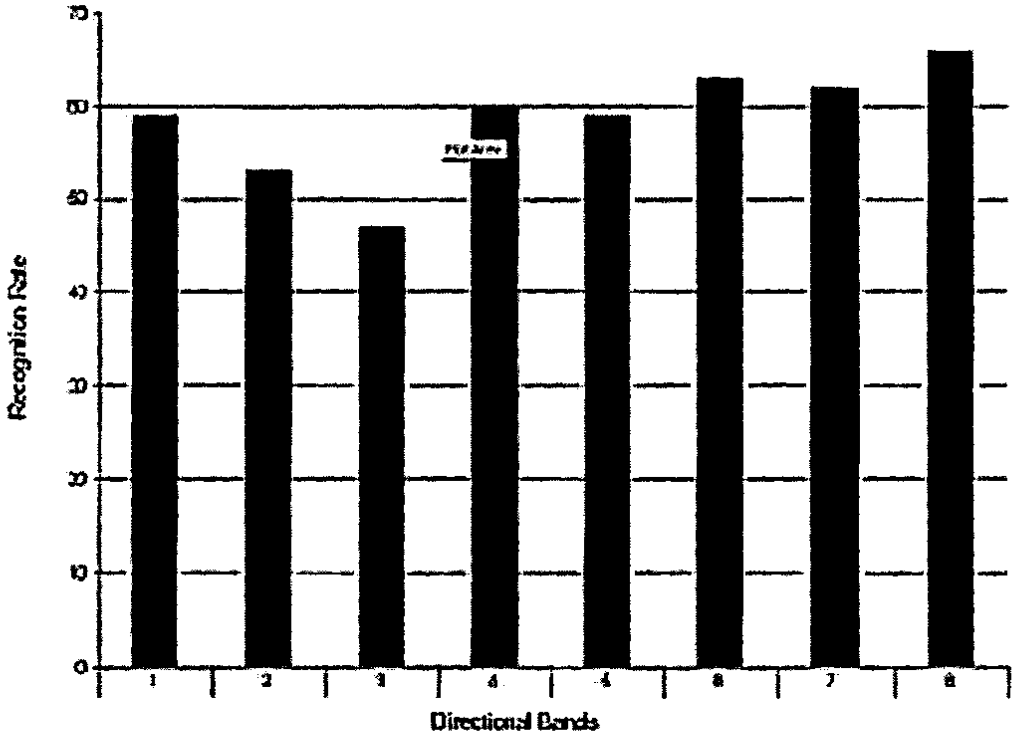

Figure 6.7 Bars showing contribution of various directional images for PCA

In this study, we have presented the face recognition system that combines Directional Filter Bank (DFB) and PCA. Because face images are very sensitive to illumination and pose variation, we anticipated that the drawback could be overcome by using DFB responses as an input of PCA. The experiment result was reasonably acceptable i.e. the directional images of DFB based on principal component vectors were successful in classification and discrimination.

Chapter-7

APPLICATION OF DECIMATION FREE DIRECTIONAL FILTER BANK TO FINGERPRINT IMAGE ENHANCEMENT

The identification of fingerprint images mainly requires matching the features of the fingerprint in question with those stored in a database. Since fingerprint identification system may receive noisy and distorted fingerprint image inputs, an efficient and robust enhancement of fingerprint images is essential for reliable fingerprint identification. In this paper, we propose a decimation-free directional filter bank (DFB) structure. It provides output in the form of directional images as opposed to directional subbands provided in previous DFBs [60,62]. The presence of directional images facilitates any further spatial processing if needed. However, we have to prepare a fingerprint image before it can be given as input to the proposed DFB structure due to the fact that fingerprints acquired are low in contrast. The preparation steps involve removing non-uniform illumination from the image. Then proposed DFB structure outputs directional images. The final enhanced result is constructed on a block-by-block basis by comparing energy of all the directional images and picking one that provides maximum energy.

7.1 Introduction

Directional analysis plays an important role in many areas and situations affecting actual life such as oil exploration, medicine, remote sensing and data analysis. There have been many proposed approaches for directional analysis in the past. The areas of applicability for this directional analysis cover almost all areas of 2-D and 3-D signal processing. Here our focus is on fingerprint images.

A fingerprint is the pattern of ridges and furrows on the surface of the fingertip. Fingerprints have been used as a means to identify individuals uniquely for a very long time, having many various purposes such as criminal identification, high security access control, credit card usage verification, and employee identification. The main reason for the popularity of fingerprints as a method of identification results forms the fact that each fingerprint of a person is unique as well as easy to access. The uniqueness of a fingerprint is exclusively determined by the local ridge characteristics and their relationships. Two most important ridge characteristics, called minutiae, are ridge ending and ridge bifurcation. Ridge ending is defined as a point where a ridge ends abruptly. A good quality fingerprint typically contains 40-100 minutiae. Examples of minutiae are shown in Figure 7.1.

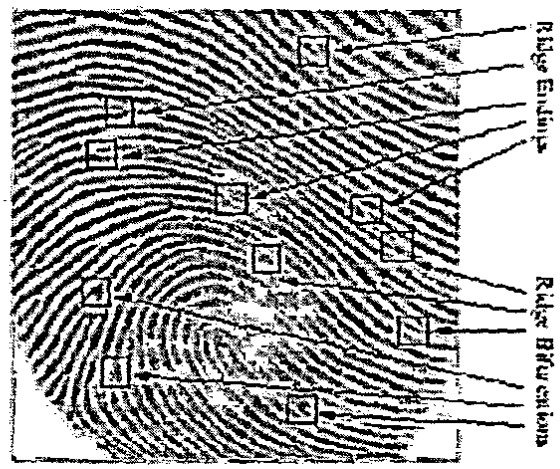

Figure 7.1 Fingerprint Image showing Local ridge characteristics

Apart from minutiae identification and extraction, high-level features can also characterize a given class of the fingerprint. The important high-level features are the core and the delta points. Based on core and delta points fingerprint images can be classified into four different pattern classes. These classes include Arch, Tented Arch, Loop (left and right) and Whorl. Figure7.2 provides some pictorial examples of high-level features.

Automatic fingerprint matching depends on the comparisons of either local ridge characteristics or the high level characteristics to make a personal identification.

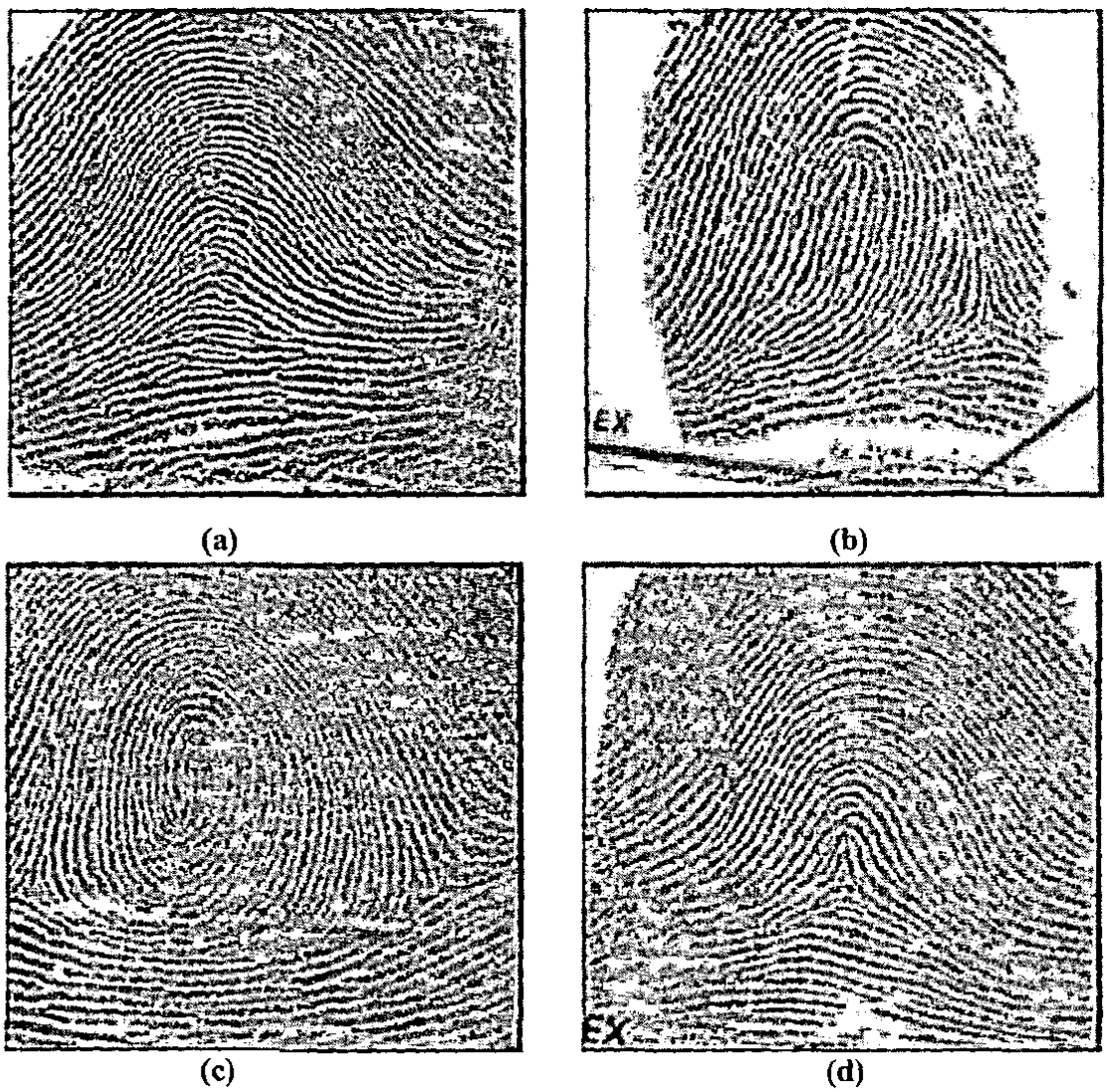

Figure 7.2 High-level features of fingerprints a) Arch. b) Loop c) Whorl. d) Tented Arch.

A critical step in fingerprint matching in both cases is to reliably extract features from the input fingerprint images. The performance of fingerprint identification mechanism relies heavily on the quality of the input fingerprint images. However, in practice due to variations in impression conditions, ridge configurations, skin conditions, acquisition devices, and non-cooperative attitude of the subjects, a significant percentage of acquired fingerprint images are of poor quality. In order, to ensure that the performance of the identification algorithm

will be robust with respect to the quality of the input digital fingerprint images, enhancement algorithms are needed which can improve the clarity of the ridge structure.

Various fingerprint enhancement techniques have been proposed in the literature. A fingerprint enhancement method based on directional Fourier domain filtering is presented [27], where direction of the pixel has been identified and then the image is being filtered and combined to get an enhanced image. The method was further improved [93], where direction calculation for a given pixel has been improved by using computationally efficient Gabor Filtering technique. However, the technique heavily depends on local direction finding mechanism which is prone to noise. An image analysis based on directional filter banks has been proposed and applied to fingerprint enhancement [60]. Later on, a visualizable directional filter bank [62] was used in correcting linear deformations in a given fingerprint image. Directional filter bank based fingerprint image enhancement was also proposed [74,94].

In this chapter, we proposed a new directional filter bank based fingerprint enhancement algorithm. The difference between the proposed algorithm and the previous techniques is the fact that we utilize directional images rather than directional sub-bands. The advantage of using directional images is that our enhancement works in the same domain as the images themselves. This helps us in using neighborhoods as compare to pixel by pixel approach used in previously suggested directional filter bank based techniques. In the sections that follow we will develop the theory of decimation free directional filter bank structure, discuss the creation of directional images, and then reconstruction of the final enhanced image.

7.2 Fingerprint Image Enhancement

A fingerprint image enhancement algorithm receives an input fingerprint image, applies a set of intermediate steps on the input image and finally outputs the enhanced image. The main steps of algorithms are as follows. We begin with a test image shown in Figure7.3 and apply various processing steps sequentially.

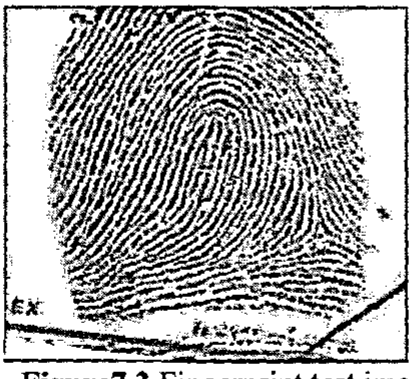

Figure7.3 Fingerprint test image

7.2.1 Non-Uniform Illumination Correction

An input fingerprint image has a varying illumination pattern that needs to be removed. Although, there are many spatial domain techniques available to get rid of non-uniform illumination structure. We opted for Homomorphic filtering to extract non-uniform

illumination of the input fingerprint image. An image a (x, y) can be expressed as a product of illumination and reflectance components i.e.

$$a(x,y) = i(x,y)\, r(x,y).$$

By taking the natural logarithm of input image a(x , y) in the spatial domain we have transformed the image into sum of its illumination and reflectance parts. This is shown in equation form as below:

$$z(x,y) = \ln\{ i(x,y) \} + \ln\{ r(x,y) \}.$$

This is followed by taking discrete Fourier transform (DFT) of the logarithmic image. Now based on the fact that illumination is a slowly-varying pattern that will appear as low frequency content in the Fourier domain. Therefore, we applied a non-ideal Butterworth Lowpass filter to extract the Lowpass region of the image. The transfer function of a Butterworth Lowpass filter of order n, and with cut off frequency D_0 at a distance from the origin is defined as:

$$H(x,y) = \frac{1}{1 + \left[D(x,y) / D_0 \right]^{2n}}$$

Where, D(x , y)is a radial distance from the origin. After filtering the image and inverse DFT has been applied to transform the filtered image from Fourier domain back to spatial domain. Finally, illumination pattern present in an image can be obtained by taking exponential of the resulting output in the spatial domain. The extracted illumination pattern can be subtracted from the test image to obtain a uniformly illuminated image as shown in Figure 7.4.

(a) (b)

Figure7.4 Illumination Adjustment: a) Non- uniformly illuminated image. b) Uniformly illuminated image.

7.3 Creation of Directional Images

This section has been divided into two sections.

7.3.1 Design of Directional Filters

The directional analysis employed in this section decomposes the spectral region of a given image into wedge-shaped passband regions. It is easily shown that these wedge-shaped regions correspond to directional components of an image. The filters related to these wedge-shaped regions are commonly referred to as fan filters.

The schematic diagram of our proposed structure is shown in Figure 4.2. The structure is in the form of a tree with two-band splits at the end of each stage, where each split increases the angular resolution by the factor of two. The first stage employs the complimentary hour-glass filters. The filters for next two stages are obtained by linear transformation of the first stage hour-glass filters. For implementing linear transformation, the uni-modular matrices M and R are utilized. The rules for the selection of these matrices are presented [62]. Once the filters for each stage are implemented, we can combine them on branch by branch basis to get the required fan filters as shown at the end of third stage in Figure 4.2.

One important difference between present proposed structure and DFB structure [62], is the absence of decimator. It was pointed out [60] that if sub-bands need to be processed for directional energy estimates, the decimation present in the conventional filter bank structure poses problem. This means that two samples located at the same spatial index (n_1 , n_2) in two different sub-bands i and j, will not necessarily correspond to same spatial region in the original image. This problem was circumvented [60] by employing nearest-neighborhood or bilinear interpolation to make all sub-bands of the same size. However, in our structure, decimators at each stage are taken out and filters are designed by linear transformation in the frequency domain to get fan filters. Furthermore, to avoid ringing artifact in the output, ideal fan filters are avoided by employing non-ideal hour-glass filters using an FIR Lowpass filter [95].

7.3.2 Directional Images

Directional images are obtained by applying all directional filters constructed in above section. Four of these directional images are shown in Figure 7.5. These directional images can be regarded as decomposition of the original image in eight pieces based on direction. Directional images contain features associated with global directions rather than local directions. By creating directional images we have divided noise of the original image into eight different directions.

7.4 Noise Removal

Noise removal is accomplished by first calculating the block based directional energy of each directional image. The directional energy of a block (X , Y) including the pixel (x , y) from the kth directional image is calculated as:

$$E_k(X,Y) = \sum_{x=0}^{m_k} \sum_{y=0}^{n_k} \left| f_k(X,Y;x,y) \right|$$

where, f k is the directional image. The noise free directional images represented by A_k are obtained by the equation.

$$A_k = \begin{cases} f_k(X,Y;x,y) & \text{if } E_k(X,Y) > T \\ F_k(X,Y;x,y) & \text{if otherwise} \end{cases}$$

Here, T represents the threshold. Figure 7.6 shows four of eight noise free directional images. Comparing these images with Figure 7.7 shows that noise has been cleaned where as features are preserved

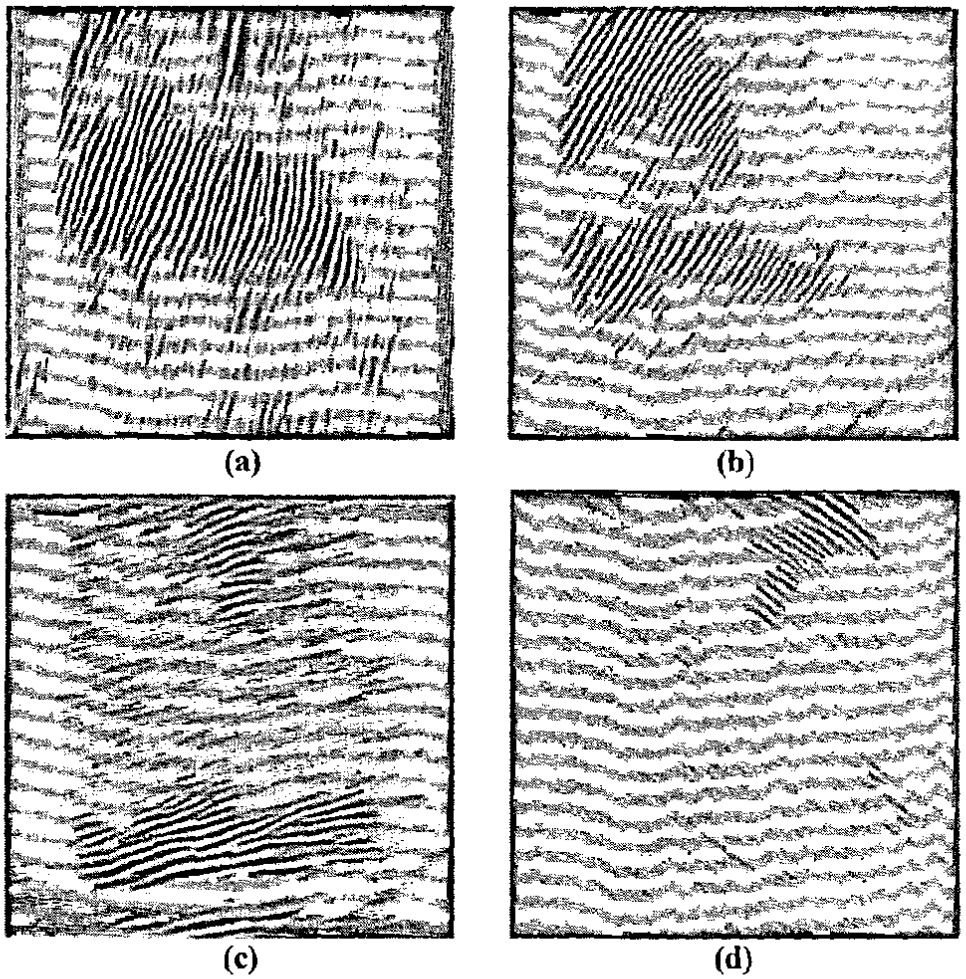

Figure7.5 Creation of directional image: a) Ridges having direction in the range 67.5-90 degrees. b) Ridges having direction in the range 45-67.5 degrees. c) Ridges having direction in the range 0-22.5 degrees. d) Ridges having direction in the range 135-157.5 degrees.

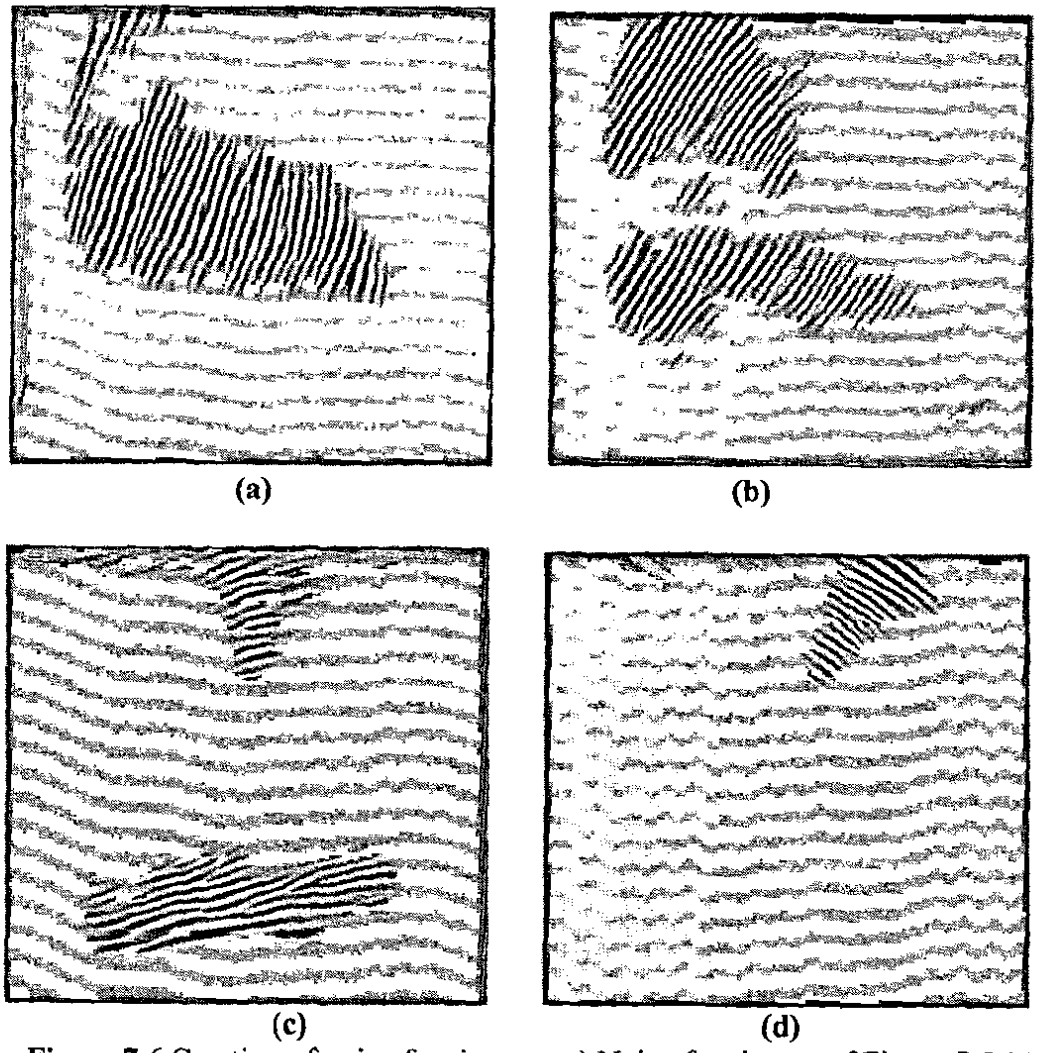

Figure 7.6 Creation of noise-free images: a) Noise-free image of Figure 7.5 (a). b) Noise-free image of Figure 7.5 (b). c) Noise-free image of Figure 7.5 (c). d) Noise-free image of Figure 7.5

7.5 Reconstruction of Enhanced Image

Enhanced image is constructed from the directional images according to the following equation:

$$f_{hf}(X, Y) = \max_{1 \le i \le 8} f_i(X, Y),$$

Where, f_{hf} is high-frequency output image from directional filter bank and f_i represents ith directional image. For every block (X , Y) of the original image we select a replacement from the eight directional images based on maximum directional energy. The final enhanced fingerprint image obtained is shown in Figure 7.7. Comparing the result with the original image shown in Figure 7.3 reveals that all the ridge structure is intact while the spatial noise has been cleaned substantially. Figure 7.8 and 9 show the results of binarization of the original image and that of the enhanced image, respectively. We see that enhanced fingerprint image results in a binary image with clear ridges and valleys.

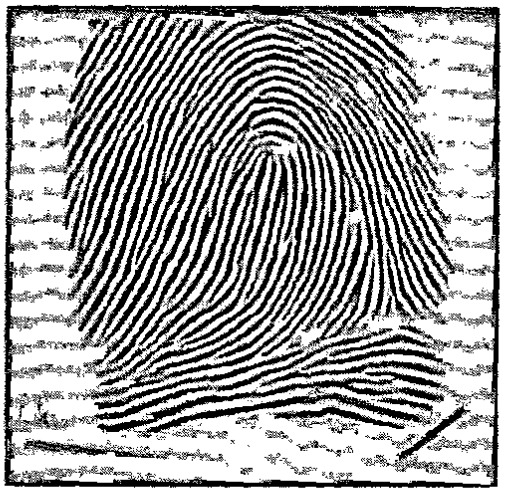

Figure7.7 Enhanced result

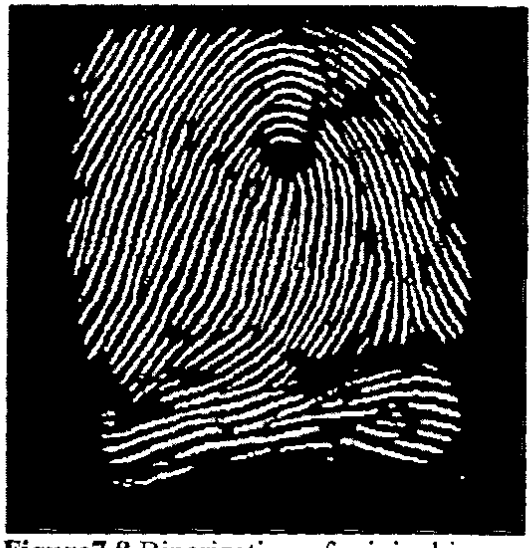

Figure7.8 Binarization of original image

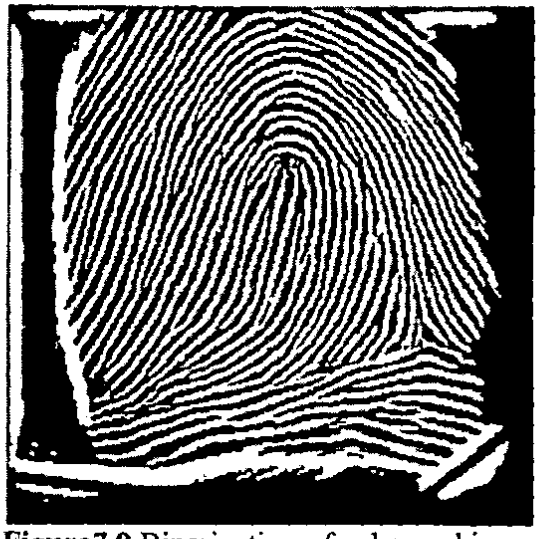

Figure7.9 Binarization of enhanced image

Chapter-8

RESULTS

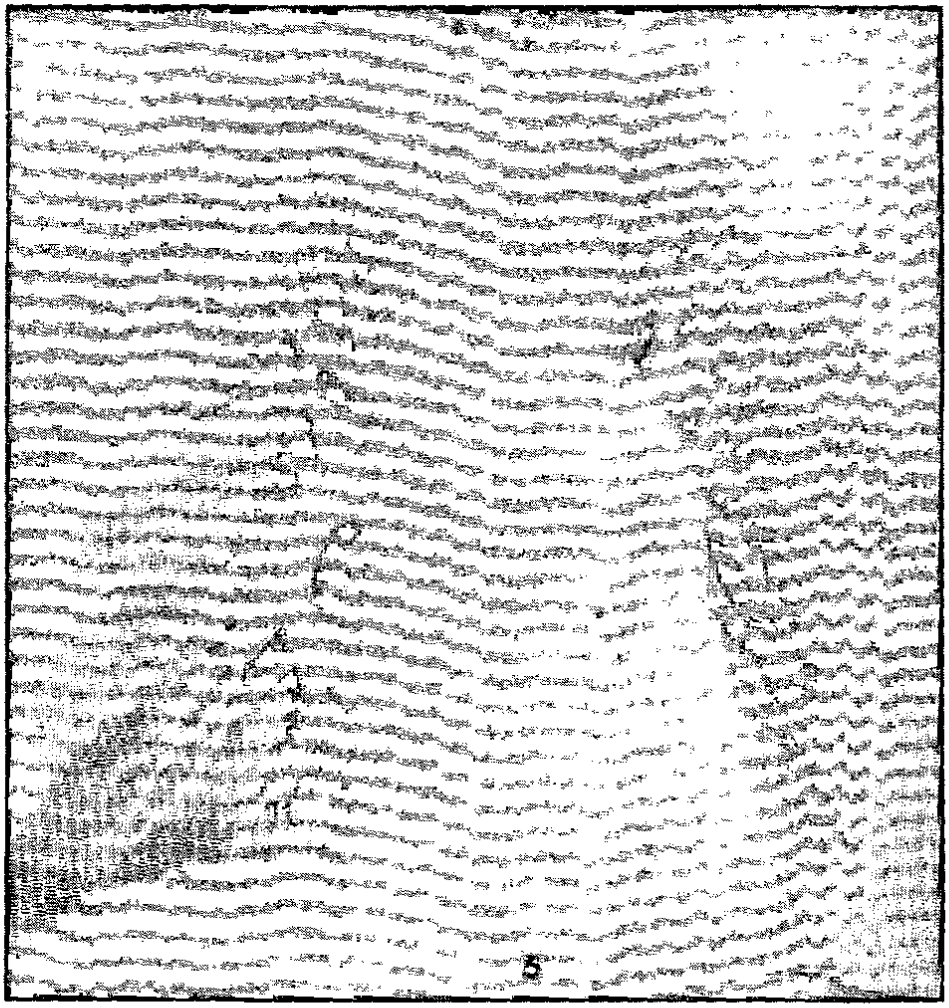

(a)

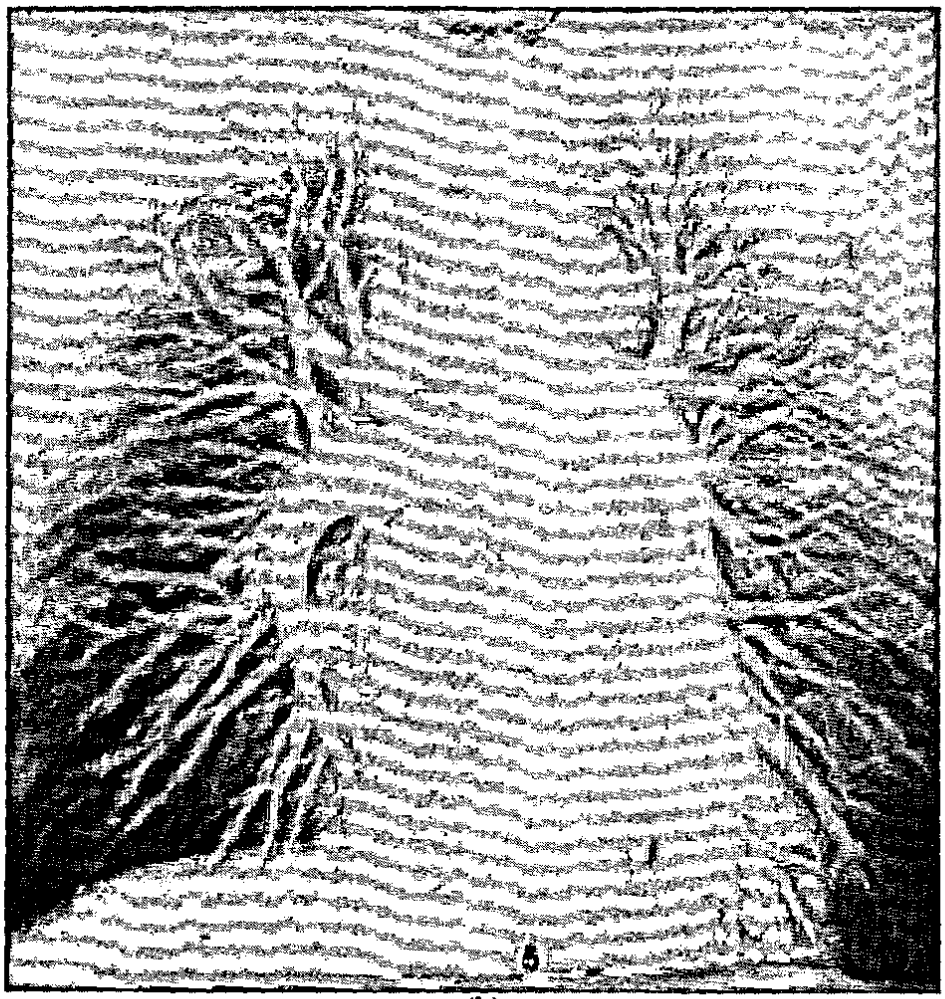

(b)

Figure 8.1 Medical Image Enhancement a) Original Image b) Enhanced Image.

(a)

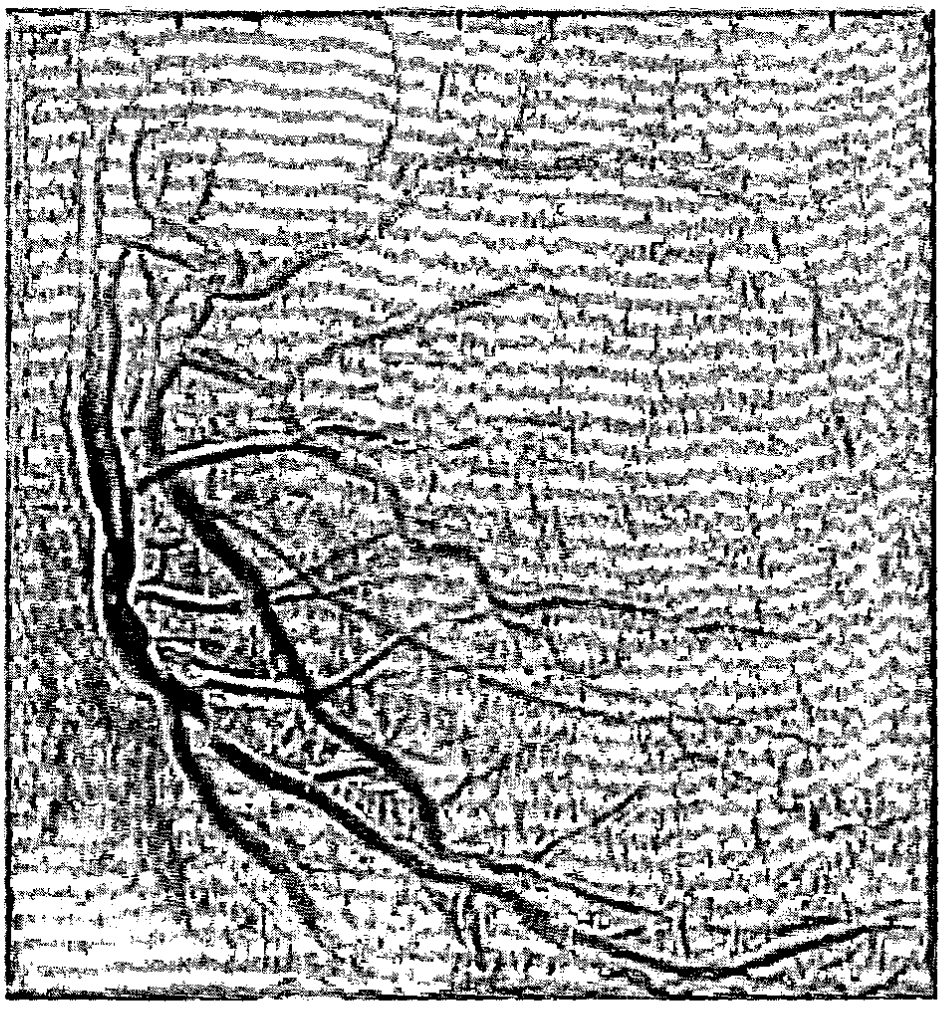

(b)

Figure 8.2 Medical Image Enhancement a) Original Image b) Enhanced Image.

(a)

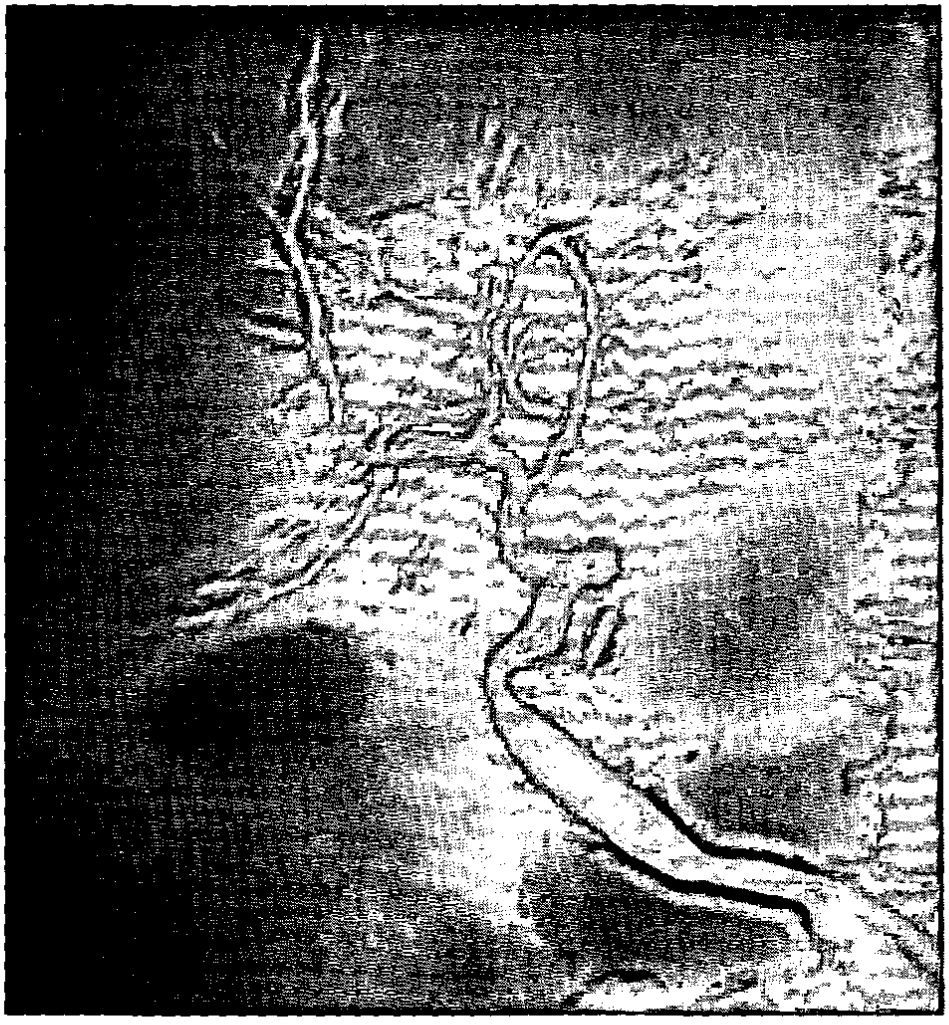

(b)

Figure 8.3 Medical Image Enhancement a) Original Image b) Enhanced Image.

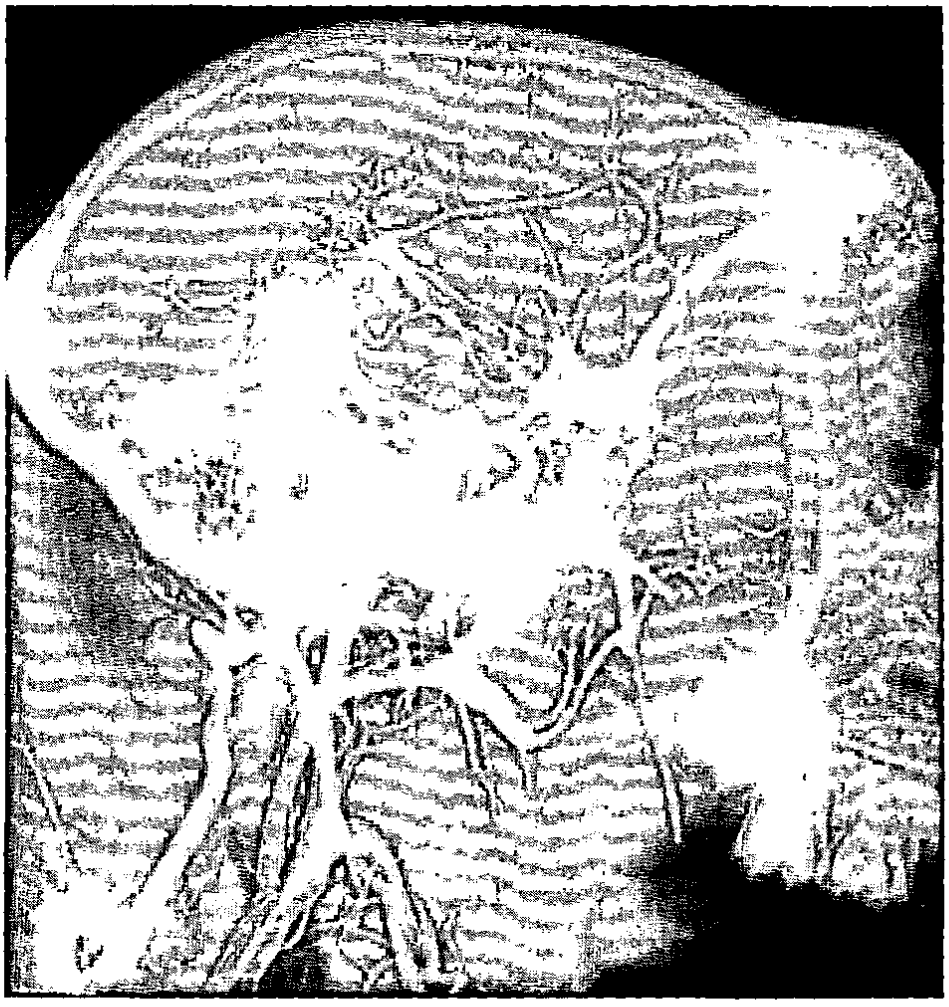

(a)

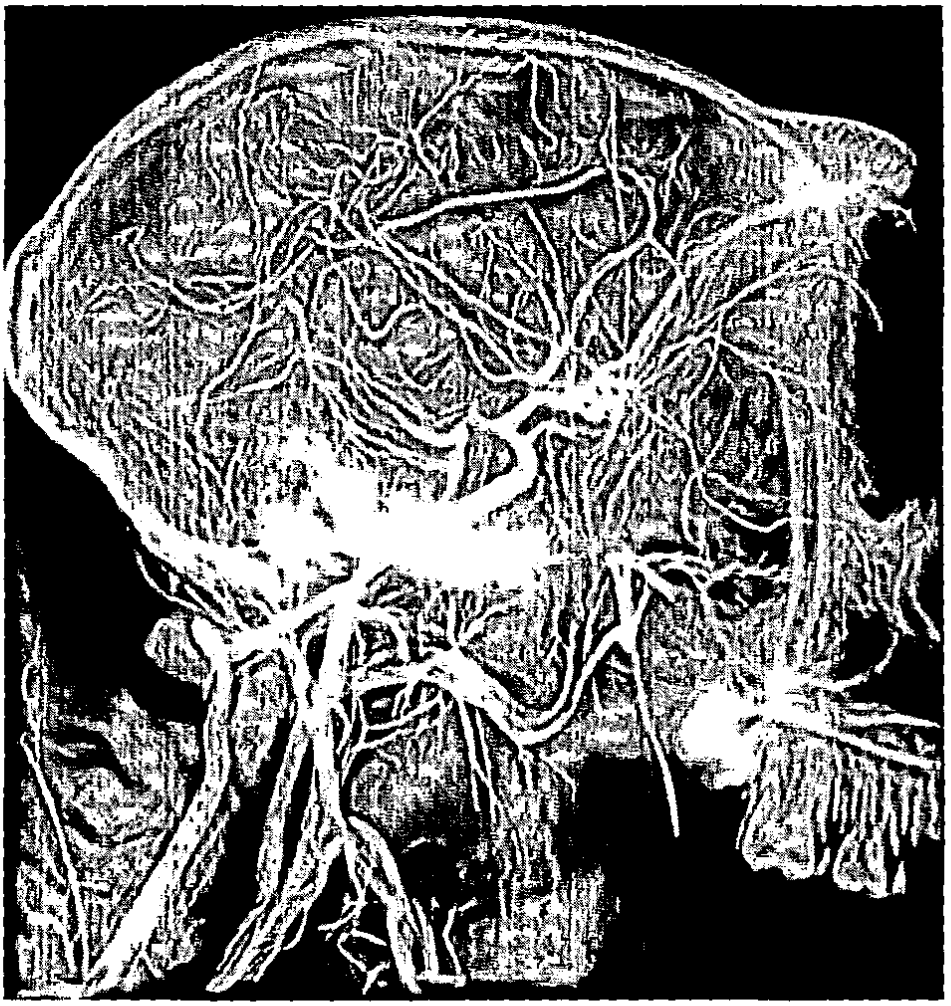

(b)

Figure 8.4 Medical Image Enhancement a) Original Image b) Enhanced Image.

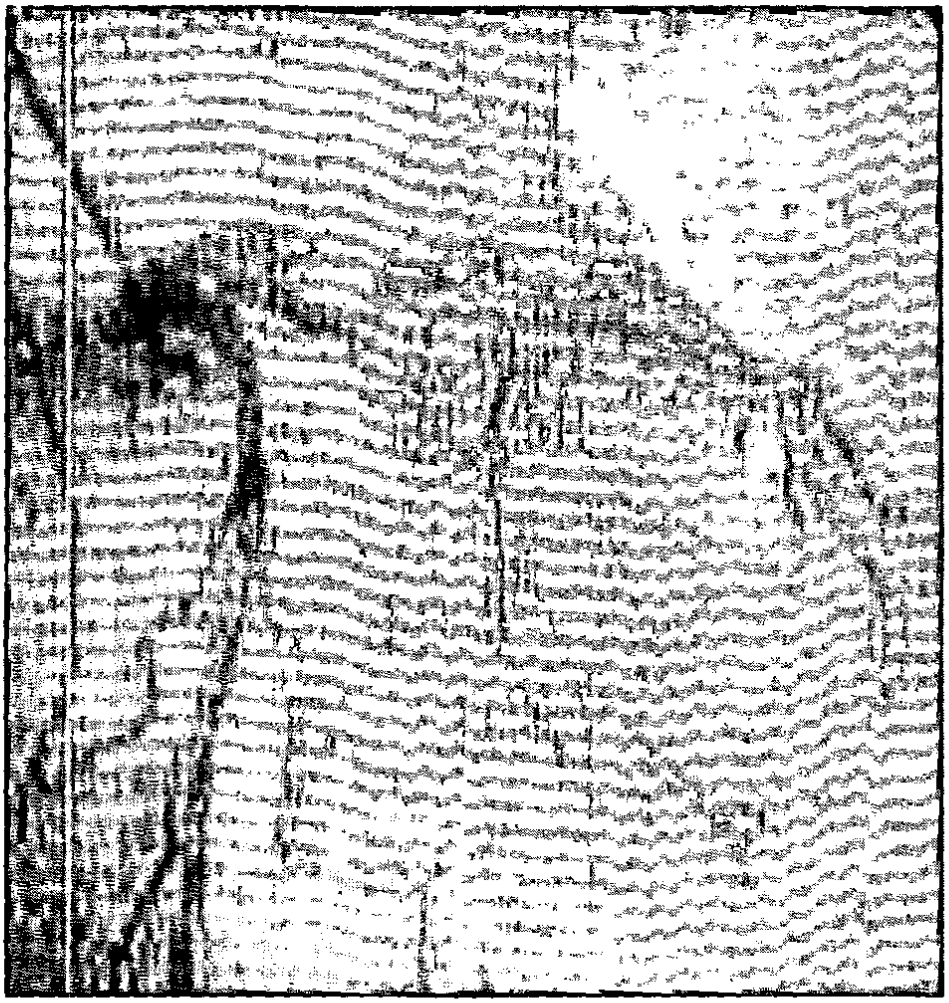

(a)

(b)

Figure 8.5 Medical Image Enhancement a) Original Image b) Enhanced Image.

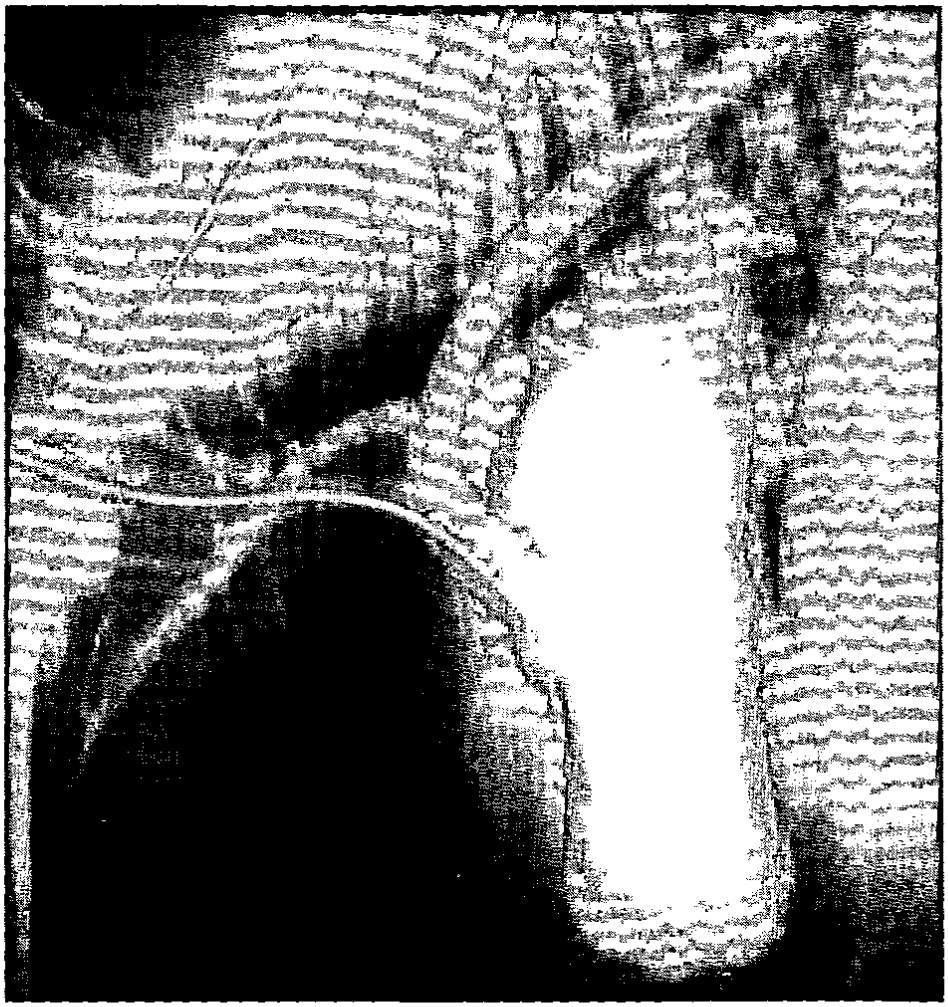

(a)

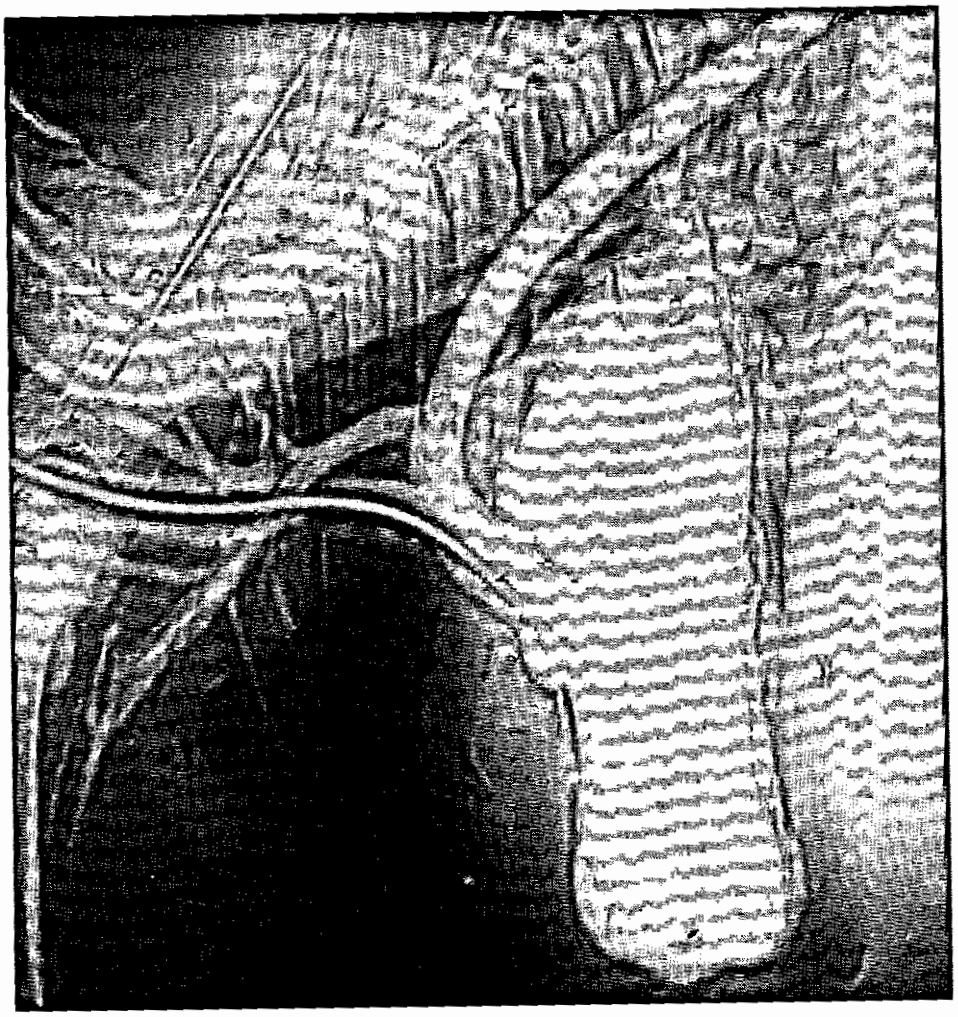

(b)

Figure 8.6 Medical Image Enhancement a) Original Image b) Enhanced Image.

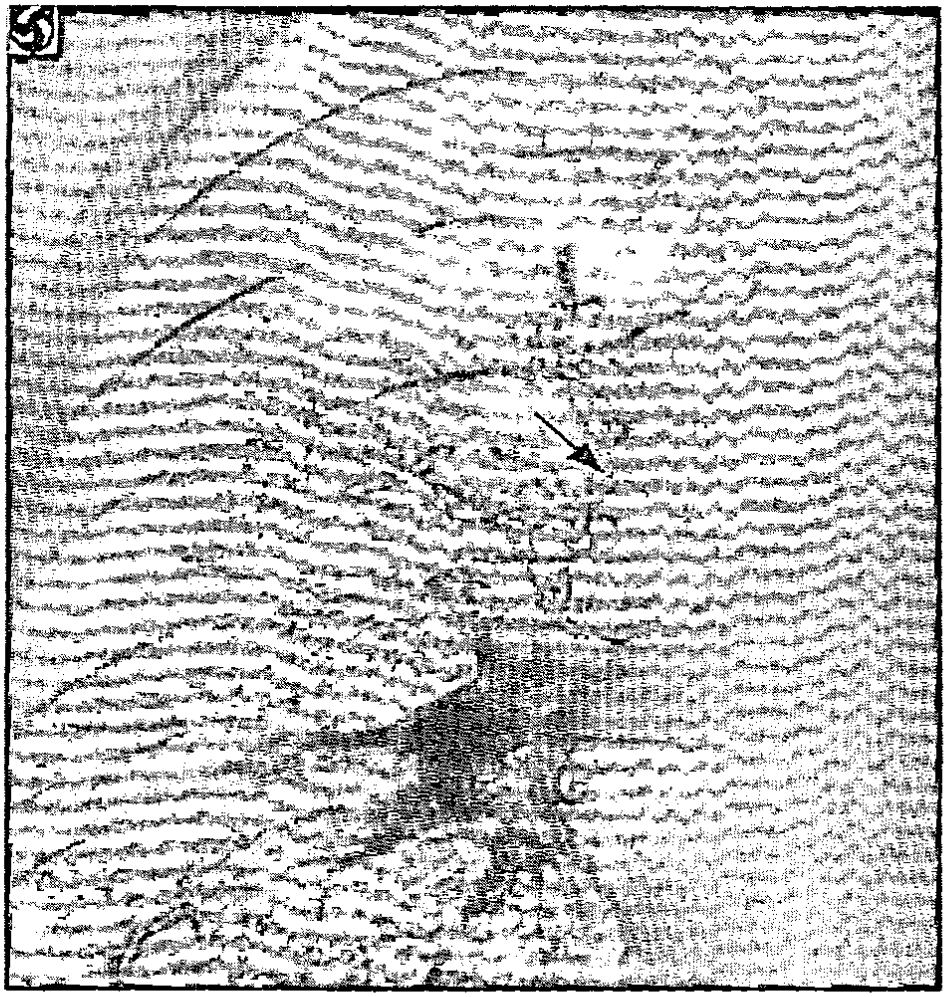

(a)

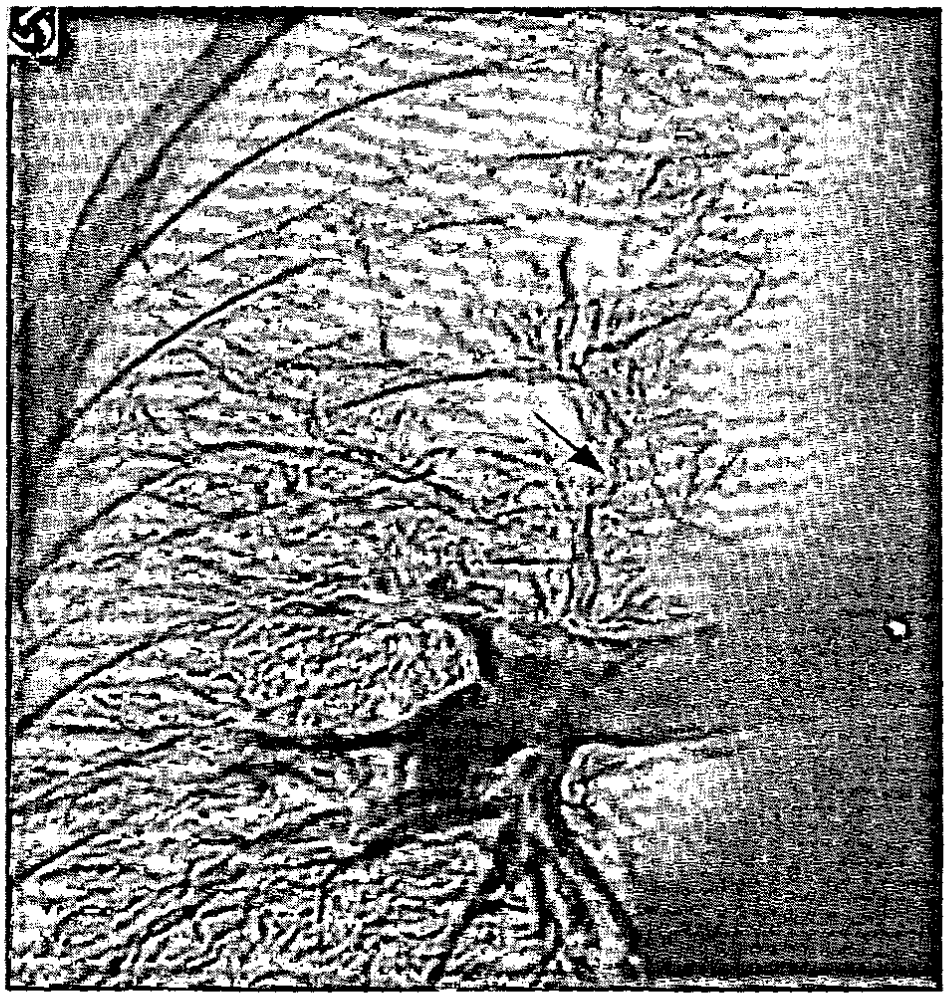

(b)

Figure 8.7 Medical Image Enhancement a) Original Image b) Enhanced Image.

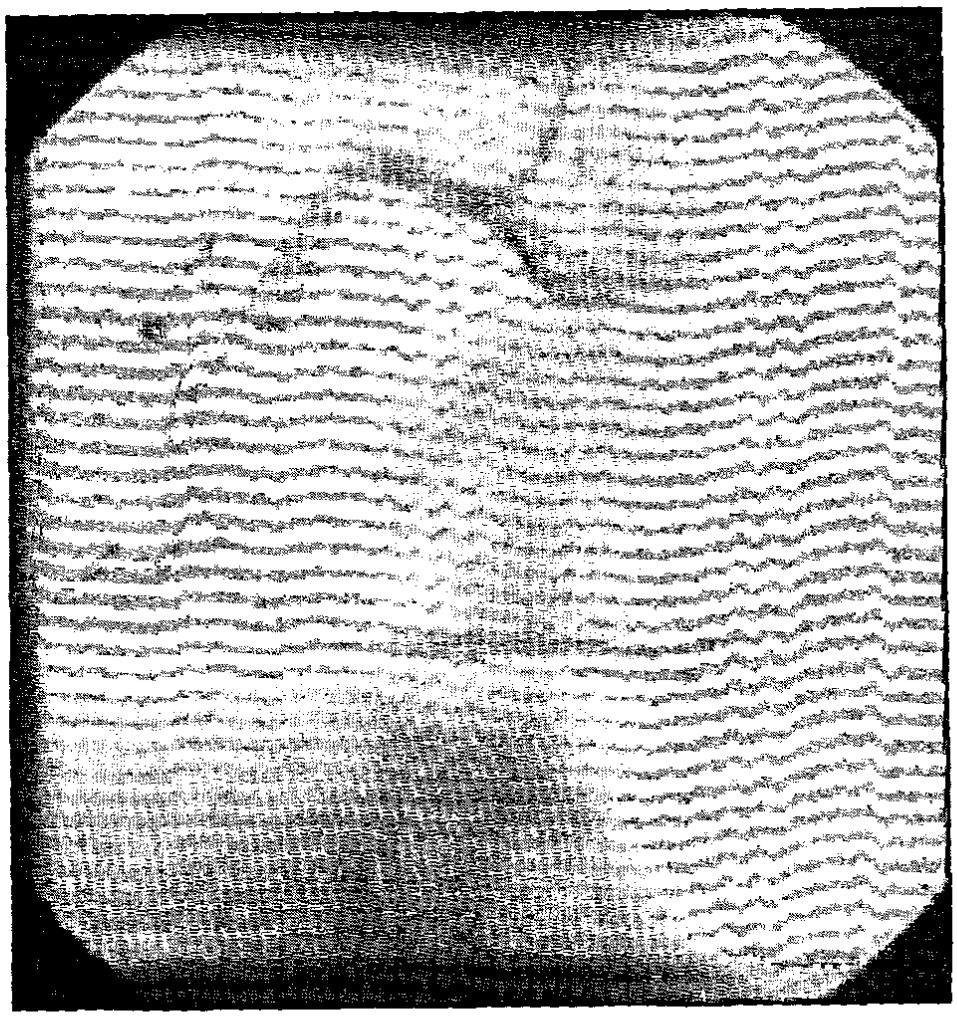

(a)

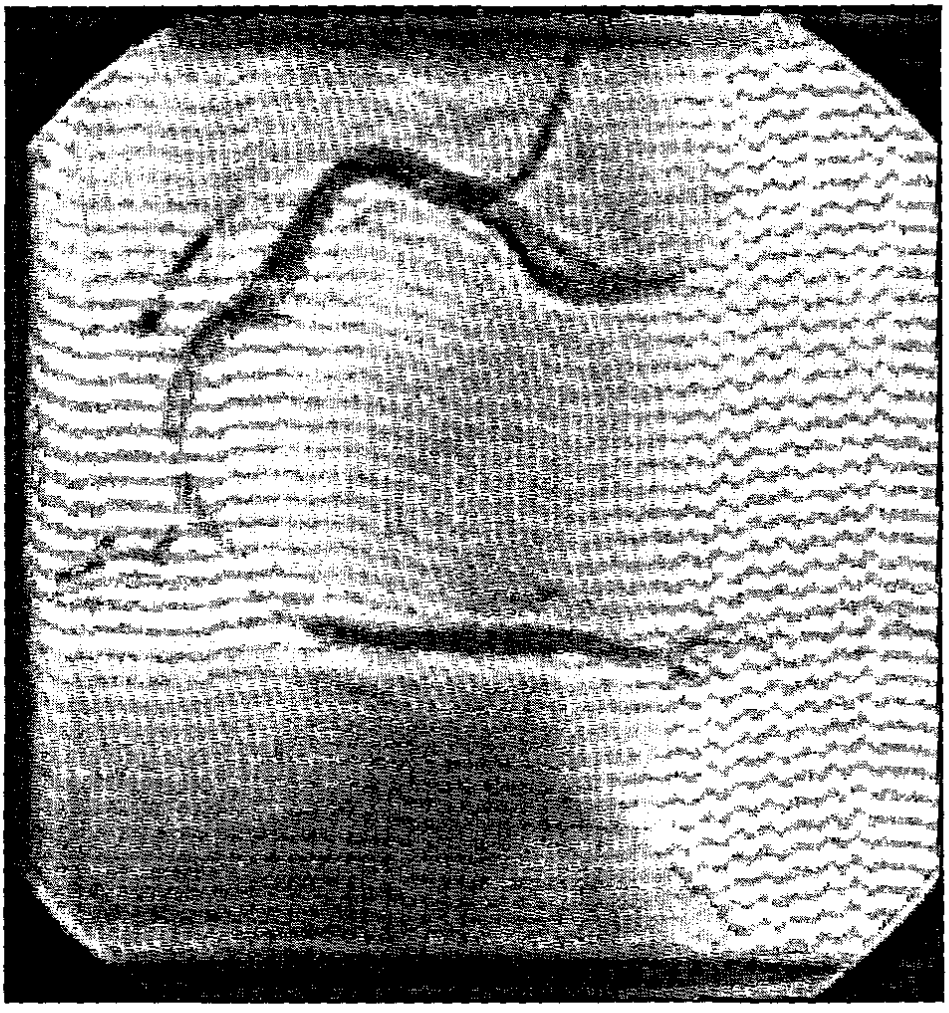

(b)

Figure 8.8 Medical Image Enhancement a) Original Image b) Enhanced Image.

Chapter-9

CONCLUSION

This thesis has explored the nature and use of decimation directional filter bank, particularly with respect to their creation, applications in image enhancement, face recognition, and fingerprint image enhancement. During the course of research performed for this thesis, a decimation free directional filter bank structure was proposed and developed, and new applications for existing areas that need directional analysis were found and examined.

9.1 Contributions

The contributions of the thesis are outlined below.

9.1.1 Decimation Free Directional Filter Bank Theory

- A decimation free directional filter bank based on Tree, and Parallel structure was developed during the course of this research.
- Directional images which are output of decimation free directional filter bank have same sizes as an input image, resulting in removal of interpolator required in the previous approach.
- Reconstruction from the directional images is accomplished by just adding all the directional images.
- Phase introduced during the filtering is no more required as the addition of all the images gives reconstruction. So, zero phase structure is designed.
- Each pixel position is comparable with the pixel present in any of the directional image, which was not the case with the previous approach.

9.1.2 Decimation Free Directional Filter Bank Applications

Decimation free directional filter bank is used for the very first time for medical image enhancement. The previous researchers has not used directional filter bank due to the fact that they require interpolation for comparison purpose, and interpolation is always an approximation.

Also it has been used for the face recognition purpose with principal component analysis, and it fifty percent better result than Gabor filtering technique.

Decimation free directional filter bank is also tuned to enhance fingerprint image, and to remove linear discontinuities form the image.

9.2 Future Work

We are trying to replace principal component analysis with directional filter bank and than feed it as an input to FLD (Fisher Linear Discriminant) for the face recognition purpose.

We are also planning to work on signature verification through decimation free directional filter bank.

APPENDIX A

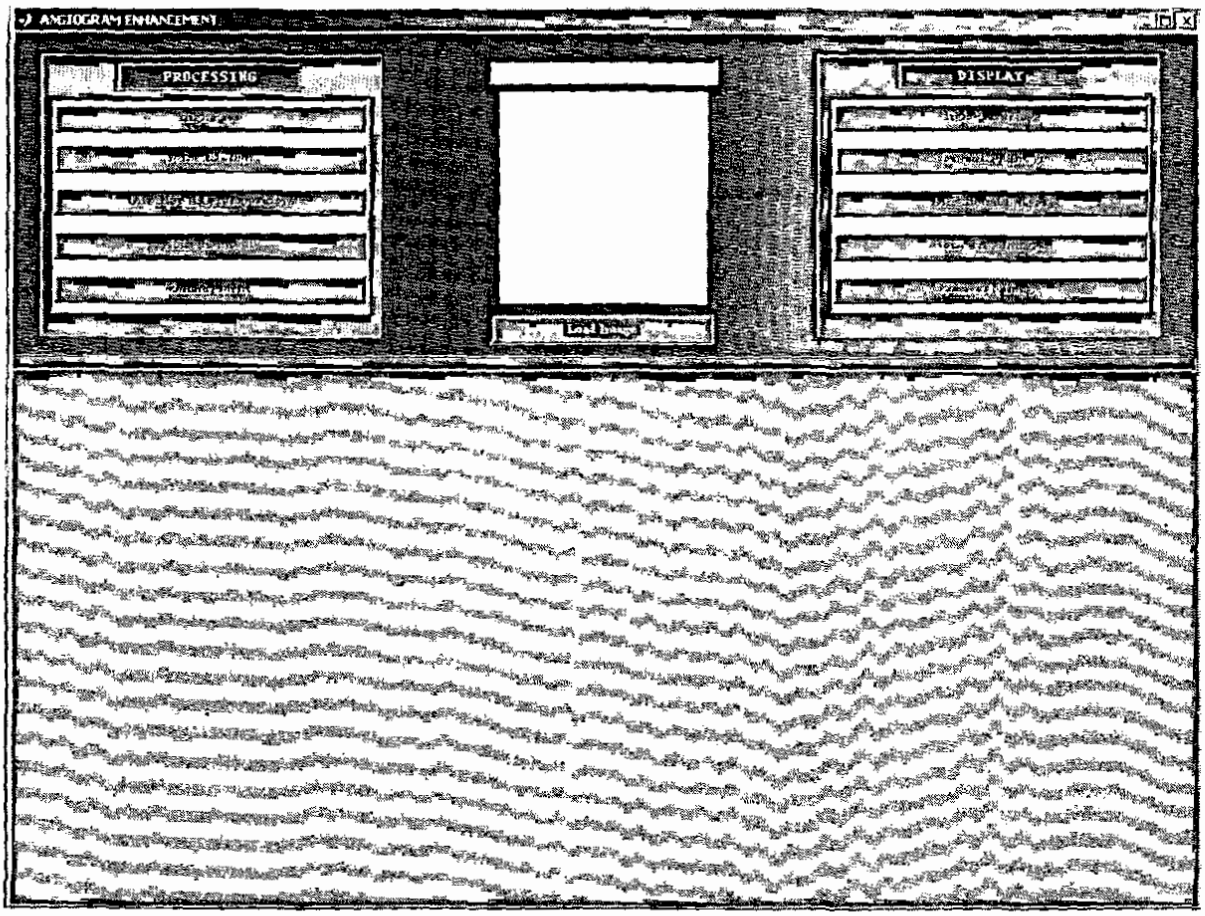

Figure A-1 Main Interface Screen of Medical Image Enhancement System.

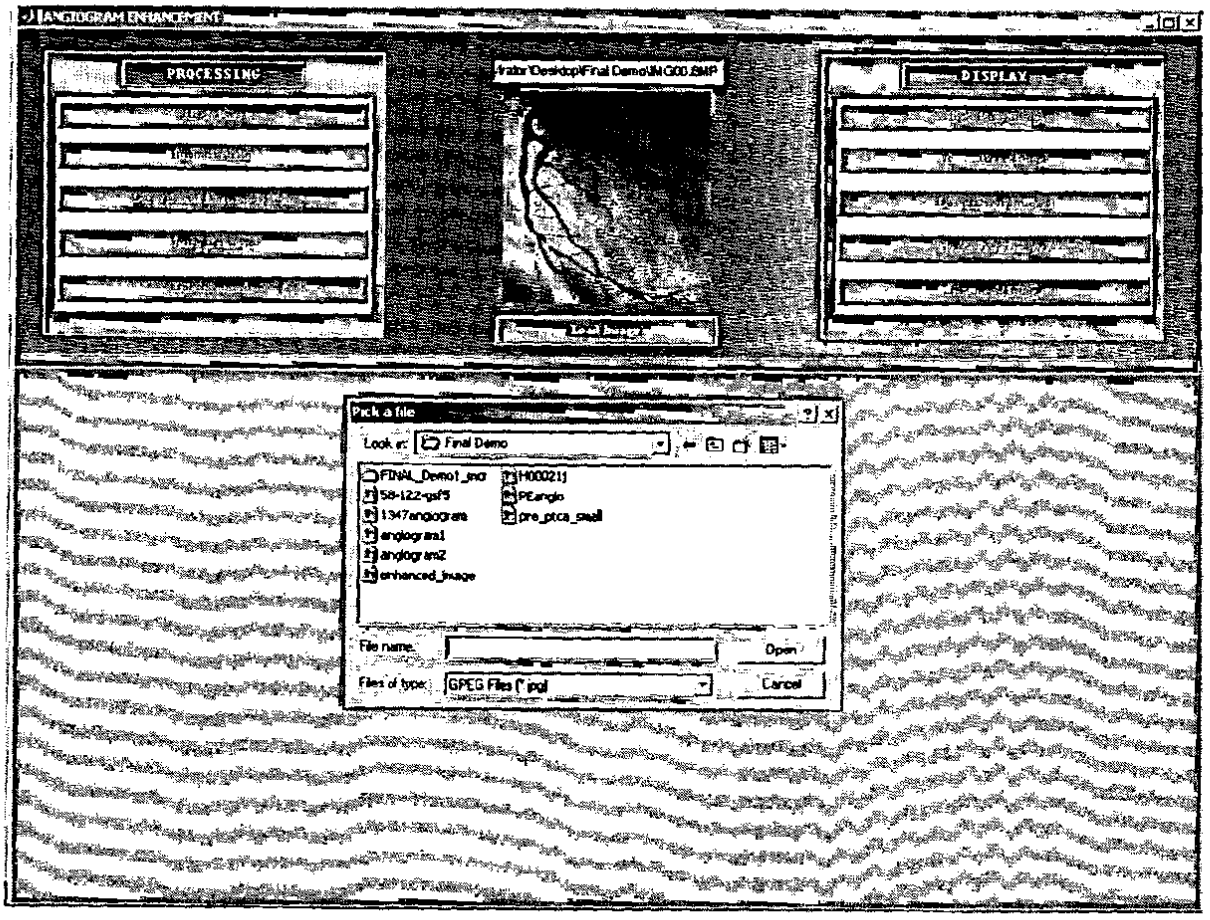

Figure A-2 Interface for Loading Medical Image.

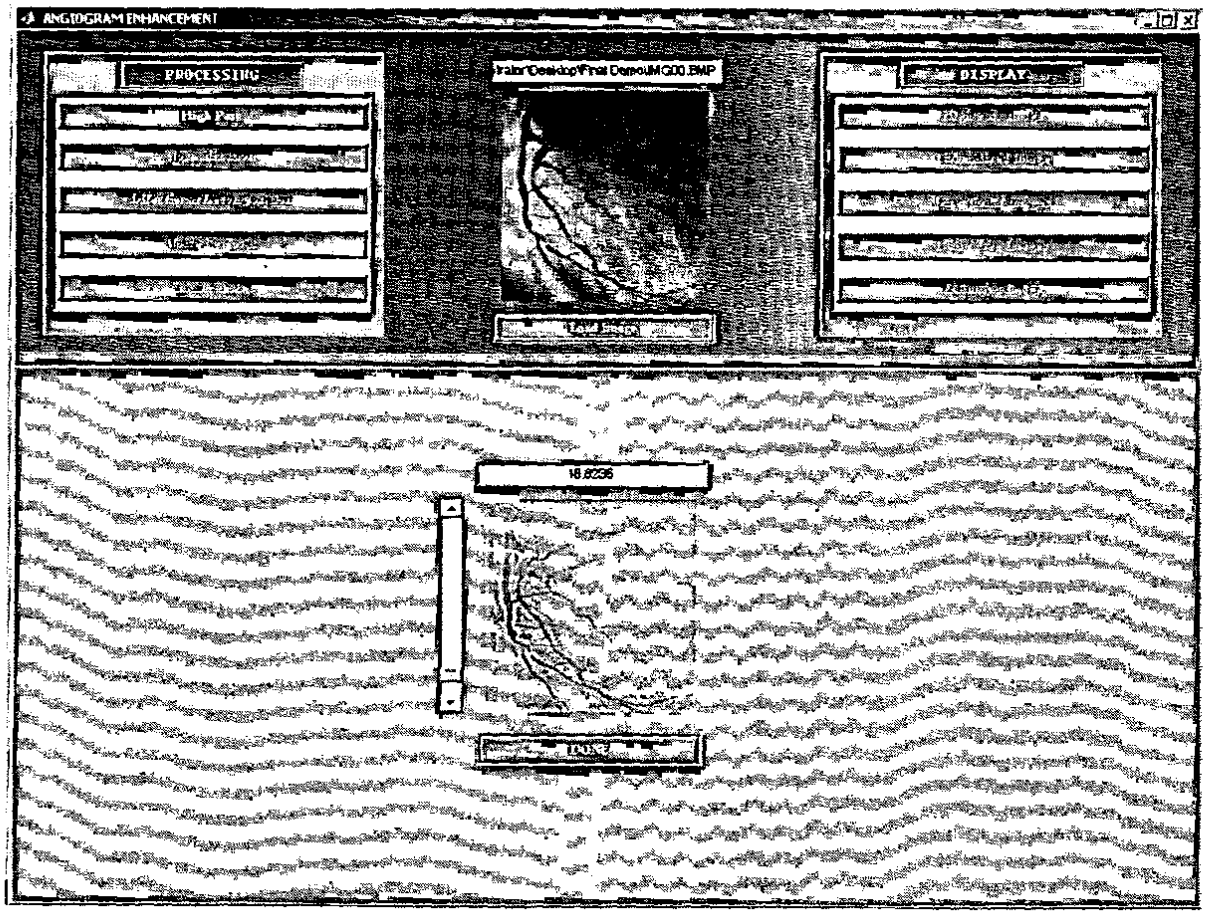

Figure A-3 High Pass of Original Image.

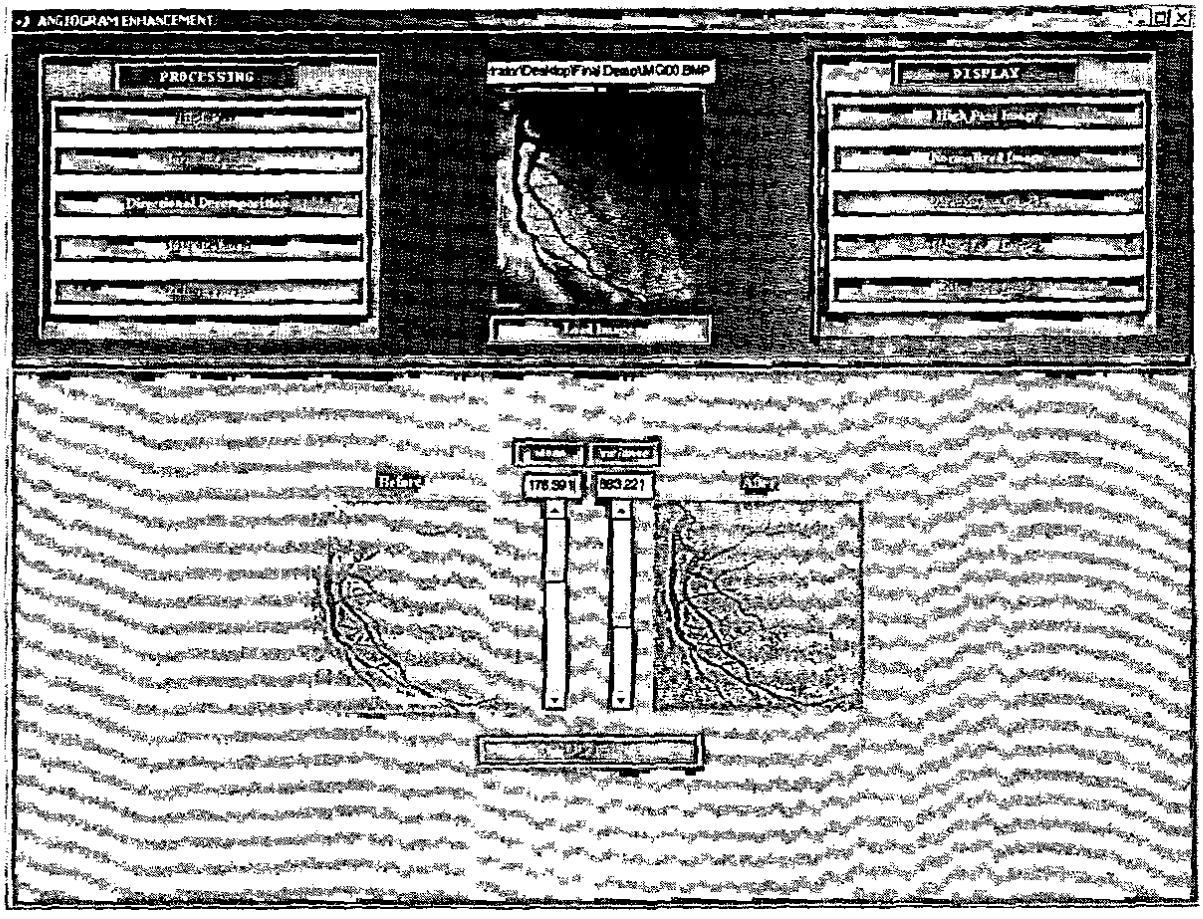

Figure A-4 Normalization of High Passed Image.

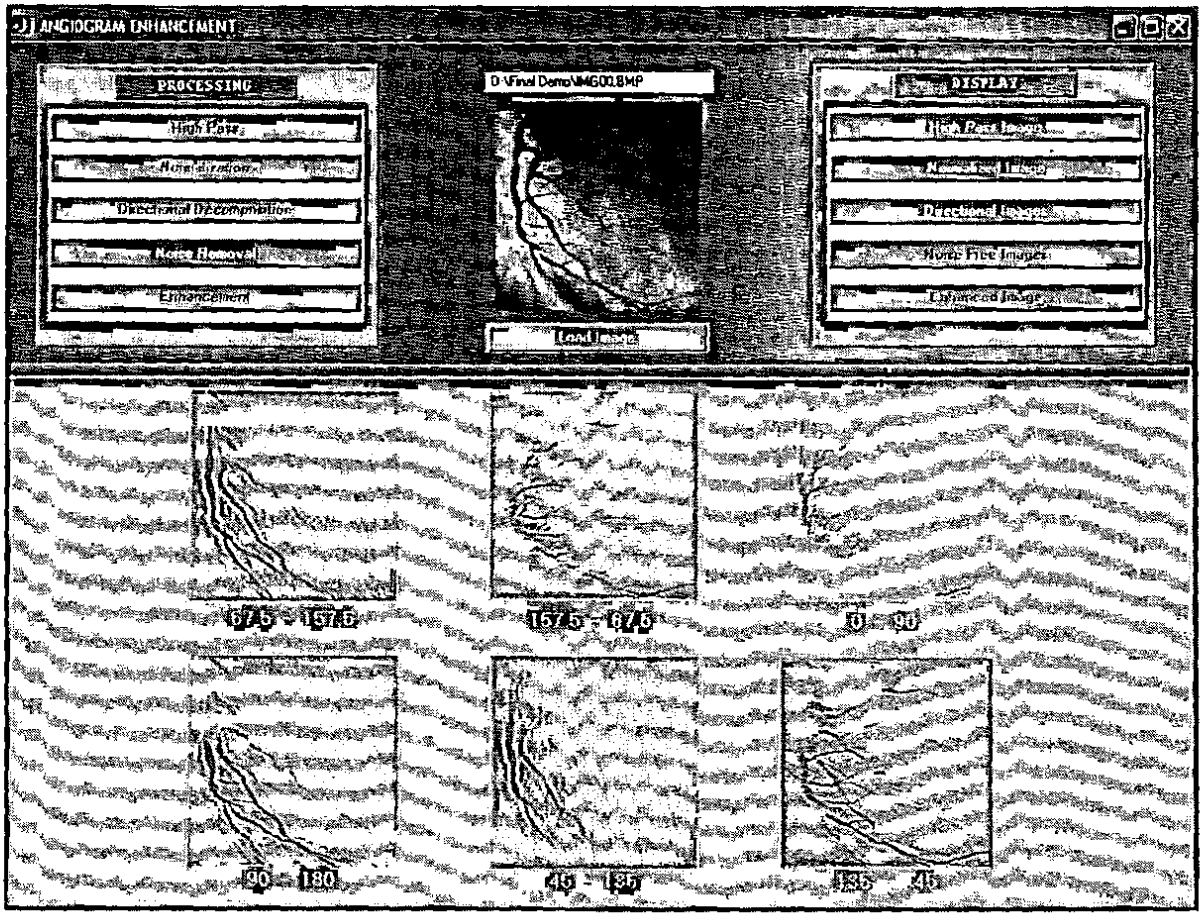

Figure A-6 Interface for Directional Decomposition Process.

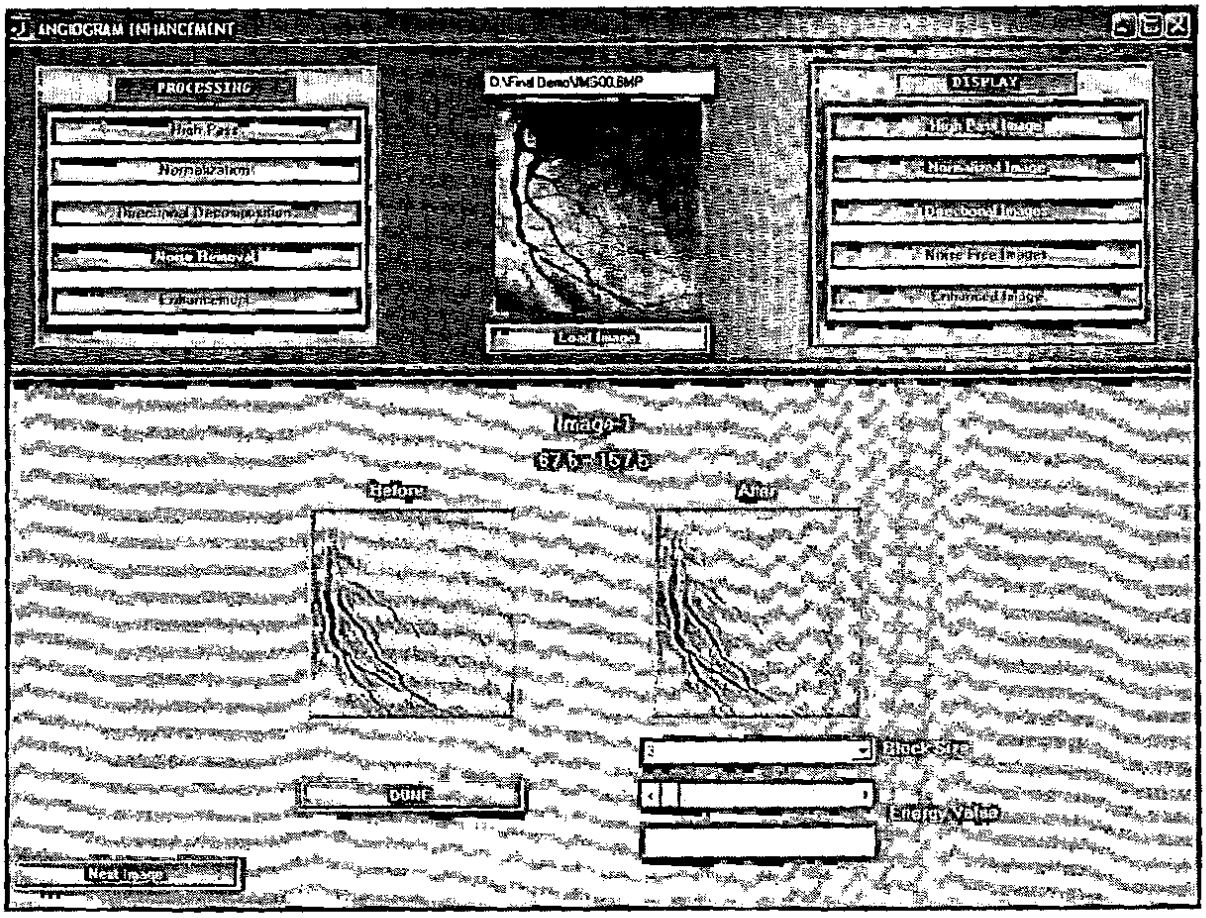

Figure A-7 Noise Removal for 1st Directional Image.

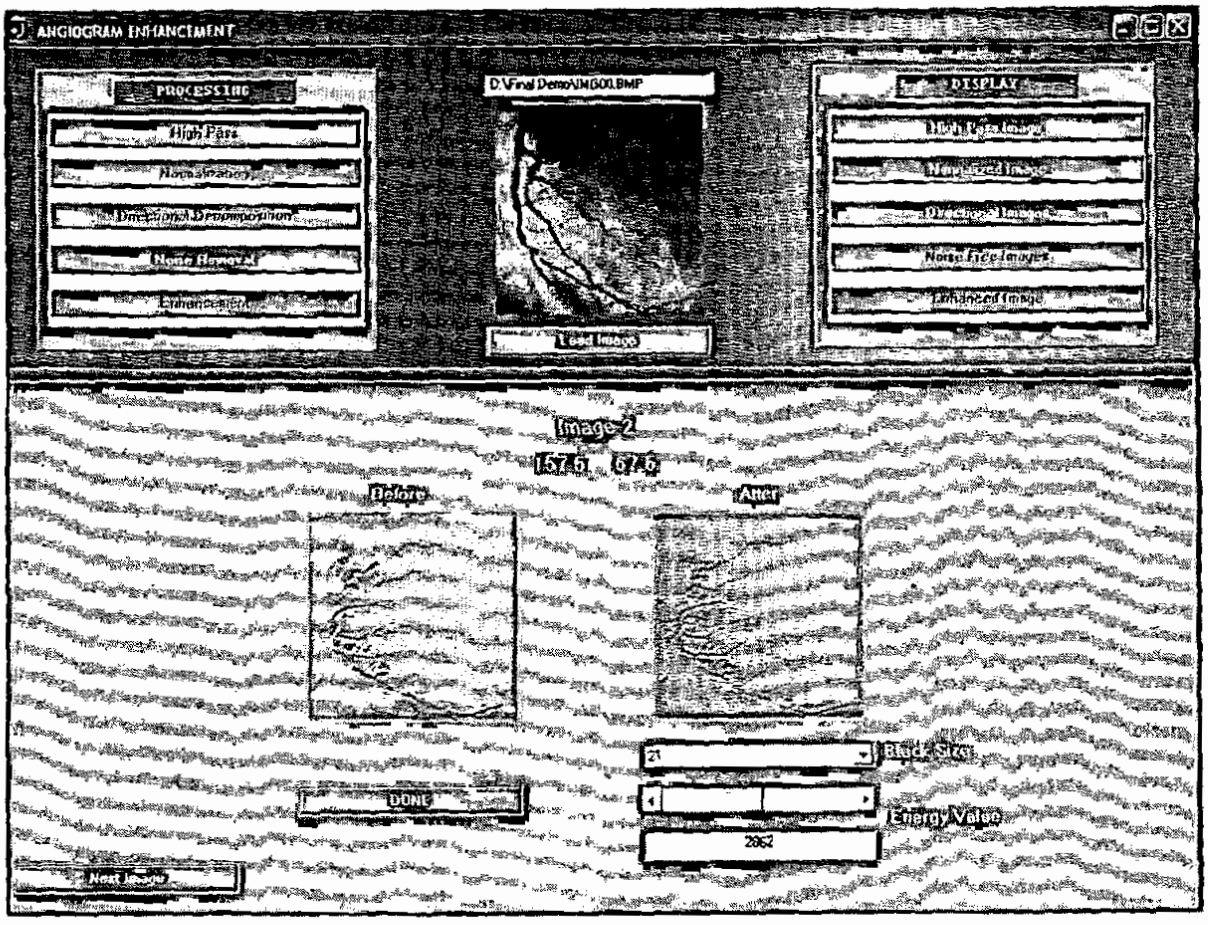

Figure A-8 Noise Removal for 2nd Directional Image.

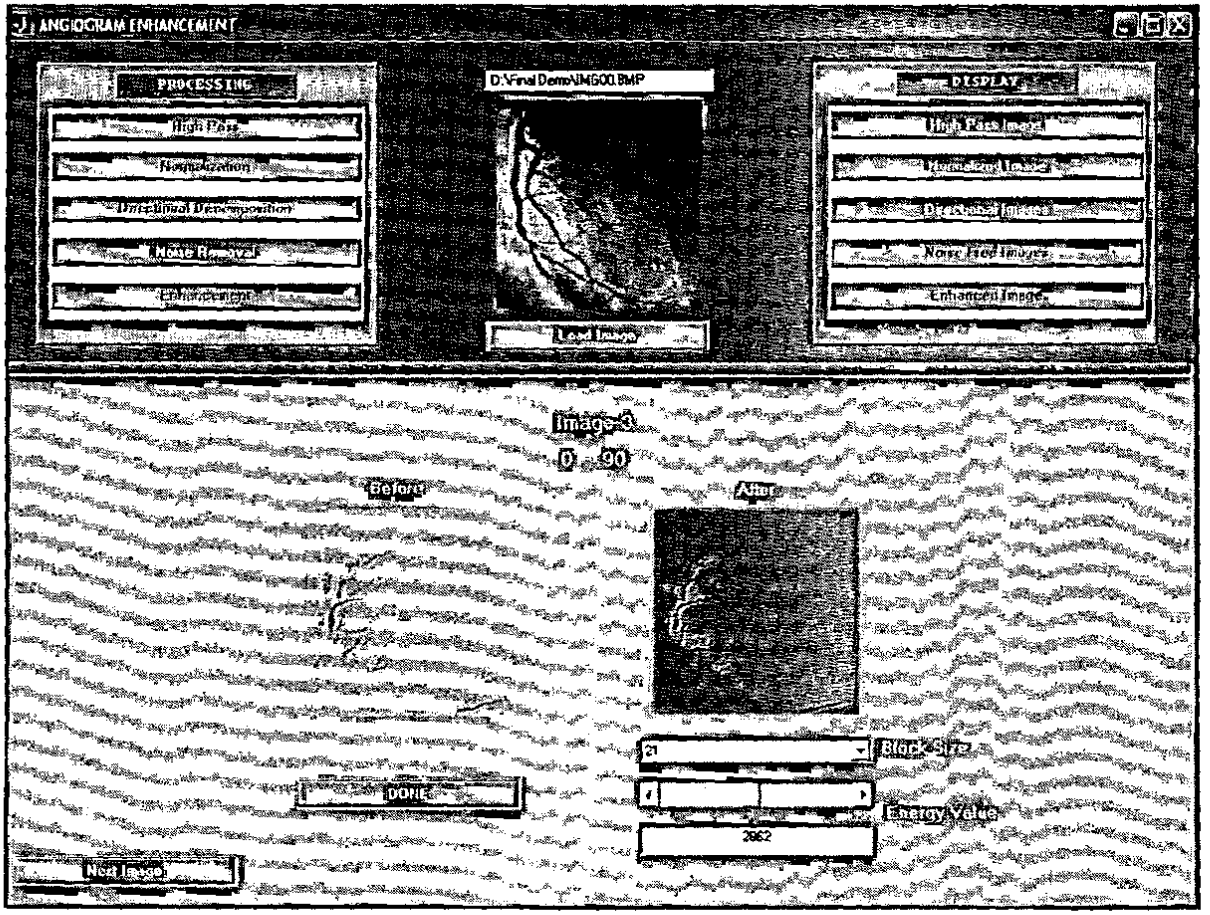

Figure A-9 Noise Removal for 3rd Directional Image.

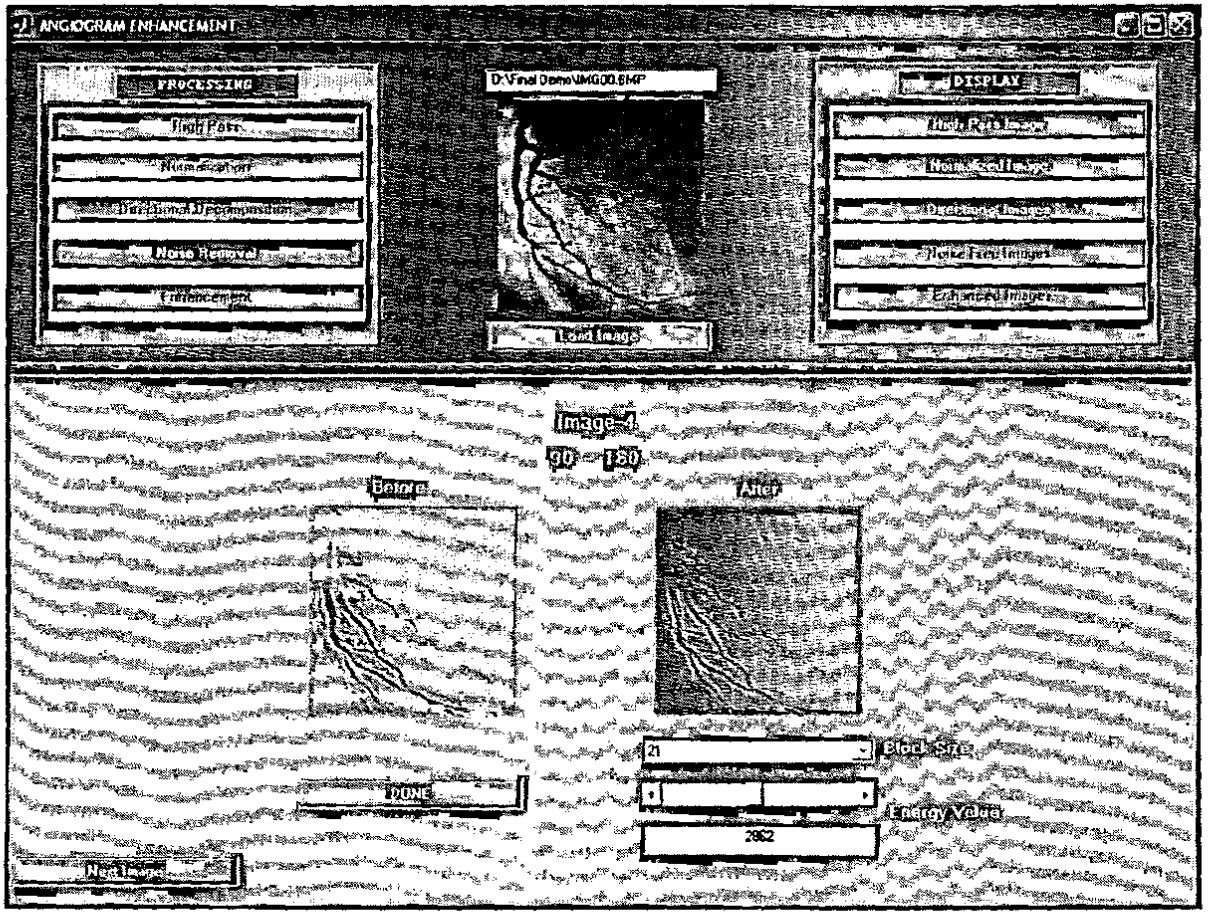

Figure A-10 Noise Removal for 4th Directional Image.

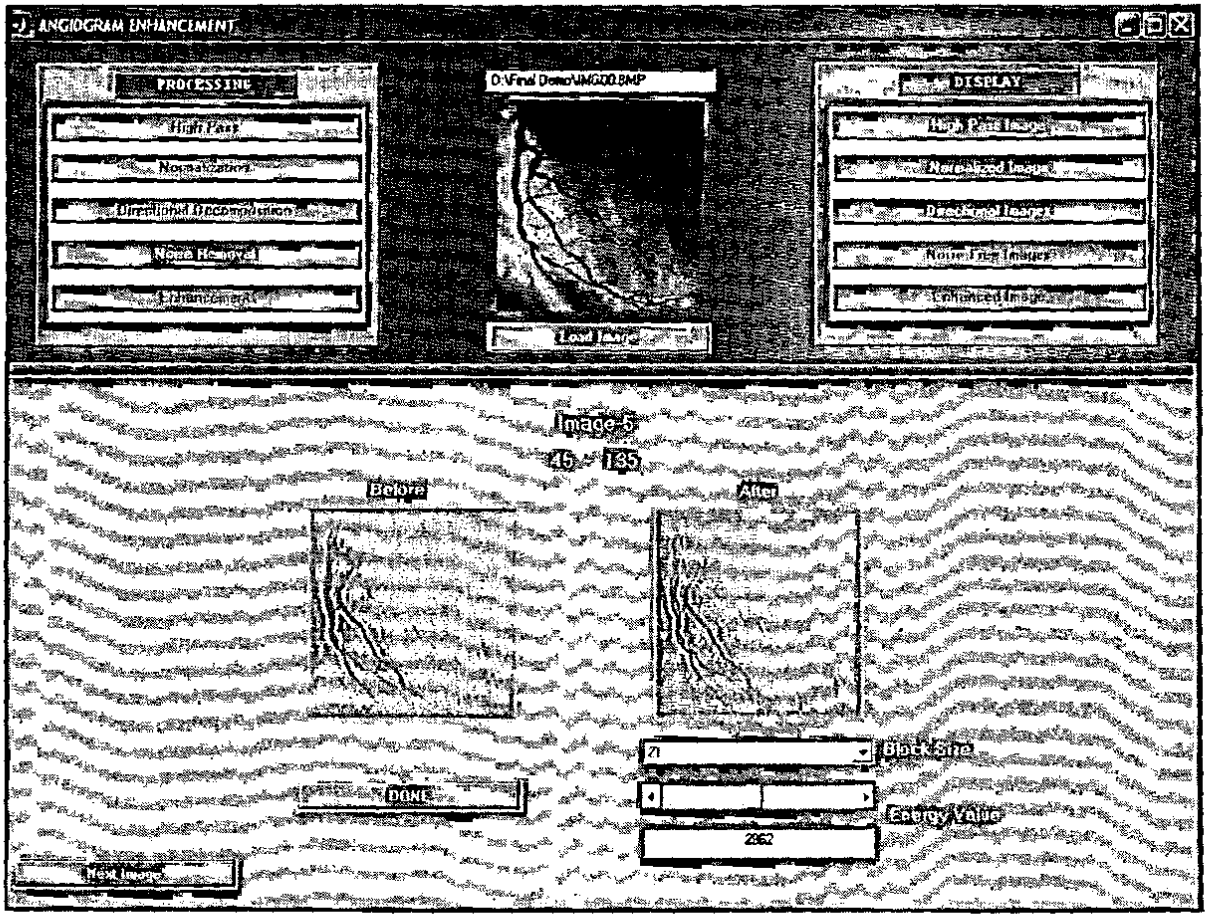

Figure A-11 Noise Removal for 5th Directional Image.

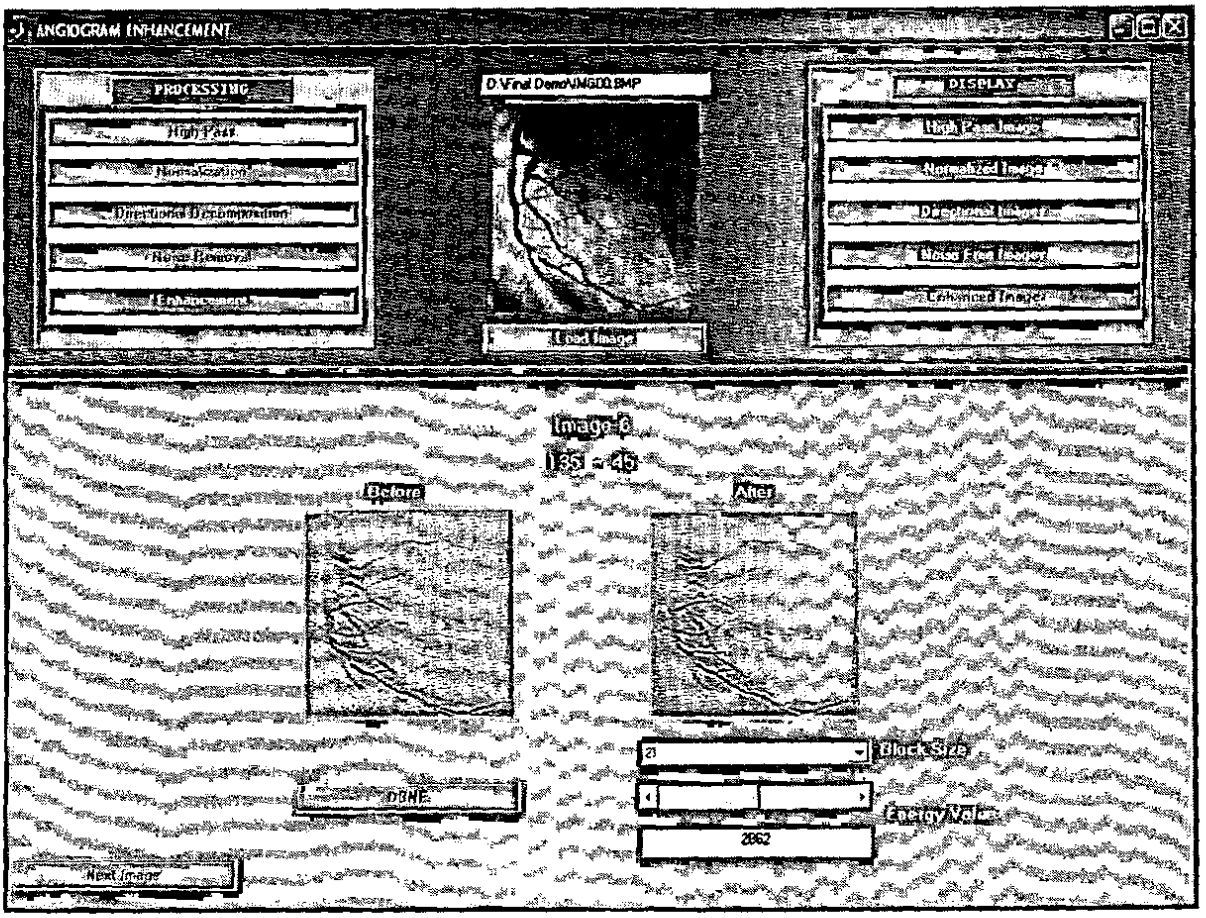

Figure A-12 Noise Removal for 6th Directional Image.

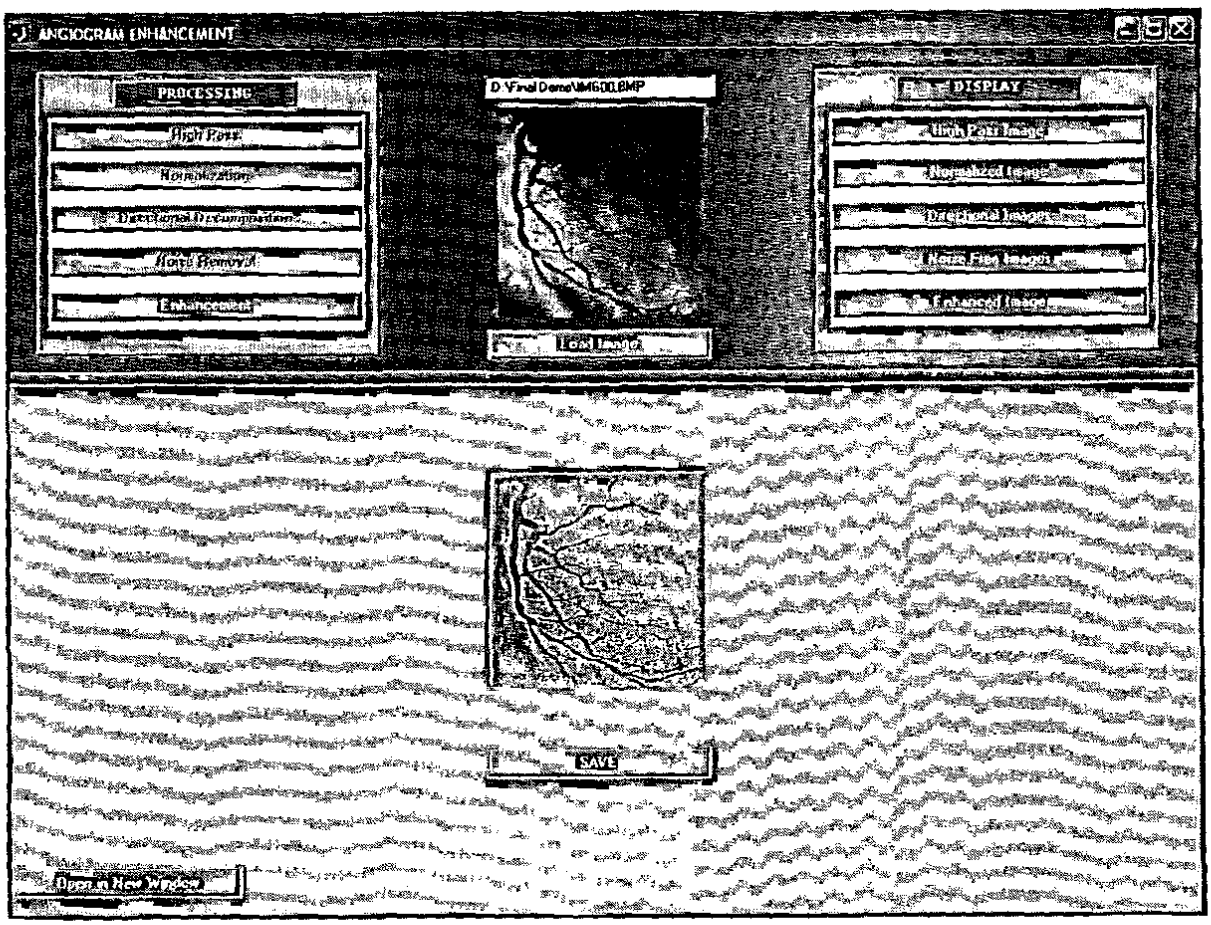

Figure A-13 Enhanced Image Interface.

RAFERENCES & BIBLIOGRAPHY

[1] M. Marta, R. Dunlay, and D. Mathis, "Terrain classification using texture for the ALV," in *Proceedings of the SPIE - International Society for Optical Engineering*, pp. 64-70, November 1989.

[2] L. M. Linnett and A. J. Richardson, "Texture segmentation using directional operators," in *Proceedings of the International Conference on Acoustics, Speech, and Signal Processing*, pp. 2309-2312, IEEE, April 1990.

[3] S. Treitel, J. L. Shanks, and C. W. Frasier, "Some aspects of fan filtering," *The Robinson Treitel Reader*, pp. 789-800, 1969. Paper originally presented at the 36th Annual International Meeting of the SEG, Houston, Texas, Nov. 0, 1966.

[4] P. Embree and J. P. Burg, "Wide band velocity filtering —the pie slice process," *Geophysics*, vol. 28, pp. 948-974, 1963.

[5] J. P. Fail and G. Gray, "Les filters en eventail," *Geophys. Prosp.*, vol. 11, pp. 131-163,1963.

[6] R. H. Tatham, J. Keeney, and L Nopon, "Application of the Tau-P transform (slant stack) in processing seismic reflection data." presented at 52nd Annual Meeting SEG, Dallas, TX, 1982, 1982.

[7] E. Peli, "Adaptive enhancement based on a visual model," *Optical Engineering, Vol.* 26, pp. 655-660, July 1987.

[8] H. Li and Z. He, "Directional subband coding of images," in *Proceedings of the IEEE International Conference on Acoustics, Speech, and Signal Processing*, pp. 1823-26, May 1989.

[9] M. Kunt, "Recent results in high-compression image coding," *IEEE Transactions on Circuits and Systems, vol.* CAS-34, pp. 1306-1336, November 1987.

[10] M. Kunt, A. Ikonomopoulos, and M, Kocher, "Second generation image coding techniques," *Proceedings of the IEEE*, vol. 73, pp. 549-574, April 1985.

[11] B. Mahesh and W. A. Pearlman, "Hexagonal sub-band coding for images," in *Proceedings of the IEEE International Conference on Acoustics, Speech, and Signal Processing*, pp. 1953-56, May 1989.

[12] E. P. Simonceili and E- H. Adelson, "Non-separable extensions of quadrature mirror filters to multiple dimensions,[11] *Proceedings of the IEEE*, pp. 652-664. April 1990.

[13] B. Mahesh and W. A. Pearlman, "Image coding on a hexagonal pyramid with noise spectrum shaping," in *Visual Communications and Image Processing IV.* pp. 764-774, SPIE, 1989.

[14] E. P. Simonceili and E. H. Adelson, "Nonseparable QMF pyramids," in *Visual Communication and Image Processing,* pp. 1242-1246, SPIE, 1989.

[15] E. Shlomot, Y. Zeevi, and W. A. Pearlman, "The importance of spatial frequency and orientation in image decomposition and coding," in *Visual Communications and Image processing II,* pp. 152-158, 1987.

[16] E. H. Adelson and E. Simonceili, "Orthogonal pyramid transforms for image coding," in *Visual Communications and Image Processing,* pp. 50-58, SPIE. 1987.

[17] W. T. Freeman and E. H. Adelson, "Steerable filters for image analysis," Technical report 126 126, Vision and Modeling Group — The Media Laboratory, Massachusetts institute of Technology, Cambridge, MASS 02139, February 1990.

[18] J. Radon, "[On the determination of functions from their integrals along certain manifolds]," *Ber. Saechs. Akad. Wiss. Liepzig, Math. Phys.,* vol. 69, pp. 262-77. 1917. in German.

[19] P. V. C. Hough, "Methods and means for recognizing complex patterns." U.S. Patent 3,069,654, 1962.

[20] R. O. Duda and P. E. Hart, "Use of the Hough transform to detect lines and curves and figures," *Comm. ACM,* vol. 15, no. 1, pp. 11-15, 1972.

[21] G. Hall, T. J. Terrel, J. M. Senior, and L. M. Murphy, "Transputer implementation of the Radon transform for image enhancement," in *Proceedings of the International Conference on Acoustics Speech and Signal Processing,* pp. 1548-51, May 1989.

[22] L. M. Murphy, "Linear feature detection and enhancement in noisy images via the Radon transform," *Pattern Recognition Letters,* vol. 4, pp. 279-84, September 1986.

[23] S. Fejes and L. Davis, "Detection of independent motion using directional motion estimation," *Computer Vision and Image Understanding,* Vol. 74, pp. 101-120, May. 1999.

[24] H. Taniguchi, A. Seki, S. Kuroda, S. Ikebata, and H. Furusawa, "A method of motion analysis using spatiotemporal image-directional temporal plane transform," *Systems and Computers in Japan,* Vol. 26, pp. 88-97, Jul. 1995.

[25] Y.P. Lin and P. Vaidyanathan, "Theory and design of two-dimensional filter banks: a review," *Multidimensional Systems and Signal Processing,* Vol. 7, pp. 263-330, July-Oct 1996.

[26] S. Sarbadhikari, J. Basak, S. Pal, and M. Kundu, "Noisy fingerprints classification with directional FFT based features using MLP," *Neural Computing & Applications,* Vol. 7, No.2, pp. 180-191, 1998.

[27] B. Sherlock, D. Monro, and K. Millard, "Fingerprint enhancement by directional Fourier filtering," *IEEE Proceedings-Vision, Image and Signal Processing,* Vol. 141, pp. 87-94, Apr. 1994.

[28] B. Mehtre, N. Murthy, S. Kapoor, and B. Chatterjee, "Segmentation of fingerprint images using the directional image," *Pattern Recognition,* Vol. 20, No. 4, pp. 429-435, 1987.

[29] R- Cappelli, A. Lumini, D. Maio, and D. Maltoni, "Fingerprint classification by directional image partitioning," *IEEE Transactions on Pattern Analysis and Machine Intelligence,* Vol. 21, pp. 402-421, May. 1999.

[30] A. Paplinski, "Directional filtering in edge detection," *IEEE Transactions on Image Processing,* Vol. 7, pp. 611-15, 1998.

[31] H. Tanaka, Y. Iwahori, and N. Ishii, "Estimation of surface orientation from directional derivatives of shading image," *International journal of Systems Science,* Vol. 26, pp. 975-981, Apr. 1995.

[32] J. De Vriendt, "Effect of sampling, quantization and noise on the performance of the second directional derivative edge detector," *Multidimensional Systems and Signal Processing,* Vol. 6, pp. 37-68, Jan. 1995.

[33] P. Huang, S. Dai, and P. Lin, "Planar shape recognition by directional flowchange method," *Pattern Recognition Letters,* Vol. 20, pp. 163-170, Feb. 1999.

[34] N. Kato, M. Suzuki, S. Omachi, H. Aso, and Y. Nemoto, " A handwritten character recognition system using directional element feature and asymmetric Mahalanobis distance," *IEEE Transaction on Pattern Analysis and Machine Intelligence,* Vol. 21, pp. 258-262, Mar. 1999.

[35] R. Cardoner and F. Thomas, "Residuals + directional gaps = skeletons," *Pattern Recognition Letters,* Vol. 18, pp. 343-353, Apr. 1997.

[36] S. Liang, M. Ahmadi, and M. Shridhar, "Segmentation of handwritten interference marks using multiple directional stroke planes and reformalized morphological approach," *IEEE Transactions on Image Processing,* Vol. 6, pp. 1195-1202, 1997.

[37] J. Taguchi, K. Kido, and K. Sano, "Directional image filter respectively adjusted to edge and flat regions," *Systems and Computers in Japan*, Vol. 30, pp. 72-78, Jul. 1999.

[38] K. Kido, J. Taguchi, and K. Sano, "Improvement of MRI image quality by a directional adaptive filter, "*Systems and Computers in Japan.* Vol. 28, pp. 69-76, Sep. 1997.

[39] Y. Sun, R. Lucariello, and S. Chiaramida, "Directional low-pass filtering for improved accuracy and reproducibility of stenosis quantification in coronary arteriograms," *IEEE Transactions on Medical Imaging,* Vol. 14, pp. 242-248, Jun. 1995.

[40] A. Shimizu, J. I. Toriwaki, and J. I. Hasegawa, "Characteristics of minimum directional difference filter which extracts circumscribed shadows in chest X-ray images," *IT,* Vol. 38, pp.587-607, March 1992.

[41] P. Trahanias and A. Venetsanopoulos, "Vector directional 61ters-a new class of multichannel image processing filters," *IEEE Transactions on Image Processing,* Vol. 2, pp. 528-534, Oct. 1993.

[42] P. Trahanias, D. Karakos, and A. Venetsanopoulos, "Directional processing of color images: theory and experimental results," *IEEE Transactions on Image Processing,* Vol. 5, pp. 868-880, Jun. 1996.

[43] K. Plataniotis, D. Androutsos, and A. Venetsanopoulos, "Color image filters: the vector directional approach," *Optical Engineering,* Vol. 36, pp. 2375-2383, Sep. 1997.

[44] K. Plataniotis, D. Androutsos, and A. Venetsanopoulos, "Color image processing using adaptive vector directional filters," *IEEE Transactions on Circuits and Systems II: Analog and Digital Signal Processing,* Vol. 45, pp. 1414-19, Oct. 1998.

[45] N. Nikolaidis and I. Pitas, "Directional statistics in nonlinear vector field filtering," *Signal Processing,* Vol. 38, pp. 299-316, Aug. 1994.

[46] J. Scharcanski and A. Venetsanopoulos, "Edge detection of color images using directional operators," *IEEE Transactions on Circuits and Systems for Video Technology,* Vol. 7, pp. 397-401, Apr. 1997.

[47] J. Bell, M. Chantler, and T. Wittig, "Sidescan sonar: a directional filter of seabed texture?," *IEE Proceedings-Radar, Sonar and Navigation,* Vol. 146, pp. 65-72, Feb. 1999.

[48] H. Yamada, K. Yamamoto, and K. Hosokawa, "Directional mathematical morphology and reformalized Hough transformation for the analysis of topographic maps," *IEEE Transactions on Pattern Analysis and Machine Intelligence,* Vol. 15, pp. 380-387, Apr. 1993.

[49] D. Androutsos, K. Plataniotis, and A. Venetsanopoulos, "Directional detail histogram for image retrieval," *Electronics Letters,* Vol. 33, pp. 1935-1936, 6 N.1997.

[50] T. Tohne, H. Koda, and H. Tanaka, "A scheme for constructing directional filters and its application to two-channel coding of images," *Systems and Computers in Japan,* Vol. 27, pp. 94-105, Mar. 1996.

[51] A. Kubrick and T. Ellis, "Perceptually based directional classified gain-shape vector quantization," *IEEE Transactions on Circuits and Systems for Video Technology,* Vol. 5, pp. 96-108, Apr. 1995.

[52] A. Ikonomopoulos and M. Kunt, "High compression image coding via directional filtering," *Signal Processing,* Vol. 8, pp. 179-203, Apr. 1985.

[53] D. Dunn, W. Higgins, and J, Wakeley, "Texture Segmentation Using 2-D Gabor Elementary Functions," *T-PAMI,* Vol. 16, pp. 130-149, 1994.

[54] J. P. Antoine and R. Murenzi, "Two-dimensional directional wavelets and the scale-angle representation," *Signal Processing,* Vol. 52, pp. 259-281, Aug. 1996.

[55] E. Simoncelli, W. Freeman, E. Adelson, and D. Heeger, "Shiftable Multi-Scale Transforms," *IT,* Vol. 38, pp. 587-607, March 1992.

[56] A, K. Jain, *Fundamentals of Digital Image Processing.* Prentice-Hall, 1989.

[57] J. Johnston, "A Filter Family Designed for use in QMF Banks," *IEEE, ICASP,* pp. 291-94, April 1980.

[58] M. J. T. Smith and T. P. Barnwell, "Exact Reconstruction Techniques for Tree-structured Subband Coders," *IEEE Trans. On Acoustics, Speech, and Signal Processing,* pp. 434-441, Jan. 1986.

[59] J. W. S. Cassels, *An Introduction to the Geometry of Numbers.* Springer-Verlag, 1959.

[60] R. H. Bamberger. *The Directional Filter Bank: A Multirate Filter Bank for the Directional Decomposition of Images.* Ph.D-thesis, Georgia Institute of Technology, November 1990.

[61] R. H. Bamberger and M. J. T. Smith, "A filter bank for the directional decomposition of images: theory and design," *IEEE Trans, on Signal Processing,* Vol. 40, pp. 882-893, April 1992.

[62] S. il Park, M. J. T. Smith, and R. M. Mersereau, "A New Directional Filter Bank For Image Analysis and Classification," *IEEE International Conference on Acoustics, Speech, and Signal Processing,* Vol. 3, pp.1417-1420, 1999.

[63] R. Bamberger and M. Smith, "Narrow band analysis of a filter bank for the directional decomposition of images," *ICASSP,* pp. 1739-42, 1990.

[77] A. Samal and P. A. Iyengar, "Automatic recognition and analysis of human faces and facial expression: A survey," *Pattern Recognition*, vol. 25, no. 1, pp. 65–77, 1992.

[78] R. Chellappa, C. L. Wilson, and S. Sirohey, "Human and machine recognition of faces: A survey," Proc. IEEE, vol. 83, no. 5, pp.705–740, 1995.

[79] J. Daugman, "Face and gesture recognition: Overview," IEEE Trans. Pattern Analysis and Machine Intelligence, vol. 19, no. 7, pp.675–676, 1997.

[80] A. Pentland, "Looking at people: Sensing for ubiquitous and wearable computing," IEEE Trans. Pattern Analysis and Machine Intelligence, vol. 22, no. 1, pp.107–119, 2000.

[81] M. Turk, and A. Pentland, "Eigenfaces for recognition," Journal of Cognitive Neuroscience, vol. 13, no. 1, pp.71–86, 1991.

[82] M. C. Burl, U. M. Fayyad, P. Perona, P. Smyth, and M. P. Burl, "Automating the hunt for volcanos on venus," in Proc.IEEE Conf. on Computer Vision and Pattern Recognition (IEEE, New York, 1994).

[83] A. Pentland, B. Moghaddam, and T. Starner, "Viewbased and modular eigenspaces for face recognition," in Proc.IEEE Conf. on Computer Vision and Pattern Recognition (IEEE, New York, 1994).

[84] C. Bregler, and S. M. Omohundro, "Surface learning with applications to lip reading," in G. Tesauro, J. D. Cowan, and J. Alspector, eds., Advances in Neural Information Processing Systems 6 (Morgan Kaufman, San Fransisco, CA, 1994, pp.43–50.

[85] H. Murase and S. K. Nayar, "Visual learning and recognition of 3-D objects from appearance," Int'l J. Comput. Vision 14, x-x (1995).

[86] J. J. Weng, "On comprehansive visual learning," Presented at the NSF/ARPA Workshop on Performance vs. Methodology in Computer Vision, Seattle, WA, June xx, 1994. Workshop on Recognition, Analysis, and Tracking of Faces and Gestures in Real-Time Systems, pp. 53–57, 1999, Greece.

[87] H. Murase, S. K. Nayar, and S. A. Nene, "General learning algorithm for robot vision," Neural and Stochastic Methods in Image and Signal Processing III, S.-S. Chen, ed., Proc. SPIE 2304, x-x, 1994.

[88] R. A. Fisher, "The use o f multiple measure in taxonomic problems," Ann. Eugenics vol. 7, pp. 179–188, 1936.

[89] D. L.Swits, and J. Weng, "Using discriminant eigenfeatures for image retrieval," IEEE Trans. Pattern Analysis and Machine Intelligence vol. 18, no. 8, pp. 831–836, 1996.

[90] P. N. Belhumeur, J. P. Hespanha, and D. J. Kriegman, "Eigenfaces vs. Fisherfaces: Recognition using a class specific linear projection," IEEE Trans. Pattern Analysis and Machine Intelligence vol. 19, no. 7, pp. 711–720, 1997.

[91] Ki-Chung Chung, Seok Cheol Kee and Sang Ryong Kim, "Face recognition using principal component analysis of gabor filter responses," in Proc. International Workshop on Recognition, Analysis, and Tracking of Faces and Gestures in Real-Time Systems, pp. 53–57, 1999, Greece.

[92] Chul-Hyun Park, Joon-Jae Lee, Mark J. T. Smith, Sang-il Park, and Kil-Houm Park "Directional filter bank-based fingerprint feature extraction and matching," IEEE Trans. on Circuits and Systems For Video Technology, vol. 14, no. 1, pp. 74–85, 2004.

[93] Hong, L. Wan, and A. Jain, "Fingerprint image enhancement algorithm and performance evaluation," *IEEE Trans on Pattern Analysis and Machine Intelligence*, vol. 20, no. 8, pp. 777-789, 1998.

[94] S. K. Oh, J. J. Lee, C. H. Park, and B. S. Kim, "New fingerprint image enhancement using directional filter bank," *WSCG*, vol. 11, no. 1, Feb. 2003.

[95] R. Ansari, "efficient iir and fir fan filters," *IEEE Trans. Circuits Syst.*, vol. CAS-34, pp. 941ñ945, Aug. 1987.